The evolutionary origins of neural crest and placodes

By

Philip Barron Abitua

A dissertation submitted in partial satisfaction of the

requirements for the degree of

Doctor of Philosophy

in

Molecular and Cell Biology

in the

Graduate Division

of the

University of California, Berkeley

Committee in charge:

Professor Michael S. Levine, Chair
Professor Richard Harland
Professor Nipam Patel
Professor Marvalee H. Wake

Spring 2015

Abstract

The evolutionary origins of neural crest and placodes

by
Philip Barron Abitua
Doctor of Philosophy in Molecular and Cell Biology
University of California, Berkeley
Professor Michael S. Levine, Chair

The sudden appearance of neural crest and neurogenic placodes in early branching vertebrates has puzzled biologists for over a century. These embryonic tissues contribute to the development of the cranium and associated sensory organs, which were crucial for the evolution of the vertebrate head. The evolution of neural crest and neurogenic placodes has been postulated as a key event leading to the appearance of new cell types that fostered the transition from filter feeding to active predation in ancestral vertebrates. However, the evolutionary origin of neural crest and neurogenic placodes has remained obscure due to the lack of embryonic data from tunicates, the closest living relative to the vertebrates. We provide evidence that the tunicate *Ciona intestinalis* possesses a cephalic melanocyte lineage (a9.49) similar to neural crest that can be reprogrammed into migrating ectomesenchyme by the targeted misexpression of *Twist*. Our results suggest that the neural crest melanocyte regulatory network predated the divergence of tunicates and vertebrates. We propose that the co-option of mesenchyme determinants, such as *Twist*, into the neural plate ectoderm was crucial for the emergence of the vertebrate “new head”.

Furthermore, we show that *Ciona intestinalis* possesses a preplacodal ectoderm (PPE) that is specified by a BMP antagonist and expresses the key regulatory determinant *Six1/2,* a developmental program conserved across vertebrates. The *Ciona* PPE is shown to produce ciliated neurons that express gonadotropin-releasing hormone (*GnRH*), a G protein-coupled receptor for relaxin-3 (*RXFP3*), and a functional cyclic nucleotide gated channel (*CNGA*), suggestive of dual chemosensory and neurosecretory activities. These observations provide the first evidence that *Ciona* possesses a neurogenic placode, which produces multifunctional sensory and neurosecretory cells related to those derived from olfactory placodes of vertebrates. In vertebrates, GnRH neuroblasts are first formed in the olfactory placode and use the axon tracts of chemosensory neurons to guide them to their final destination in the hypothalamus. Tracing experiments have shown that olfactory and GnRH neurons form a direct neuronal circuit. We speculate that the PPE-derived neurons in *Ciona* resemble an ancestral cell type, a progenitor to the complex neuronal circuit that integrates sensory information and neuroendocrine control in vertebrates.

This dissertation is dedicated to Donna Clarke Carollo, my high school biology teacher. Thank you for inspiring me!

Acknowledgments

I would like to thank everyone who positively impacted my life to help me get to this rather unexpected position of earning a PhD from the University of California Berkeley.

As a small child growing up I often struggled in school. I was often frustrated with my performance in comparison to my peers. Learning didn't always come easy, but my mother always assured me that I was smarter than the average bear. I was a late bloomer to say the least.

In high school Mrs. Clarke introduced me to the tiny world of the cell. I was mesmerized by the microscopic world and remember staying up past my bedtime reading Molecular Biology of the Cell in my closet. My grades improved enough to get accepted at the University of Texas at Austin, where I continued my pursuit of molecular and cell biology.

As a junior I took developmental biology with John Wallingford. His first lecture was so enthralling that I asked if I could volunteer in his lab directly afterwards. He gave me that opportunity and I made the best of it. Concurrently I was enrolled in an upper division microscopy course taught by Malcolm Brown, the cellulose enthusiast. Brown's course was extremely challenging. We had to write lengthy lab reports in a short span of time, which turned out to be an extremely useful skill to have developed (*wink wink*). It was in this course that I was exposed to the beautiful world of electron microscopy.

I surmised that the technique of electron microscopy could be applied to my undergraduate work on frogs in John Wallingford's lab. John took the chance on the idea and bought me diamonds and gold (a diamond knife for ultrathin sectioning and gold particles for immunolabeling). Dwight Romanovic, the technician in the core facility, showed me the ropes and helped me develop my electron microscopy skills. These efforts allowed me to co-author three papers during my undergraduate career. For the third paper, my scanning electron micrograph of a multi-ciliated cell ended up on the cover of Nature Cell Biology!

John Wallingford practically made my decision for me when it came time to apply for grad school. He thought I should go to Berkeley, no question. After the interview, I was quickly contacted by David Weisblat who immediately offered me the position. In some strange turn of events I ended up joining Mike Levine's lab, even after hearing the ring of fire story. Truth be told I was attracted by *Ciona intestinalis* as developmental biology system. I hadn't really considered the field of evo-devo but it ended up the focus of my rotation project and it turned out to be a rather lucrative angle.

Alberto Stolfi, lovingly referred to as Junior by Mike, was my mentor in the Levine lab. As a senior graduate student, Alberto stressed to me the idea of time management. He told me that although six years seems like a lot, your time in grad school is not infinite. So instead of rushing in my final couple of years I decided to push myself to the limit during my first and second year. I quickly identified the neural crest project and ran with it. I took the American approach of research, which is throwing everything at the wall and hoping something sticks. Throughout this period Alberto was tremendously helpful in teaching me techniques in molecular biology. He was a cloning god! Often times people from other labs would come by just to ask, “what would Alberto do?”

Working for Mike Levine is not easy. He pushes you to your physical and mental limit. I am not certain this is a good thing, but I can tell you it sure is effective. We had our difficult times, periods of ignoring each other, passive aggressive emails and straight up aggressive ones, but overall his demeanor is passable. In the end Mike’s lab is as good as any to spend grad school in, if slaving away your twenties is something that interests you. At least you’re likely to publish well if you apply yourself. As Mike always says, “papers are the currency of science.” And of course I am grateful that he was so invested in my research and progress.

Misery enjoys company. I am not sure I would have handled the working conditions without Blair Gainous to confide in. Blair was always willing to listen to my problems and was there to discuss my project with. He is a true stand up guy and very tidy roommate. Thanks buddy!

I would like to thank all my current and future co-authors, Clare Hudson, Takehiro G. Kusakabe, Hitoyoshi Yasuo, Nicolas Haupaix, Eileen Wagner, Christopher J. Winchell, Ignacio A. Navarrete, Cathy Sirour, Kaori Kamata, Masashi Nakagawa, and Motoyuki Tsuda.

Last but certainly not least I would like to thank my beautiful, loving girlfriend Angela Kaczmarczyk. She has been tremendously supportive and tolerant of my sometimes extreme work ethic. I am very happy to have met Angela here at Berkeley and look forward to continuing our journey in Boston. We have started a family together by adopting our little baby Nameko, the cutest cat of all time. Hopefully we will expand our family in the not too distant future. Earning a PhD has been the most challenging hurdle I have yet to face. I can’t imagine accomplishing it without the unconditional love from Angela.

Thank you everyone!

Table of contents

Chapter I:

Introduction

The origin of the vertebrates is a question that seeks to explain the beginnings of our early ancestors who diverged from other invertebrate chordates (i.e. tunicates and amphioxus) 550 million years ago. It is thought that two whole rounds of genome duplication at the base of the vertebrates facilitated this transition[1]. This event provided the raw genetic material for the evolution of entirely new gene families[2] and even the evolution of new cell types[3]. Two of these cell types, neural crest and placodes, are considered so unique by many researchers that they are often considered 'vertebrate innovations'[4].

The disparate between neural crest and placodes seen in vertebrates, and homologous cell types in amphioxus was so great that it likely seemed correct to think of them as *de novo* innovations. However, within the last decade it was discovered that tunicates and not cephalochordates (amphioxus) are the closest living relative to vertebrates[5]. All of a sudden, this finding revitalized tunicates as a model system for evolutionary and developmental (evo-devo) studies on vertebrate origins and subsequently became the focus of my dissertation.

Ciona intestinalis is a member of the tunicates, and is affectionately referred to as a sea squirt due to its ability to expel water from its siphons like a squirt gun. *Ciona* is a marine invertebrate chordate that spends its adult life as a sessile filter feeder, which can be found in copious amounts attached to docks around the world due to its invasive nature.

Despite its unusual appearance, often being mistaken from some kind of sponge, the early development of *Ciona* closely resembles our own. *Ciona* embryos undergo gastrulation to form all three germ layers, neurulation produces a hollow neural tube, and they exhibit a swimming larval period controlled by motor ganglion cells[6,7]. In these ways *Ciona* is like a streamlined proto-vertebrate. However, they lack two cell types known as neural crest and placodes.

Neural crest is a remarkable cell type that migrates throughout the embryo, giving rise to most of the cranium, peripheral nervous system, pigment cells, and other derivates[8,9]. Placodes are equally impressive in their potential, contributing to sensory organs involved in sight, smell, and hearing, as well as producing the anterior pituitary, which has vital neuroendocrine functions[10].

Neural crest cells form at the border between then neural plate (future central nervous system) and the adjacent ectoderm. This region is defined by a set of transcription factors referred to as 'neural plate border genes.' Activated downstream of these genes is the next tier of transcription factors known as 'neural crest specifiers.' These genes in turn activate the final set of genes called 'neural crest effectors,' which include transcription factors like *Mitf* and cell

biology genes such as the *KIT* receptor[11]. This cascade of genes is organized into a gene regulatory network (GRN).

The neural crest GRN is an excellent tool for studying evo-devo, because it provides a conserved model of neural crest development across all vertebrates. This can be used as a basis for identifying homologous cell types in invertebrate chordates such as *Ciona*, which is explained in detail in Chapter II. However, this model is not without its caveats. A single GRN cannot accurately describe all the various cell types that neural crest produce.

In chapter II we home in on a single cell type that we identify as the best neural crest homolog in *Ciona* based on its position within the embryo, its conserved gene expression, and its differentiation into a melanocyte. Other embryological comparisons of neural crest have been made with amphioxus but those studies have only showed the conserved expression of the 'neural plate border genes' and a single 'neural crest specifier,' *snail*[3].

Despite our comparison of the melanocyte lineage to neural crest in vertebrates, there are still two key differences. First, the *Ciona* melanocyte lineage does not produce other derivatives such as neurons, cartilage, or bone. Second, the lineage does not undergo a long-range migration that is typically exhibited by neural crest. In Chapter II an evolutionary scenario is proposed for the acquisition of both of these characteristics.

In Chapter III, using live imaging, we identify that the *Ciona* melanocyte cell lineage undergoes a previously unrecognized cell division. Furthermore, we detail how Ephrin-mediated ERK1/2 signaling controls the number of melanocytes in the tadpole. Interestingly, in vertebrates ERK1/2 signaling has been implicated in neural crest development. It is conceivable, that a deregulation of ERK1/2 signaling was involved in the expansion of neural crest derived melanocytes in vertebrates.

Neurogenic placodes, like neural crest, are considered a unique defining feature of vertebrates. They too arise from the neural plate border, however they are restricted to the anterior-most region[12]. The evolution of neurogenic placode is less contentious than neural crest evolution in part because it is a relatively smaller field. Previous researchers have likened the anterior border of the *Ciona* neural plate to the anterior pituitary of vertebrates[13,14]. However, this structure is said to lack neurogenic potential.

We broaden our focus in Chapter IV and show that the placodal homolog of *Ciona*, defined by conserved *Six1/2* expression, does indeed produce neurons. We look at a wide range of genes expressed in multiple placode derivatives in vertebrates and ponder if the equivalent neurons in *Ciona* could represent an ancestral cell type. This theory postulates that distinct, yet related cell types in extant vertebrates may have evolved from a single multifunctional cell in an earlier ancestor. The ancestral cell hypothesis was originally applied to an organ in amphioxus to explain the link between the olfactory circuit and hypothalamus[15]. In light of the revised phylogeny we provide more compelling evidence for such an ancestral cell in *Ciona* as described in Chapter IV.

Chapter II:

Identification of a neural crest rudiment in a non-vertebrate chordate

Summary

Neural crest arises at the neural plate border, expresses a core set of regulatory genes, and produces a diverse array of cell types including ectomesenchyme derivatives that elaborate the vertebrate head[8,16]. The evolution of neural crest has been postulated as a key event leading to the appearance of new cell types that fostered the transition from filter feeding to active predation in ancestral vertebrates[9]. However, the origin of neural crest remains controversial, since homologous cell types have not been unambiguously identified in non-vertebrate chordates[3,16]. Here we show that the tunicate *Ciona intestinalis* possesses a cephalic melanocyte lineage (a9.49) similar to neural crest that can be reprogrammed into migrating ectomesenchyme by the targeted misexpression of *Twist*. Our results suggest that the neural crest melanocyte regulatory network predated the divergence of tunicates and vertebrates. We propose that the co-option of mesenchyme determinants, such as *Twist*, into the neural plate ectoderm was crucial for the emergence of the vertebrate "new head"[9].

Introduction

Whole-genome phylogenetic analyses place the tunicates as the true sister clade to vertebrates[5], and consequently they are well suited for investigating the evolutionary origins of neural crest. In a previous report on the mangrove tunicate, a migratory cell population originating from the vicinity of the neural tube was likened to neural crest[17]. However, subsequent studies of eleven additional tunicates provided unequivocal evidence that these cells arise from the mesoderm flanking the neural tube[18]. It was then suggested that a mesoderm-derived mesenchyme lineage (A7.6) in Ciona possessed some of the properties of neural crest[19], although these cells do not arise from the neural plate border and lack expression of key neural crest regulatory genes.

Results

We present evidence that the a9.49 cell lineage of Ciona embryos represents a rudimentary neural crest. It arises at the neural plate border and expresses several neural plate border genes, as well as a number of neural crest specification genes, including *Id*, *Snail*, *Ets*, and *FoxD*[1,6,19-22] (Fig. 1a, Appendix

A). In vertebrates, Mitf directly activates several target genes required for melanogenesis of neural crest-derived melanocytes, including *Tyr* and *TRP*[23]. In tunicates, *Mitf* is expressed in the a9.49 lineage[24], which can be labeled via electroporation of a *Mitf* reporter plasmid (*Mitf>GFP*) (Fig. 1b). The posterior daughters of the lineage (a10.97) intercalate at the dorsal midline and form the gravity-sensing otolith and melanocyte of the light detecting ocellus (Fig. 1c)[25]. We sought to understand the basis for the differential specification of these pigmented cells.

Wnt signaling plays a conserved role in neural crest induction, and promotes melanocyte formation from cephalic neural crest in zebrafish[26]. Both a10.97 cells express *Tcf/Lef*, the transcriptional effector of Wnt signaling[22], thus Wnt might also play a role in Ciona melanogenesis. We found that *Wnt7* is expressed along the dorsal midline just posterior to the presumptive ocellus (Fig. 1b), suggesting that it might serve as a positional cue to trigger differentiation of the posterior a10.97 melanocyte.

Wnt signaling was selectively perturbed in the a9.49 lineage using the *Mitf* enhancer (Fig. 1c-f). A *bγ-crystallin* reporter was used to distinguish the melanocytes since it is expressed in the otolith but not the ocellus (Fig. 1c). Both pigmented precursors were converted to ocelli upon misexpression of *Wnt7* (Fig. 1d). A similar transformation was observed upon targeted expression of a stabilized form of *b*-catenin, the coactivator of *Tcf* (Fig. 1e). In contrast, misexpression of a dominant-negative form of *Tcf* (*Mitf>dnTCF*) produced the reciprocal transformation: both a10.97 melanocytes differentiated into otoliths and expressed the *bγ-crystallin* reporter (Fig. 1f).

Supernumerary otoliths were induced by the expression of a constitutively active form of the *Ets1/2* transcription factor (Fig. 1g and Appendix B). Co-electroporation of *Mitf>Wnt7* transformed these extra otoliths into ocelli (Fig. 1h). These results suggest that Wnt7 signaling specifies the ocellus and suppresses the development of the otolith. To determine the underlying mechanism we sought to identify neural crest specification genes that are selectively activated in the presumptive ocellus in response to Wnt7 signaling.

In vertebrates, Foxd3 has been shown to repress melanogenesis of neural crest cells via downregulation of *Mitf*[23,27]. In Ciona, *FoxD* is directly activated by the accumulation of nuclear *b*-catenin in the early embryo, indicating a potential link between Wnt signaling and *FoxD* expression[28]. We found that *FoxD* is selectively expressed in the presumptive ocellus, (Fig. 2a, b) adjacent to the expression of *Wnt7* in the dorsal midline (Fig. 1b). A *FoxD* enhancer recapitulates this expression in the presumptive ocellus (Fig. 2c), and is dependent on Wnt signaling, as expression is lost in the presence of *dnTCF* (Fig. 2d).

To investigate the role of FoxD in melanogenesis, we expressed variants of *FoxD* in the midline of the CNS, including the a9.49 lineage, using 5' regulatory sequences from the *Msx* gene (Fig. 1a, Appendix C). Targeted expression of either full-length *FoxD* or the N-terminal third of *FoxD* (non-DNA binding) abolished expression of the *Mitf>GFP* reporter gene (Fig. 2e, f, Appendix C).

However, misexpression of a constitutive repressor form of *FoxD* (DNA binding domain fused to a WRPW repressor motif) had little effect on *Mitf* expression (Appendix C). These results suggest that FoxD represses *Mitf* independent of its DNA binding domain, which is consistent with its mode of regulation in avian embryos, where Foxd3-mediated repression of *Mitf* is thought to occur through the sequestration of the transcriptional activator Pax3[27].

Our results suggest a simple gene regulatory network (*Wnt7*→*FoxD*⊣*Mitf*) for the differential specification of the otolith and ocellus in the Ciona tadpole (Appendix D). Both a10.97 cells express *Mitf* prior to neurulation and during the convergence of the two cells along the dorsal midline of the anterior neural tube. Subsequently, the posterior a10.97 cell receives a localized Wnt7 signal and activates *FoxD*, which attenuates *Mitf* leading to diminished pigmentation in the ocellus. *Mitf* expression is sustained in the anterior a10.97 cell, which forms the densely pigmented otolith.

Zebrafish employ a remarkably similar mechanism to specify neural crest-derived pigmented melanophores and iridophores, which derive from a common bi-potent Mitf+ progenitor[23]. The conservation of this network strengthens the argument that the a9.49 lineage of Ciona represents a rudimentary neural crest. However, the a9.49 lineage lacks some of the defining properties of cephalic neural crest, such as long-range migration and the potential to form ectomesenchyme derivatives.

We therefore sought to identify vertebrate neural crest determinants that are not expressed in the Ciona a9.49 lineage. In vertebrates, the craniofacial mesenchyme is derived from primary mesoderm and the ectomesenchyme arising from cephalic neural crest[8,29]. Both sources of cranial mesenchyme express the conserved mesodermal determinant *Twist*[30] and produce diverse cranial tissues including muscle, cartilage and bone. In tetrapods, it appears that only the cephalic neural crest expresses *Twist* and produces ectomesenchyme[30-32], whereas trunk neural crest lacks *Twist* expression and generates non-ectomesenchymal derivatives (e.g. neurons, glia and melanocytes)[8]. Disruption of *Twist* activity causes severe cephalic neural crest phenotypes, including defects in cell migration and survival, as well as morphological defects of the skull vault and heart[30,31,33].

There are three *Twist*-related genes in Ciona. In this study we focused on the one most similar to *Twist1* in vertebrates (Appendix E). In Ciona, *Twist* is expressed solely in mesoderm-derived mesenchyme (Fig. 3a). It is not expressed in any region of the neural plate, including the a9.49 lineage. *Twist*-expressing mesoderm undergoes long-range migration (Fig. 3b) and produces a number of diverse tissues in juveniles and adults, including body wall muscles, tunic cells (which populate the protective covering of the adult), and blood cells[34]. The migration and differentiation of these mesoderm tissues are inhibited when *Twist* expression is reduced[34].

To determine whether ectomesenchyme could be formed in Ciona, we misexpressed *Twist* in the a9.49 lineage using the *Mitf* enhancer (Fig. 3c, d). The

manipulated cells exhibit a mesenchymal phenotype, including protrusive activity, proliferation and long-range migration, which was not observed by the misexpression of other related genes (Supplementary Movie 1, Appendix F). Moreover, misexpression of *Twist* in the notochord and motor ganglion causes some disruptions in terminal differentiation, but does not transform these tissues into mesenchyme (Appendix G). The reprogrammed a9.49 cells exhibit expression of mesenchyme genes, including *ERG* (Appendix H), which is expressed in the ectomesenchyme of mouse embryos[35]. The affected lineage was visualized in juveniles using reporters for *Tyr*, a gene that is activated by Mitf in melanocytes[23] (Fig. 3e,f). Normally the a9.49 derivatives are located solely in an anterior region of the CNS (Fig. 3e). In contrast, embryos expressing *Mitf>Twist* result in juveniles with ectopic a9.49 cells (Fig. 3f). The reprogrammed cells appear to produce mesodermal derivatives, such as tunic cells based on their location and their distinct, rounded morphology (Appendix I).

Additional evidence for the reprogramming of the a9.49 lineage was obtained with Kaede, a photoconvertible fluorescent protein that was previously used in Ciona to trace the formation of the CNS[36]. Here, embryos were co-electroporated with *Mitf>Twist* and *Tyr>Kaede*, which mediate expression in the a9.49 lineage (Fig. 4a). Tailbud embryos that were not exposed to UV light show no red fluorescence (Fig. 4b) and result in juveniles that have only green a9.49 descendants (Fig. 4c). In contrast, tailbud embryos treated with UV (Fig. 4d, e) develop into juveniles that display red cells throughout the body. Control juveniles lacking *Mitf>Twist* exhibit the expected expression solely in the CNS (Appendix J). Finally, time-lapse microscopy was used to examine the *Mitf>Twist* expressing cells in juveniles. Some of these cells migrate like the normal tunic cells derived from the mesenchyme (Fig. 4g, Supplementary Movie 2). Thus, the misexpression of *Twist* appears to be sufficient, in part, to reprogram the a9.49 lineage into ectomesenchyme.

Discussion

The mesenchymal properties of neural crest were proposed to be the last features to appear during its evolution[4,9]. Our studies of the non-vertebrate chordate *Ciona intestinalis* support this hypothesis. We propose that cephalic neural crest arose from the co-option of one or more mesenchyme determinants (e.g. *Twist*) in a rudimentary neural crest cell type. Thus, this enigmatic cell population should not be considered a vertebrate innovation but rather an elaboration of an ancestral chordate gene network.

Methods

Embryo preparation and imaging

Ciona intestinalis adults were obtained, *in vitro* fertilized, and electroporated for transient transgenesis as described[37]. For each electroporation, typically 70 µg of DNA was resuspended in 100 µl buffer. Embryos were fixed at the appropriate developmental stage for 15 minutes in 4% formaldehyde. The tissue was then cleared in a series of washes of 0.01% Triton-X in PBS. Actin was stained overnight with Alexa-647-conjugated phalloidin at a dilution of 1/500. Samples were mounted in 50% glycerol in PBS with 2% DABCO for microscopy. Differential interference contrast microscopy was used to obtain transmitted light micrographs with a Zeiss Axio Imager A2 using the 40x EC Plan Neofluar objective. Confocal images were acquired on a Zeiss LSM 700 microscope using a plan-apochromat 20x or 40x objective. Confocal stacks contained approximately 50 optical slices at a thickness of 1-2 µm each. Images were rendered in 3D using Volocity 6 with the 3D opacity visualization tool. For time-lapse microscopy, larvae and juveniles were anesthetized in artificial seawater supplemented with 0.04% tricaine mesylate in glass bottom dish. Time-lapse images were taken on a Zeiss LSM 700 microscope at intervals of 3-4 minutes.

Molecular cloning

The University of California Santa Cruz Genome Browser Gateway facilitated the identification of conserved non-coding sequences between *Ciona intestinalis* and *Ciona savignyi*. Primers (Appendix K) were used to PCR amplify these putative enhancer sequences which were cloned into a pCESA vector using either AscI/NotI restriction sites for *Prop1, Twist,* and *βγ-crystallin* or AscI/XhoI for *Mitf*. The *Mitf* enhancer sequence was cloned 5' of a basal FOG promoter. The LacZ coding sequence of the pCESA vector was replaced with UNC-76 GFP, UNC-76 mCherry, H2B mCherry, eGFP, or Kaede. The *ZicL*, *Msx*, *FoxD*, *Tyr*, *TRP*, *Brachyury*, and *DMBX* enhancers have been previously described[7,21,22,28,37]. A similar cloning strategy was used to create misexpression vectors using Not1/EcoR1 sites for control group A bHLH genes, *Wnt7*, *FoxD*, and *FoxD* N-term or NotI/BlpI sites for stabilized *β-catenin* and *Twist* (Appendix K). The *FoxD:DBD:WRPW* coding sequence was made by amplifying the DBD of *FoxD* (Appendix K), which was subcloned into a pCESA vector containing an HA:NLS peptide and a WRPW repressor motif using NheI/SpeI sites. Additional coding sequences for *Ets:VP16*, *Ets:WRPW*, and *dnTCF*, were subcloned from existing expression vectors[22].

***In situ* hybridization and immunohistochemistry**

The double fluorescent *in situ* hybridizations and immunohistochemistry were performed as described[37] using linearized cDNA clones for *Wnt7* (cilv33g04), *FoxD* (citb8o13), *ERG* (cilv04i11), *Mech2* (cicl04m09), and *Twist* (cicl20p07) from Nori Satoh's (OIST, Okinawa, Japan) cDNA library.

Kaede lineage tracing

Embryos electroporated with *Tyr>Kaede* and co-electroporated with *Mitf>LacZ* or *Mitf>Twist* were developed in the dark until the late tailbud stage. Tailbuds expressing Kaede were then photoconverted with UV using the DAPI filter on a Zeiss Stereo Lumar.V12 for 3 minutes. Embryos were then continuously reared in the dark to the juvenile stage and prepared for imaging.

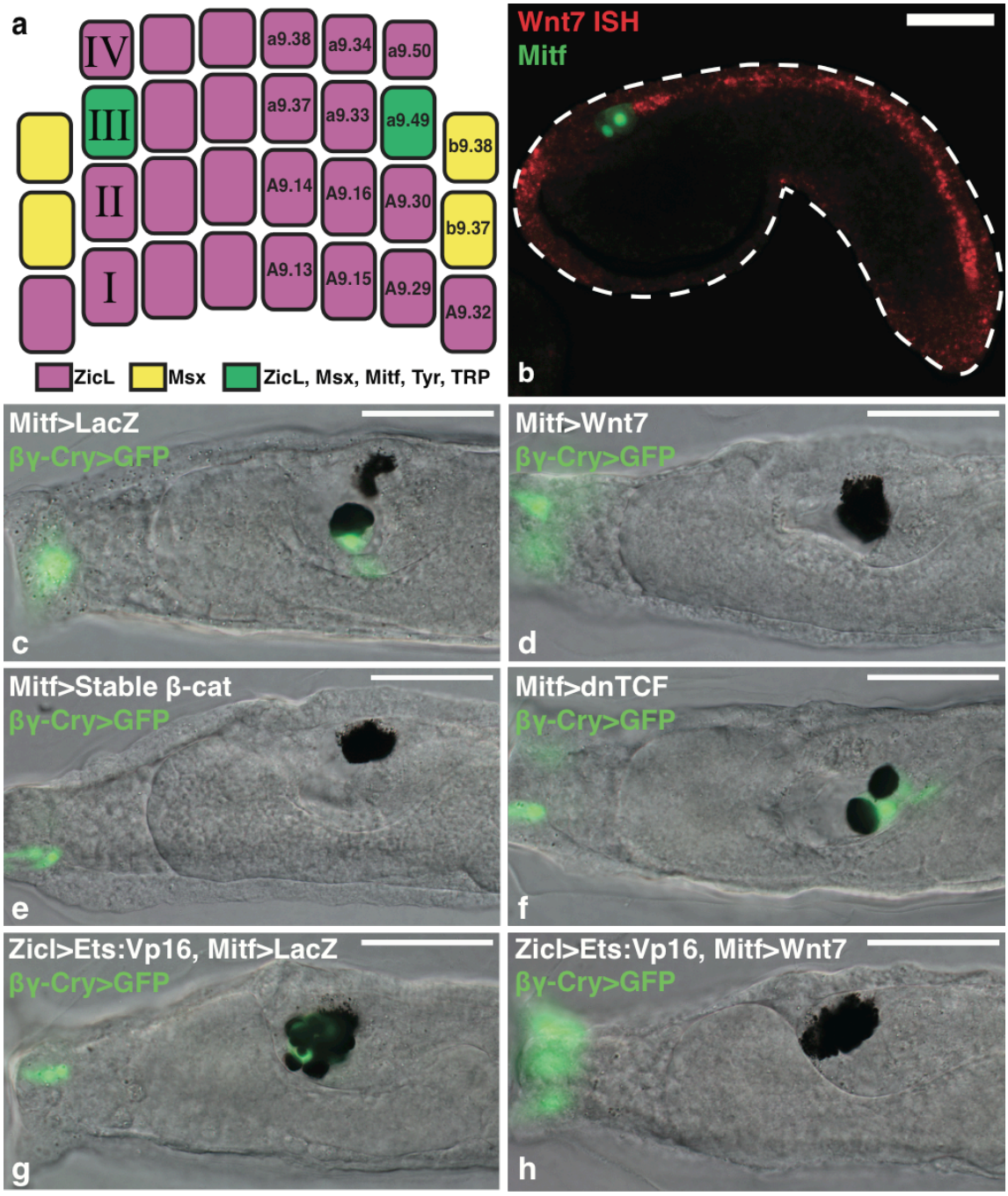
a
IV
III
II
I
a9.38
a9.34
a9.50
a9.37
a9.33
a9.49
b9.38
A9.14
A9.16
A9.30
b9.37
A9.13
A9.15
A9.29
A9.32
ZicL
Msx
ZicL, Msx, Mitf, Tyr, TRP
Wnt7 ISH
Mitf
b
Mitf>LacZ
βγ-Cry>GFP
c
Mitf>Wnt7
βγ-Cry>GFP
d
Mitf>Stable β-cat
βγ-Cry>GFP
e
Mitf>dnTCF
βγ-Cry>GFP
f
ZicI>Ets:Vp16, Mitf>LacZ
βγ-Cry>GFP
g
ZicI>Ets:Vp16, Mitf>Wnt7
βγ-Cry>GFP
h

Figure 1 | Wnt signaling promotes ocellus formation. a, Gastrula stage schematic indicates the lineage specific expression of enhancers in this study. **b**, Tailbud electroporated with *Mitf>LacZ* detected with an antibody (green), and hybridized with a *Wnt7* probe (red). **c**-**f**, Larvae electroporated with *βγ-crystallin>GFP* marks the otolith and anterior palps. **c**, Co-electroporated with *Mitf>LacZ* (166/196 had an otolith and ocellus). **d**, Co-electroporated with *Mitf>Wnt7* (172/205 had two ocelli). **e**, Co-electroporated with *Mitf>stable β-catenin* (189/205 had two ocelli). **f**, Co-electroporated with *Mitf>dnTCF* (100/205 had two otoliths). **g**,**h**, Larvae electroporated with *Zicl>Ets:VP16* and *βγ-crystallin>GFP*. **g**, Co-electroporated with *Mitf>LacZ* (75/100 had extra otoliths). **h**, Co-electroporated with *Mitf>Wnt7* (only 11/100 had extra otoliths). Scale bars, 50 μm.

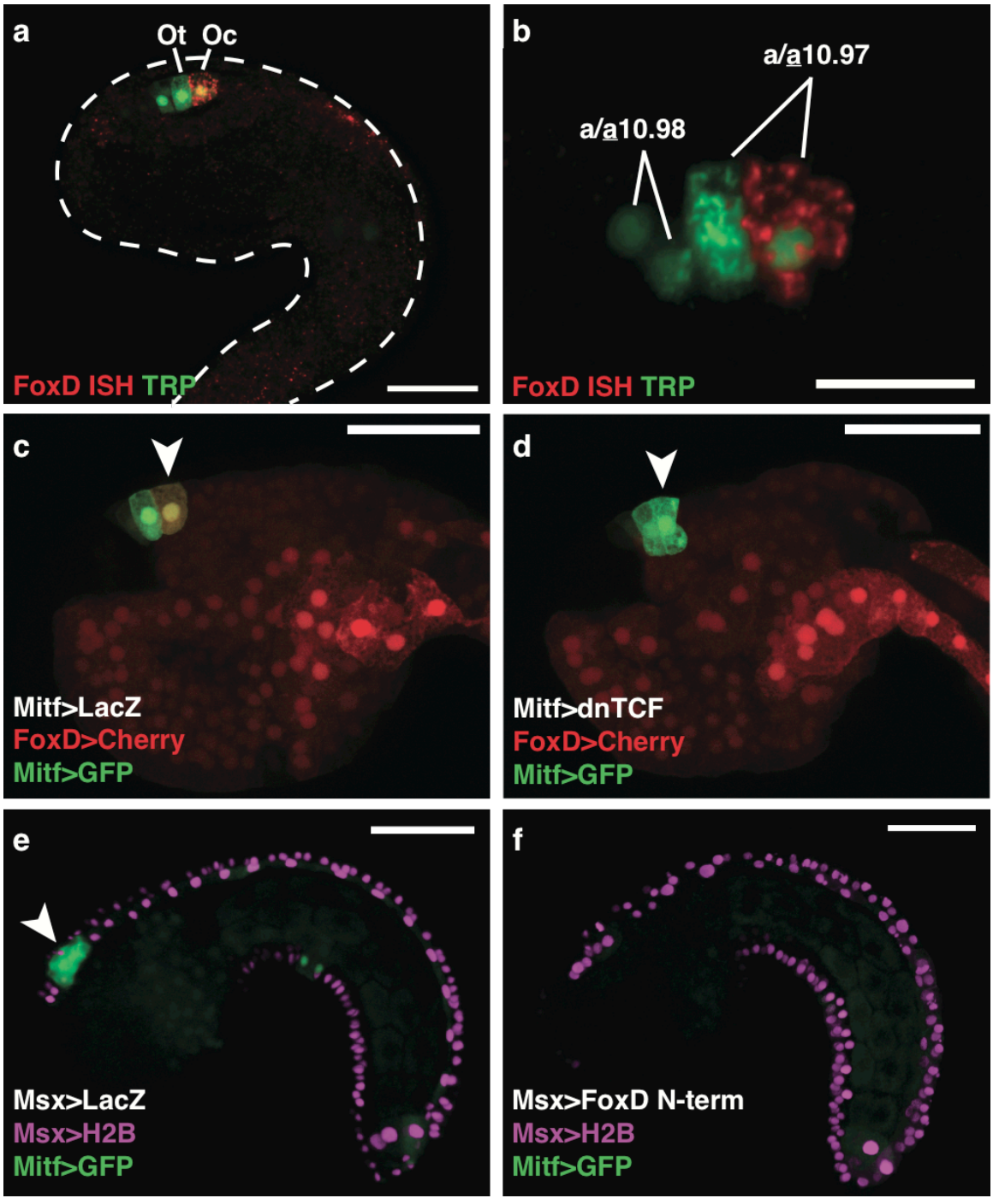
a
Ot
Oc
FoxD ISH TRP
b
a/a10.97
a/a10.98
FoxD ISH TRP
c
Mitf>LacZ
FoxD>Cherry
Mitf>GFP
d
Mitf>dnTCF
FoxD>Cherry
Mitf>GFP
e
Msx>LacZ
Msx>H2B
Mitf>GFP
f
Msx>FoxD N-term
Msx>H2B
Mitf>GFP

Figure 2 l FoxD represses *Mitf* in the ocellus. a, Tailbud electroporated with *TRP>LacZ* detected with an antibody (green) marking the precursors of the otolith and ocellus, and hybridized with a *FoxD* probe (red). **b**, *FoxD* is expressed in the posterior a10.97 cell. **c**-**d**, Tailbuds electroporated with *FoxD>mCherry* and *Mitf>GFP.* Arrowheads mark the presumptive ocellus. **c**, Co-electroporated with *Mitf>LacZ* (126/180 expressed *mCherry*). **d**, Co-electroporated with *Mitf>dnTCF* (only 30/180 expressed *mCherry*). **e**-**f**, Tailbuds electroporated with *Msx>H2B mCherry*, and *Mitf>GFP.* Arrowhead shows GFP expression in a9.49 derivatives. **e**, Co-electroporated with *Msx>LacZ.* **f**, Co-electroporated with *Msx>FoxD* N-term. Scale bars 50 μm (**a**, **c**-**f**); 25 μm (**b**)**.**

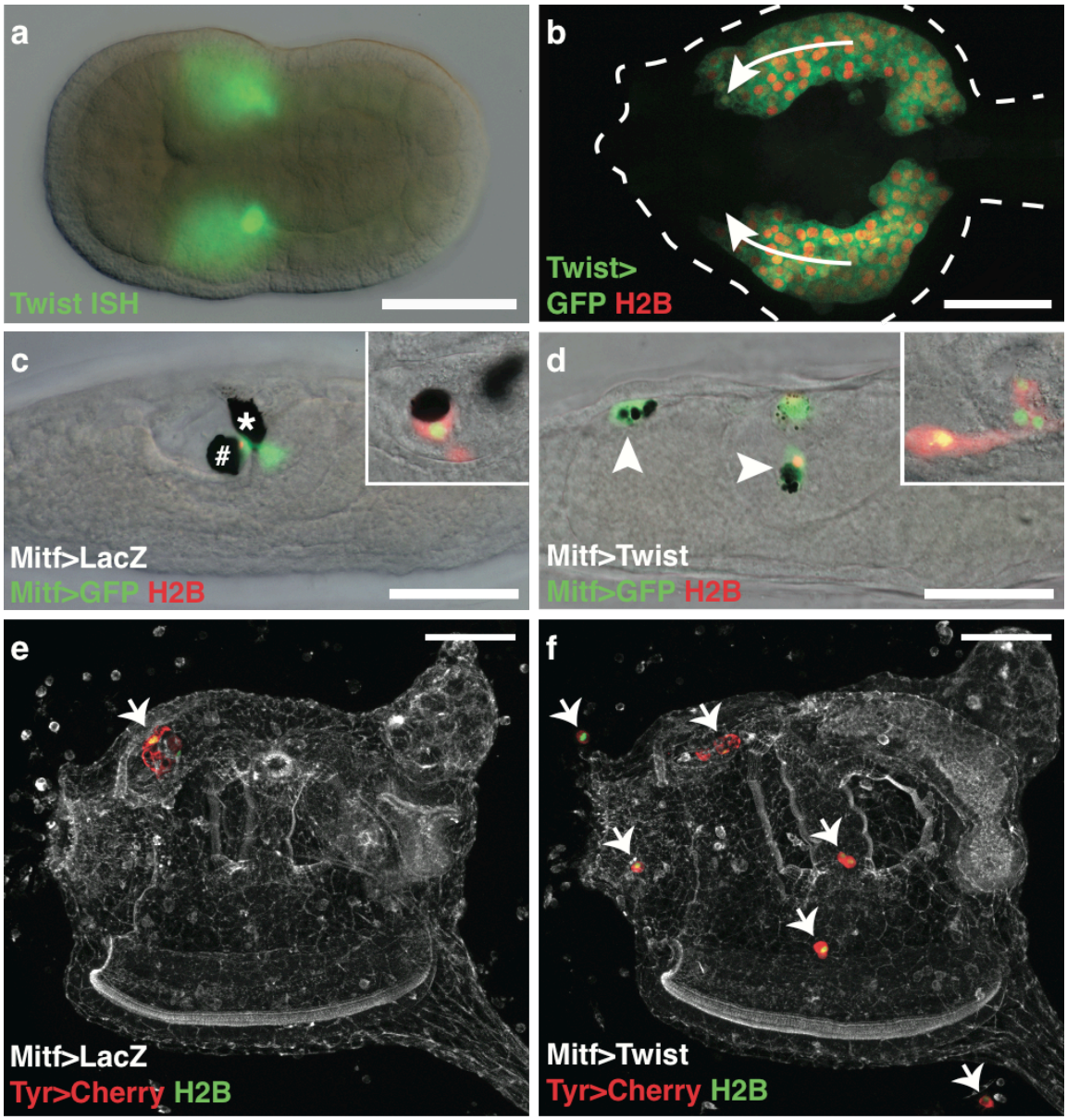
a
Twist ISH
b
Twist>
GFP H2B
c
*
#
Mitf>LacZ
Mitf>GFP H2B
d
Mitf>Twist
Mitf>GFP H2B
e
Mitf>LacZ
Tyr>Cherry H2B
f
Mitf>Twist
Tyr>Cherry H2B

Figure 3 l Twist reprograms the a9.49 lineage. a, Neurula hybridized with a *Twist* probe. **b**, Tailbud during mesenchyme migration (arrows) co-electroporated with *Twist>GFP* and *Twist>H2B mCherry.* **c**,**d**, Larvae electroporated with *Mitf>GFP, and Mitf>H2B mCherry*. Insets show lineage marked with *Tyr>mCherry,* and *Tyr>H2B YFP.* **c**, Co-electroporated with *Mitf>LacZ.* # and * mark the otolith and ocellus, respectively. **d**, Co-electroporated with *Mitf>Twist.* Arrowheads indicate ectopic position of a9.49 derivatives. **e**,**f**, Juveniles electroporated *Tyr>mCherry,* and *Tyr>H2B YFP.* Arrows indentify the position of a9.49 derivatives. **e**, Co-electroporated with *Mitf>LacZ.* **f**, Co-electroporated with *Mitf>Twist.* Scale bars, 50 μm.

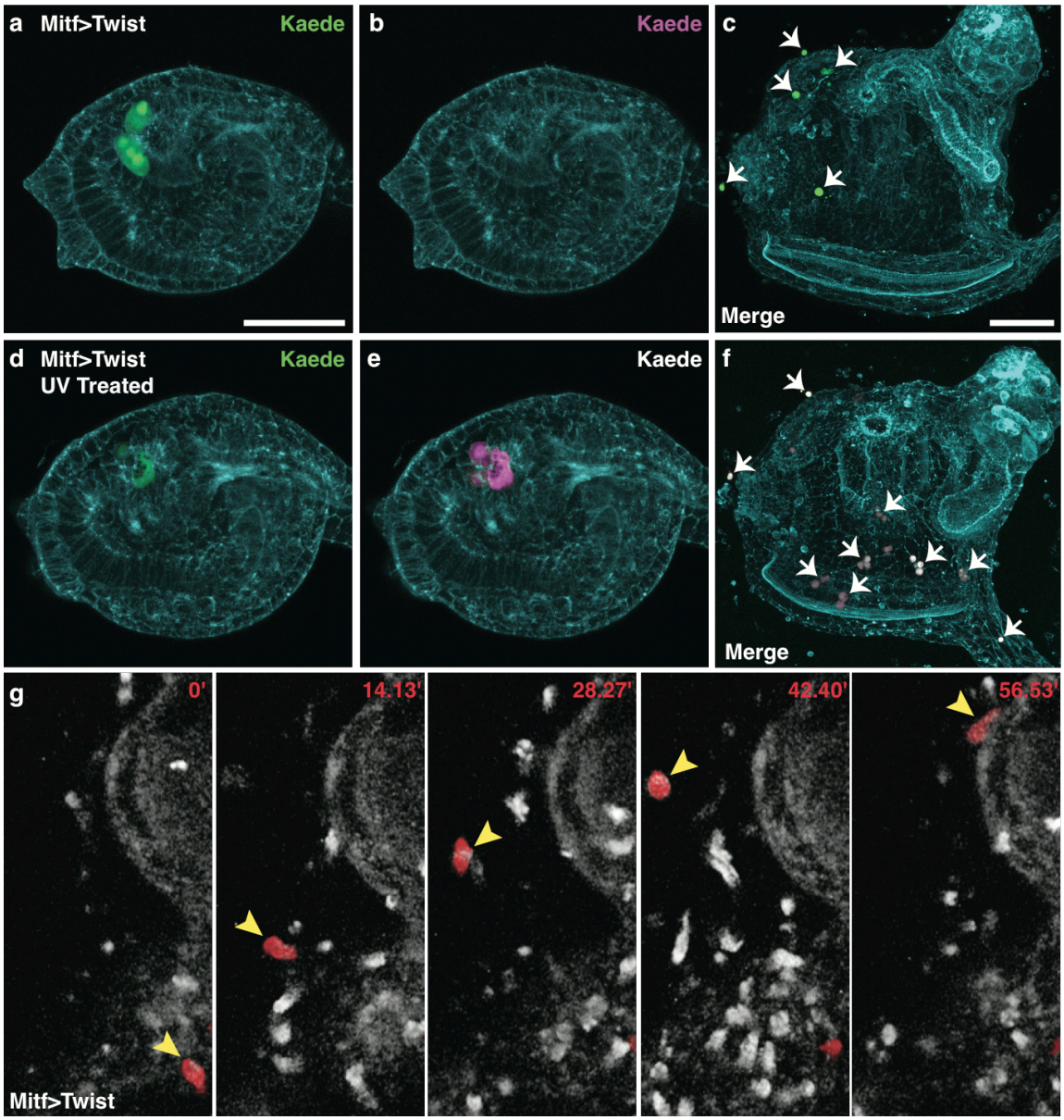
a Mitf>Twist
Kaede
b
Kaede
c
Merge
d Mitf>Twist
UV Treated
Kaede
e
Kaede
f
Merge
g
0'
14.13'
28.27'
42.40'
56.53'
Mitf>Twist

Figure 4 l Lineage tracing of reprogrammed a9.49 cells. a-f, Ciona electroporated with *Mitf>Twist* and *Tyr>Kaede*. **a**,**b**, Non-UV treated tailbud shows only green fluorescence **c**, Embryo never exposed to UV results in a juvenile with only green ectopic cells (arrows). **d**,**e**, UV treated tailbud shows green and red fluorescence respectively. **f**, UV treated embryo results in a juvenile with green and red ectopic cells (arrows). **g**, Time-lapse frames of Supplementary Movie 2 (minutes indicated) shows the migration of reprogrammed a9.49 cell labeled with *Tyr>mCherry* (arrowhead). Scale bars, 50 μm.

Chapter III:

Ephrin-mediated restriction of ERK1/2 activity delimits the number of pigment cells in the *Ciona* CNS

Summary

Recent evidence suggests that ascidian pigment cells are related to neural crest-derived melanocytes of vertebrates. Using live-imaging, we determine a revised cell lineage of the pigment cells in *Ciona intestinalis* embryos. The neural precursors undergo successive rounds of anterior-posterior (A-P) oriented cell divisions, starting at the blastula 64-cell stage. A previously unrecognized fourth A-P oriented cell division in the pigment cell lineage leads to the generation of the post-mitotic pigment cell precursors. We provide evidence that MEK/ERK signals are required for pigment cell specification until approximately 30 minutes after the final division has taken place. Following each of the four A-P oriented cell divisions, ERK1/2 is differentially activated in the posterior sister cells, into which the pigment cell lineage segregates. Eph/ephrin signals are critical during the third A-P oriented cell division to spatially restrict ERK1/2 activation to the posterior daughter cell. Targeted inhibition of Eph/ephrin signals results in, at neurula stages, anterior expansion of both ERK1/2 activation and a pigment cell lineage marker and subsequently, at larval stages, supernumerary pigment cells. We discuss the implications of these findings with respect to the evolution of the vertebrate neural crest.

Introduction

The ascidian pigment cells form part of the ocellus and the otolith, light and gravity sensing organs, respectively[38,39]. Previously, the ascidian pigment cells have been proposed as the evolutionary precursors of the vertebrate retinal pigment epithelium or pineal organ, based on expression of gene markers and the probable function of the ocellus pigment cell in shielding the photoreceptors[40,41]. However, recent evidence using a larger panel of genes supports a closer evolutionary relationship to the cephalic neural crest of vertebrates[42,43]. This hypothesis is strengthened by the acquisition of migratory properties upon the misexpression of Twist, a cell behavior exhibited by neural crest.

Of the four founder embryonic lineages of *Ciona* (A- and B- of the vegetal hemisphere and a- and b- of the animal hemisphere), the central nervous system (CNS) derives from three lineages, A-, a- and b-[44]. This study is concerned with the a-line neural lineages, from which the pigment cells arise. a-line neural lineages separate from the epidermal lineage at the 32-cell stage for the medial lineages and at the 64-cell stage for the lateral lineage, to generate one row of 6

cells at the 64- to 76-cell stage (Fig. 1)[45]. These cells then divide twice along the anterior-posterior axis to generate four rows of six cells at the 6-row neural plate stage (Fig. 1). The 6-row neural plate is arranged with row I posterior-most and row VI anterior-most[46]. The a-line cells comprise rows III-VI (pink cells in Fig. 1) and the A-line cells, rows I and II. Of the a-line cells, only rows III and IV will undergo neurulation and contribute to the CNS, where they generate the anterior part of the sensory vesicle, which is the ascidian larval brain[44,47-50]. The anterior two rows, V and VI, generate the palps, an adhesive organ, as well as non-neural epidermis[51,52]. The pigment cell lineage is situated in the lateral-most cell of row III. Between the 6-row neural plate and the 12-row neurula stages, each row of cells divides in a specific sequence, with row II cells dividing first, followed by row I, then row III and V and lastly row IV and VI[46]. In each row, cells in the medial four columns divide prior to those in the lateral columns. At the 12-row neural plate stage, the pigment cell lineage is segregated into the posterior row III (IIIp) cell, a10.97. As we will describe in this manuscript, the a10.97 pigment cell precursors undergo a further and final round of cell division along the anterior-posterior axis, whereby the posterior-positioned daughters, a11.193, intercalate at the midline to become the pigment cells of the otolith and ocellus.

FGFs are secreted ligands that bind to a class of receptor tyrosine kinases, the FGF receptors (FGFRs), and predominantly activate the Ras/MEK/ERK cascade. FGF/ERK signaling is implicated in a vast range of processes during vertebrate neural development including the induction of neural crest[53-55]. During ascidian neural development, FGF/ERK signaling is responsible for the specification of different cell types. It is involved in the process of neural induction of a-line neural lineages at the 32-cell stage[56] and later during patterning of the developing neural plate and neural tube[22,42,52,57-59]. Recently, Eph/ephrin signaling via RasGAP has been shown to limit the spatial extent of activation of ERK1/2 during several developmental cell fate choices in *Ciona* embryos including during neural development[37,59-62]. Here we investigated the role of Eph/ephrin signaling and the MEK/ERK pathway during pigment cell specification at neural plate stages of *Ciona intestinalis* development.

Results

It has previously been shown that differential ERK1/2 activity between rows III/IV (CNS) and V/VI (palp) at the 3-row neural plate stage (Fig. 1) accounts for acquisition of their distinct genetic programs[52]. ERK1/2 is subsequently differentially activated between rows III and IV at the 6-row neural plate stage with ERK1/2 active in row III cells (Fig. 2A)[58]. This pattern of ERK1/2 activation is required for the differential fate specification of these two sister rows (Fig. 2C). We inhibited MEK/ERK signal transduction by applying U0126, an inhibitor of the MAP kinase kinase, MEK1/2, at precise developmental time points. The following markers were used to assess neural plate patterning: *FoxC* (rows V and VI), *Dll-B* (epidermis and rows V and VI), *ZicL* (rows III and IV), *Six3/6* (row IV), *Mitf* and

Trp (row III)[42,52,63]. As reported previously, application of U0126 at the 76-cell stage disrupts the choice between row III/IV and row V/VI fates[52]. Genes expressed in rows III and IV (*ZicL, Six3/6, Trp* and *Mitf*) were lost and genes normally restricted to rows V and VI (*FoxC* and *Dll-B*) were ectopically expressed in rows III and IV (Fig. 2B, C). In contrast, application of U0126 after the separation of rows III/IV and V/VI, at the early gastrula 3-row neural plate stage (approximate stage 11+)[64], resulted in loss of row III gene expression (*Trp, Mitf*) and ectopic expression of the row IV gene, *Six3/6* in row III. Thus inhibition of MEK1/2 signals at these two successive time points results, in each case, in a distinct posterior to anterior fate transformation of sister cells. In the first instance, differential activation of ERK1/2 specifies row III/IV over V/VI fate and then, following division of row III/IV cells, differential ERK1/2 promotes row III over row IV fates.

There are several examples during *Ciona* embryogenesis whereby Eph/ephrin signals control the spatial extent of ERK1/2 activation[37,59-62]. Three ephrin ligands are expressed in the neural lineages during neural plate and neurula stages and the receptor *Eph3* is expressed ubiquitously, becoming upregulated in the pigment cell lineage soon after the 6-row neural plate stage (Appendix L)[20,65]. These gene expression profiles suggest that Eph/ephrin signals could also be involved in the modification of ERK1/2 activity during neural plate patterning. In order to address this possibility, we expressed a dominant negative form of the Eph receptor Eph3, *Eph3ΔC*[61], in the a-line neural lineages. For this, we used the *Dmrt* promoter which drives expression throughout the a-line neural lineages from the 64-cell stage and has previously been used to disrupt gene function at the 3-row neural plate stage[52,66]. Following electroporation of *Dmrt>Eph3ΔC,* we observed that expression of *FoxC, Dll-B, ZicL*, *Six3/6 Mitf* and *Trp* were unaffected at the 6-row neural plate stage (Fig. 2B,C). Consistently, the spatial pattern of ERK1/2 activation at the 6-row neural plate stage was not perturbed in these embryos (Fig. 2A). We conclude that Eph/ephrin signals are not required to generate the spatial pattern of ERK1/2 activation in the neural plate during the 3-row or 6-row neural plate stages.

Despite little effect on the neural plate genes analyzed, we consistently observed ectopic formation of pigment cells in larvae resulting from embryos electroporated with *Dmrt>Eph3ΔC* (Fig. 3). In some cases, five or more pigment cells could be observed. This result suggests that Eph/ephrin signals play a role in neural patterning. We thus set out to understand how Eph/ephrin signals are involved in this process.

In order to study the role of Eph/ephrin signals in pigment cell formation, we first observed the pigment cell lineage in detail, revealing a previously unrecognized cell division (Fig. 4, Supplementary Movie 3). We analyzed the time-lapse sequence of embryos electroporated with *Dmrt>H2BYFP* (Histone 2B fused with YFP, magenta in images) to label rows III through VI and *ZicL>H2BCFP* (green in images) to label rows I through IV. These reporters are thus co-expressed in rows III and IV allowing for the delineation of cell lineages.

Analyzing the time-lapse sequence revealed a further cell division of the a10.97 cell, which was previously described as a postmitotic pigment cell precursor[48,67]. The pigment cell lineage and cell positions in the neural tube are thus modified to account for this additional division (Fig. 4G). We also recognized this extra division by analyzing *Trp* expression every 15 minutes from the 6-row neural plate stage until the early tailbud stage (Fig. 5A-H). *Trp* expression begins at the 6-row neural plate stage in a9.49 (Fig. 5A). Following cell division of a9.49, *Trp* expression is observed in both daughter cells, but rapidly becomes stronger in the posterior-positioned a10.97 compared to its anterior sister cell, a10.98 (Fig. 5B-D). Next, a10.97 divides into a11.194 and a11.193, both cells retain *Trp* expression and converge towards the midline (Figs. 4D, 5E), touch (Figs. 4E, 5F) and begin to intercalate (Fig. 5G). Finally, these cells are positioned with the two smaller a11.194 cells side by side, anterior to the two larger a11.193 pigment cell precursors intercalated at the midline (Fig. 4F, G; Supplementary Movie 3).

Since patterning of the 6-row neural plate was not affected by inhibition of Eph/ephrin signaling (Fig. 2), we hypothesized that the supernumerary pigment cells observed following inhibition of Eph/ephrin signals resulted from a failure to control the spatial extent of ERK1/2 activation after the 6-row neural plate stage. We first analyzed precisely when pigment cell specification is dependent on MEK/ERK signals. We applied U0126 to embryos every 15 minutes from the 6-row neural plate stage to the early tailbud stage, when pigment cell formation has been shown to occur independently of MEK1/2 signaling[22]. We monitored the precise developmental stage at which embryos were placed in U0126 by analyzing a sample of embryos at each time point for *Trp* expression (Fig. 5A-I). We then assessed the presence of pigmented cells in resultant larvae (Fig. 5J). This analysis shows that pigment cell formation requires MEK1/2 signaling until approximately 30 minutes after the pigment cell lineage has undergone its final cell division (corresponding approximately to the embryonic stage shown in Figure 5G). Following this time point U0126-treatment had little effect on specification of pigment cells, albeit their pigmentation was somewhat reduced.

We showed that pigment cell specification requires an intact MEK1/2 signaling pathway until around 30 minutes after the final cell division of this lineage (Fig. 5). Consistent with a direct requirement for the pathway during pigment cell specification, we found that ERK1/2 remains active in the pigment cell lineage following the 6-row neural plate stage. When the neural plate consists of 12-rows of cells (in this analysis all row III cells and medial row IV cells had completed division), ERK1/2 activation was preferentially detected in the posterior daughters of rows III and IV (row IIIp and IVp) (Fig. 6A). At this stage, the pigment cell lineage is segregated into a10.97, the lateral-most cells of row IIIp (Fig. 1, 6A). At the early tailbud stage (corresponding to the stage in Figure 5F), we observed higher ERK1/2 activity in a11.193, the posterior daughter of a10.97, compared to the anterior daughter a11.194 (Figure 6D). Thus, ERK1/2 is continuously differentially activated in the pigment cell lineage following each successive A-P oriented cell division, consistent with an ongoing

and direct requirement for MEK/ERK dependent signals for pigment cell specification (Figure, 5, 6).

Differential ERK1/2 activity is involved in differential fate specification at both the 3-row and the 6-row neural plate stages (Figure 2) (Wagner and Levine, 2012). We showed that Eph/ephrin signals are not involved in the spatial control of ERK1/2 or neural plate patterning at these stages (Figure 2). However, we found that Eph/ephrin signals are required to restrict the number of pigment cells (Figure 3). We also found that ERK1/2 is continuously activated in the pigment cell lineage during neurulation, until the early tailbud stage (Figure 6). Focusing on the 12-row neural plate stage we found that Eph/ephrin signals are required to restrict ERK1/2 activation to the posterior daughter cells of row III and IV (row IIIp and row IVp) (Fig. 6B). In *Dmrt>Eph3ΔC* embryos, ERK1/2 activation was observed in both the anterior and posterior daughter cells of rows III and IV. This effect was particularly prominent in the pigment cell lineage with strong ectopic ERK1/2 activation in a10.98, the anterior sister cell of a10.97. Consistent with a critical role for Eph/ephrin signals in restricting pigment cell fate to the a10.97 lineage, we observed ectopic expression of *Trp* in a10.98 in *Dmrt>Eph3ΔC* embryos (Fig. 7). In these experiments, we also occasionally (3% of embryo halves) observed persistence of *Trp* expression in row IV cells. It is not clear to us why this happens, since we do not see ectopic expression of row III genes in row IV at the 6-row stage in *Dmrt>Eph3ΔC* embryos. Similar results were obtained using an early-active promoter, *Fog*, to drive *Eph3ΔC* in all ectodermal cells from the 16-cell stage (Appendix M)[68]. Conversely, treatment of embryos with U0126 from the 6-row neural plate stage resulted in a strong reduction of *Trp* expression (Fig.7). Thus, Eph/ephrin signals are required to restrict ERK1/2 activity at the 12-row neurula stage, but not at earlier stages (3-row and 6-row).

The spatial control of ERK1/2 activation by Eph/ephrin signals is mediated by p120RasGAP in *Ciona*[62]. This is also likely to be the case during pigment cell specification since electroporation of a dominant negative version of RasGAP, *RG (R818E),* resulted in a similar phenotype of supernumerary pigment cells in larvae and ectopic activation of ERK1/2 in 12-row neurula, but not 6-row neural plate stage embryos (Figs. 2, 3, and 6).

A role for Eph/ephrin at the 12-row stage is consistent with the formation of more than five pigmented cells that we frequently observed in *Dmrt>Eph3ΔC* larvae, since transformation of a10.98 into a a10.97-like fate should result in a pool of eight *Trp*-positive cells instead of the usual four. The presence of more than four pigmented cells also suggests that the subsequent fate choice between a11.194 and a11.193 is also perturbed in many *Dmrt>Eph3ΔC* larvae. We are currently unable to say whether this is an indirect effect associated with the presumptive loss of (for example) row IIIa fates, or whether Eph/ephrin signals are directly involved in the spatial control of ERK1/2 activation and the segregation of pigment cell fate between a11.193 and a11.194 cells. Analyzing the role of Eph/ephrin in this process would require targeted disruption of Eph/ephrin signals after the 12-row neural plates stage. Differentially expressed

markers of a11.193 and a11.194 would also be required to correctly address the role of FGF and Eph/ephrin signals during this fate choice.

Finally, we did not find any evidence that the choice between ocellus and otolith fates requires Eph/ephrin signals. In a pool of embryos electroporated with *Dmrt>Eph3ΔC* we counted an average of 1.5 otolith and 1.4 ocellus-type pigmented cells (n=299) compared to control embryos, which exhibited an average of 0.8 otolith and 1.2 ocellus-type pigment cells (n=324). The preferential increase in otolith pigmentation is consistent with a previous study where the ectopic activation of Ets results in extra pigments cells of the otolith-type, a fate choice governed by Wnt7, which serves as a positional cue for specifying the posterior ocellus pigment cell[42].

Discussion

We document an additional division of the pigment cell lineage, which was previously described to become post-mitotic following nine cell divisions after fertilization in *Ciona*[67]. We found that disruption of Eph/ephrin signals results in supernumerary pigment cells in larvae. Our results show that ephrin/Eph/RasGAP signaling is required during the 12-row neural plate stage, but not at earlier neural plate stages, to restrict ERK1/2 activation to the posterior daughters of row III (IIIp, as well as row IVp). Removal of this control mechanism results in ectopic activation of ERK1/2 in row IIIa and ectopic *Trp* expression in a10.98.

FGF/MEK/ERK-driven cell fate choices generate cell diversity at multiple steps during ascidian embryogenesis[22,37,56-59,69-73]. Even within the a-line neural lineage, there are many examples. At the 32-cell stage, the a5.3 cell divides to produce the a6.6 cell and the a6.5 cell. The a6.5 cell exhibits ERK1/2 activation in response to the neural inducing FGF signal and adopts a neural fate while the a6.6 cell, with no ERK1/2 activation, adopts an epidermal fate[56,57]. Restriction of ERK1/2 activation to the neural precursor depends upon ephrin signals[60]. At this stage, a-line neural cells contain both CNS and palp lineages. These cells are prevented from precociously activating the CNS-specific program by a time delay mechanism involving a pair of Blimp1-like zinc finger repressors[66].

From the 3-row neural plate stage, differential ERK1/2 activation is used repeatedly to specify the posterior-most cell fates during at least four successive rounds of A-P oriented cell divisions in the a-line neural lineages. During each division the pigment cell lineage segregates into the posterior cells. At the 3-row neural plate stage, CNS lineages (row III/IV) segregate from palp lineages (row V/VI) with FGF/MEK/ERK promoting CNS over palp fate in row III/IV[52]. Differential activation of ERK1/2 between rows III/IV and V/VI may be achieved simply by the restricted expression of the inducing ligand, since *Fgf9/16/20* is expressed in row I/II cells, adjacent to the row III/IV cells (Appendix L)[6]. At the 6-row neural plate stage, ERK1/2 activation is restricted to row III of the a-line neural plate. Localized expression of FGF ligands (*Fgf9/16/20* and *Fgf8/17/18*) in

row II might also account for the differential activation of ERK1/2 between rows III and IV (Appendix L)[22,58]. At this stage, differential ERK1/2 activation also drives the cell fate choices between row I and row II sister cells of the A-line neural plate with ERK1/2 activated in row I cells, though it is not clear how this differential activation pattern is established[58].

Here we described an additional differential activation of ERK1/2 in row III and row IV derivatives following their division into rows IIIa, IIIp, IVa and IVp, whereby ERK1/2 activation is again associated with the posterior daughter cells in row IIIp and row IVp (Fig. 6). We show that ERK1/2 activation is spatially restricted to the posterior rows by Eph/ephrin signals. This mechanism is unlikely to be confined to the pigment cell lineage choice between a10.97 and a10.98 fates, since ectopic ERK1/2 activation is seen broadly in rows IIIa and IVa following inhibition of Eph/ephrin signals. It is not yet clear which ephrin ligands are involved in this process. *ephrin-Ad* is expressed in rows V-VI from the 6-row neural plate stage and may therefore be involved in the restriction of ERK1/2 activity between rows IVa and IVp (Appendix L)[52]. *ephrin-Ac* and *ephrin-Ab* are expressed in discrete domains of the neural plate in close proximity to row III and thus might be involved in the spatial control of ERK1/2 activation between row IIIa and IIIp cells (Appendix L). On the other hand, early in development the *Eph3* receptor is expressed ubiquitously, then shortly after the 6-row stage it is upregulated in the pigment cell lineage. Interestingly this upregulation depends on MEK/ERK signaling, suggesting that MEK/ERK signals render this cell lineage particularly sensitive to Eph/ephrin signals during subsequent stages (Appendix L). Based on *ephrin* and *Fgf* ligand and receptor expression profiles, it is unclear how such a precise spatial pattern of ERK1/2 activation is achieved at the 12-row neural plate stage. It is possible that other mechanisms are also involved, however our data suggest that Eph/ephrin plays an essential role in establishing this pattern (Figure 5).

Following the MEK/ERK-mediated specification of a10.97 as the pigment cell lineage, these cells divide into a11.194 and a11.193 and the posteriorly positioned a11.193 cells become pigmented. It is not yet clear how this fate choice between a non-pigmented and pigmented cell fate is achieved, although differential ERK1/2 may be involved since ERK1/2 is preferentially activated in a11.193. Additional differentially expressed gene markers of a11.193 and a11.194 would be required to address this issue. To determine whether Eph/ephrin signals are involved will necessitate a means to block signaling specifically after the 12-row neural plate stage. The fact that five or more pigment cells are frequently observed in *Dmrt>Eph3ΔC* larvae, suggests that this fate choice is also perturbed in this experimental context.

Finally, the two a11.193 cells from both sides of the neural plate intercalate at the midline and adopt either an ocellus or otolith fate. The post-mitotic pigment cell precursors have been shown to form an equivalence group in another ascidian species, *Halocynthia roretzi*. These cells intercalate at random and the posteriorly positioned cell adopts the ocellus fate[25,44]. We did not find any

evidence that Eph/ephrin signals are involved in this final fate choice. In *Ciona,* this fate choice is controlled by Wnt7 signals, whereas BMP-Chordin antagonism has been implicated in *Halocynthia*[42,74].

If the pigment cell lineage resembles the evolutionary precursors of the vertebrate neural crest, it is relatively easy to envisage how these cell types could both increase in number and adopt a migratory capacity. Simple deregulation of signaling pathways leads to quite a dramatic increase in pigment cell number (Fig. 3)[22,42]. A subset of these cells would then need to acquire the expression of a mesenchyme-promoting factor such as *Twist* in order for a primordial neural crest to develop[42].

Methods

Embryo experiments and constructs

Adult *Ciona intestinalis* were purchased from the Station Biologique de Roscoff (France) or M-Rep (San Diego, CA). Cell nomenclature, lineage and the fate maps are previously described[44,48]. Ascidian embryo culture has been described[75]. Electroporation was carried out as described[37]. U0126 (Calbiochem) was added to artificial seawater at 2mM. All data was pooled from at least two independent experiments.

For the electroporation constructs, the upstream sequences *ZicL*, *Tyr*, *Mitf*, *Dmrt*, *Msx* and *Fog* are previously described[42,52,62,68]. These were used to drive expression of *LacZ*, *mCherry*, *Eph1DC Histone 2B* (*H2B*), *unc76GFP*, *Eph3ΔC.* , *RG (R818E)*. Following electroporation, embryos were selected at gastrula stages for correct morphology. In Figure 4 *Dmrt>dnEph3* electroporated embryos were co-electroporated with *Trp>mCherry*. Only fluorescent (i.e. electroporated) embryos were counted for this experiment, in all other experiments, all embryos were counted. In order to assess ocellus and otolith pigment cell type, embryos were mounted in 80% glycerol and slightly compressed. Ocellus type or otolith type pigment cells were defined based on pigment granule morphology; such that tiny dispersed granules were defined as ocellus type and larger, round or flower shaped granules were defined as otolith. The number of ocellus type pigment cells was likely underestimated since it was more difficult to distinguish individual ocelli from one another. In both control and electroporated embryos, even very large ocelli were counted as one.

In situ hybridization and immunofluorescence

In situ hybridization was carried out as previously described[76,77]. Dig-labeled probes were synthesized from the following *Ciona* cDNA clones: *Trp*[57], *FoxC* (cilv050a24)[65], *ZicL* (cicl002e04)[28], *Mitf* (cilv41b12)[42], *Six3/6* (cicl021e08), *Dll-B* (cicl022f04), *ephrinAc* (ciad074h16), *ephrinAb* (cieg037l08), *ephrinAd*

(ciad008n17), *Eph3* (cieg009e01), *FgfR* (citb040h06), *Fgf9/16/20* (citb007k01) and *Fgf8/17/18* (citb002j04) are all described[65]. Clone numbers refer to clones from the Release 1 Gene Collection Plates[78]. For *Dll-B* in situ hybridization, DAPI staining was used to verify cell identity. In some batches of embryos, *Dll-B* was also detected in row IV. These batches of embryos were removed from the analysis. For *Trp* in situ hybridization in Figure 5, it should be noted that the intensity of the *Trp* signal increases with developmental time. At the 6-row neural plate stage, the color reaction was developed for approximately 12 hours, whereas at the early tailbud stage, the color reaction time was approximately 2 to 3 hours.

dpERK1/2 immunofluorescence is described previously[62]. LacZ immunofluorescence is described previously[59] except that anti-b-galactosidase (Molecular Probes, A11132) was used at 1/500 and the secondary antibody used was goat anti-rabbit Alexa Fluor 488 (Molecular Probes, A11008) at 1/1000.

In our analysis, we refer to embryos as the 6-row neural plate stage to indicate that no row of a-line cells has divided, though cells in row II have sometimes divided. We refer to the 12-row neurula stage to indicate that row III cells have divided. Embryos in Fig. 2, 6 and Appendix L were mounted in VECTASHIELD/DAPI (Vector Laboratories). Embryos in Figs. 2,5,6,7 and appendices were photographed on an Olympus BX51 using a Leica DFC310FX camera and those in Figs. 3 and 4G on a Zeiss Axio Imager AZ using a SPOT RT3 camera.

Time-lapse movie

The time-lapse sequence was obtained using a Zeiss LSM 700 microscope using a plan-apochromat 20x objective. Confocal stacks contained 20 optical slices at a thickness of approximately 1mm each and were taken every 3 minutes for 2 hours. Images were rendered in 3D using Volocity 6 with the 3D opacity visualization tool.

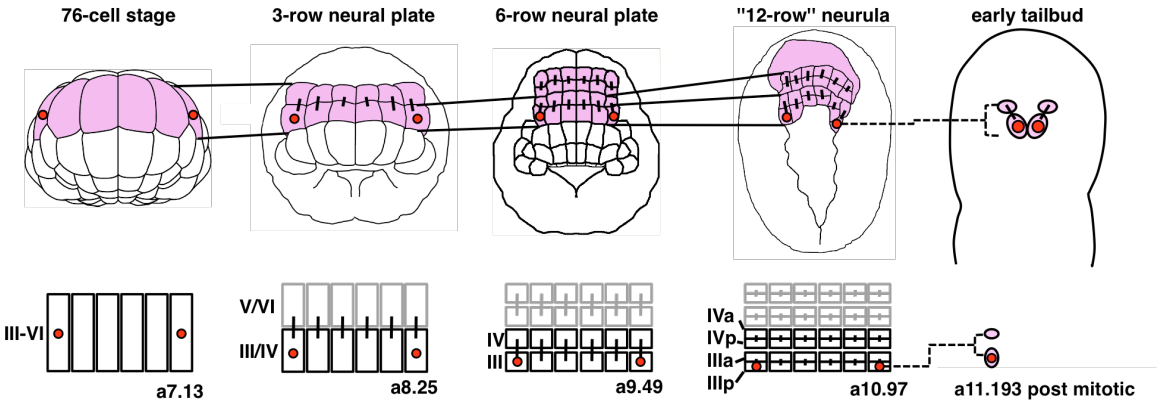
76-cell stage
3-row neural plate
6-row neural plate
"12-row" neurula
early tailbud
III-VI
a7.13
V/VI
III/IV
a8.25
IV
III
a9.49
IVa
IVp
IIIa
IIIp
a10.97
a11.193 post mitotic

Figure 1 | The a-line neural lineages of *Ciona*. Throughout the indicated stages, the a-line derived neural plate cells are colored pink in the illustrated embryos. Below the embryo illustrations are simplified schematics of the a-line derived neural plate, with the row III-IV CNS lineages in black and the row V-VI palp lineages in grey. Bars indicate sister cell relationships. A red dot indicates the pigment cell lineage at each stage with the corresponding cell nomenclature indicated. After segregation from the non-neural ectoderm, the a-line neural lineage is a single row of six cells at the 76-cell stage. During gastrulation, the six a-line neural precursors divide along the anterior-posterior axis, making two rows of six cells. Together with the single row of A-line neural precursors, this makes a 3-row neural plate. All cells of the 3-row stage divide in a specific order to generate the 6-row stage. The 6-row neural plate then divide in an asynchronous but predictable order (see text for details) to produce 12-rows of neural plate cells in neurula embryos. At this stage the pigment cell lineage is positioned in the lateral column in row IIIp. This cell undergoes one final division to produce a11.194 and a11.193 prior to their intercalation at the midline (see also Supplementary Movie 3 and Fig. 4).

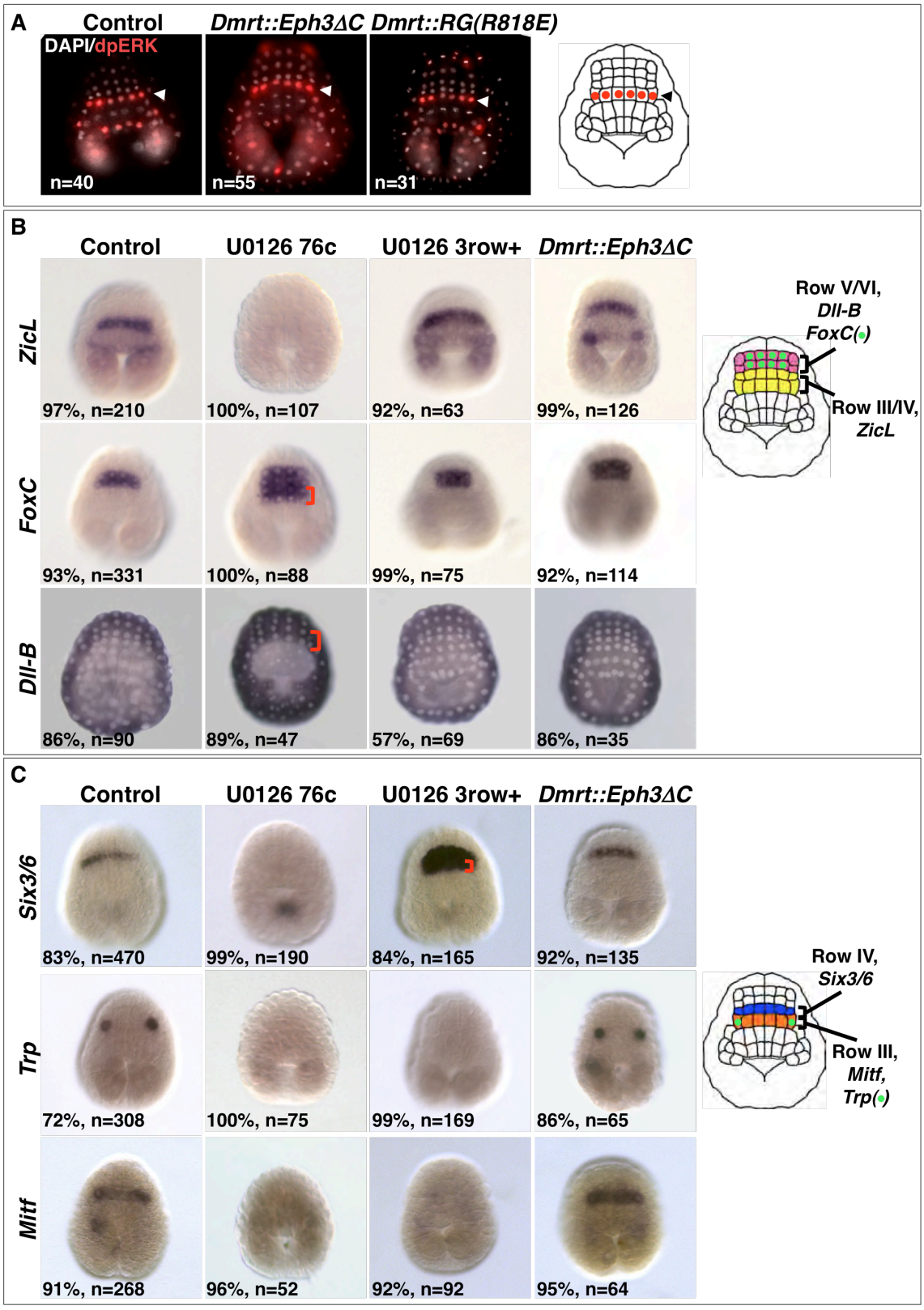
A
Control
Dmrt::Eph3ΔC
Dmrt::RG(R818E)
DAPI/dpERK
n=40
n=55
n=31
B
Control
U0126 76c
U0126 3row+
Dmrt::Eph3ΔC
ZicL
97%, n=210
100%, n=107
92%, n=63
99%, n=126
FoxC
93%, n=331
100%, n=88
99%, n=75
92%, n=114
Dll-B
86%, n=90
89%, n=47
57%, n=69
86%, n=35
Row V/VI,
Dll-B
FoxC(•)
Row III/IV,
ZicL
C
Control
U0126 76c
U0126 3row+
Dmrt::Eph3ΔC
Six3/6
83%, n=470
99%, n=190
84%, n=165
92%, n=135
Trp
72%, n=308
100%, n=75
99%, n=169
86%, n=65
Mitf
91%, n=268
96%, n=52
92%, n=92
95%, n=64
Row IV,
Six3/6
Row III,
Mitf,
Trp(•)

Figure 2 | Role of MEK1/2 and Eph/ephrin signals at the 3-row and 6-row neural plate stage. Experimental conditions are indicated above each column of panels. **a**, dpERK1/2 immunofluorescence at the 6-row neural plate stage showing ERK1/2 activation in row III (arrowhead). **b**,**c**, Analysis of gene expression following various treatments. U0126 was added to embryos at the 76-cell stage (76c), or at the late 3-row neural plate stage when endoderm invagination is well underway (3row+). An embryo illustration on the right shows the control expression domains. Percentages indicate the proportion of embryos that the panel represents. For the *Dll-B* U0126 3row+ panel, the remaining embryos showed *Dll-B* expression in rows III and IV, although this was often weaker than in rows V and VI, and/or patchy. The red brackets indicate ectopic expression.

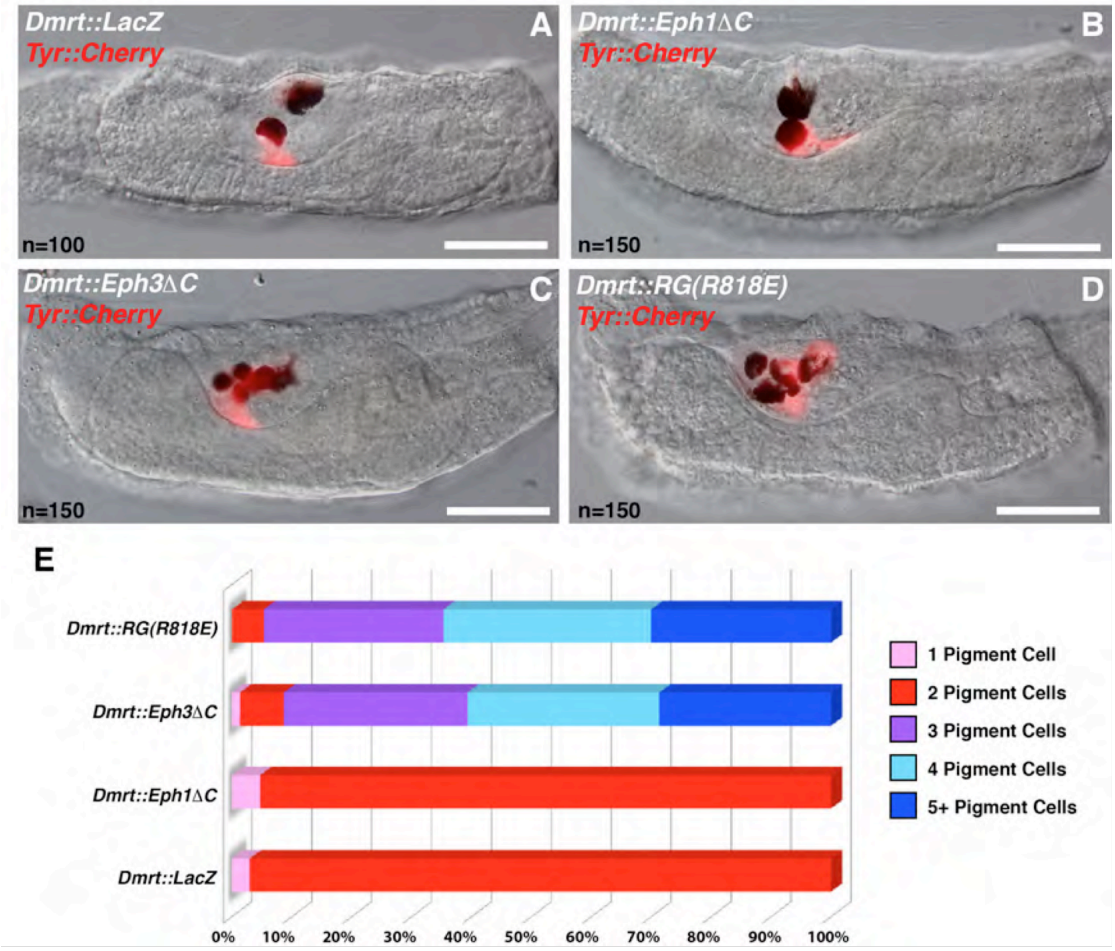
Dmrt::LacZ
Tyr::Cherry
A
n=100
Dmrt::Eph1ΔC
Tyr::Cherry
B
n=150
Dmrt::Eph3ΔC
Tyr::Cherry
C
n=150
Dmrt::RG(R818E)
Tyr::Cherry
D
n=150
E
Dmrt::RG(R818E)
Dmrt::Eph3ΔC
Dmrt::Eph1ΔC
Dmrt::LacZ
0%
10%
20%
30%
40%
50%
60%
70%
80%
90%
100%
1 Pigment Cell
2 Pigment Cells
3 Pigment Cells
4 Pigment Cells
5+ Pigment Cells

Figure 3 | Inhibition of Eph/ephrin signaling results in excess pigment cells. a-d, Embryos were electroporated with the constructs indicated on the panels. *Dmrt>Eph1DC* and *Dmrt>LacZ* were used as controls for electroporation, showing that the results were specific to disruption of Eph3 and RasGAP. Co-electroporation with *Tyr>mCherry* (red) shows that the pigment cells derive from *Tyrosinase* positive cells. The graph **e** shows the proportion of embryos with the number of pigment cells indicated in the key, following electroporation. In embryos exhibiting five or more pigment cells, it was difficult to distinguish each pigment cell, so these embryos were scored as 5+. Scale bars, 50μm.

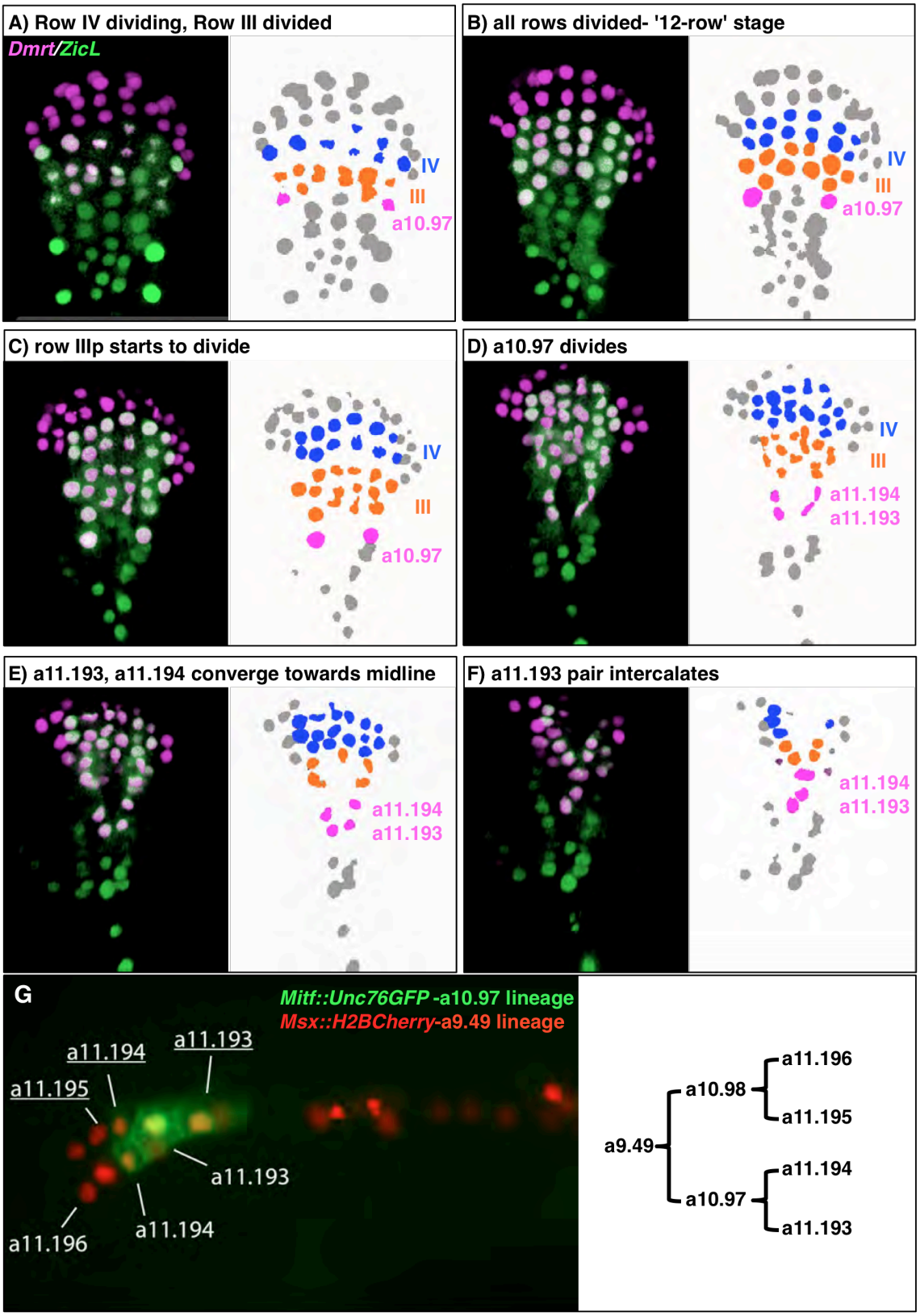
A) Row IV dividing, Row III divided
Dmrt/ZicL
IV
III
a10.97
B) all rows divided- '12-row' stage
IV
III
a10.97
C) row IIIp starts to divide
IV
III
a10.97
D) a10.97 divides
IV
III
a11.194
a11.193
E) a11.193, a11.194 converge towards midline
a11.194
a11.193
F) a11.193 pair intercalates
a11.194
a11.193
G
Mitf::Unc76GFP -a10.97 lineage
Msx::H2BCherry-a9.49 lineage
a11.194
a11.193
a11.195
a11.193
a11.196
a11.194
a9.49
a10.98
a11.196
a11.195
a10.97
a11.194
a11.193

Figure 4 | A revised pigment cell lineage. This figure accompanies Supplementary Movie 3. **a-f**, Embryos were electroporated with *ZicL>H2BCFP* (green) to label rows I-IV and *Dmrt>H2BYFP* (magenta) to label rows III-VI. Still images from the movie are shown on the left. On the right are the same still images with false-labeled nuclei to highlight the positions of row III and IV derivatives in orange and blue respectively. The a10.97 lineage is marked in pink, highlighting the extra division. **g**, An embryo electroporated with *Mitf>Unc76GFP* (green), *Msx>H2BmCherry* (red) to show the lineage derivatives of a10.97 and a9.49 respectively. The position of each cell is labeled on the tailbud stage embryo.

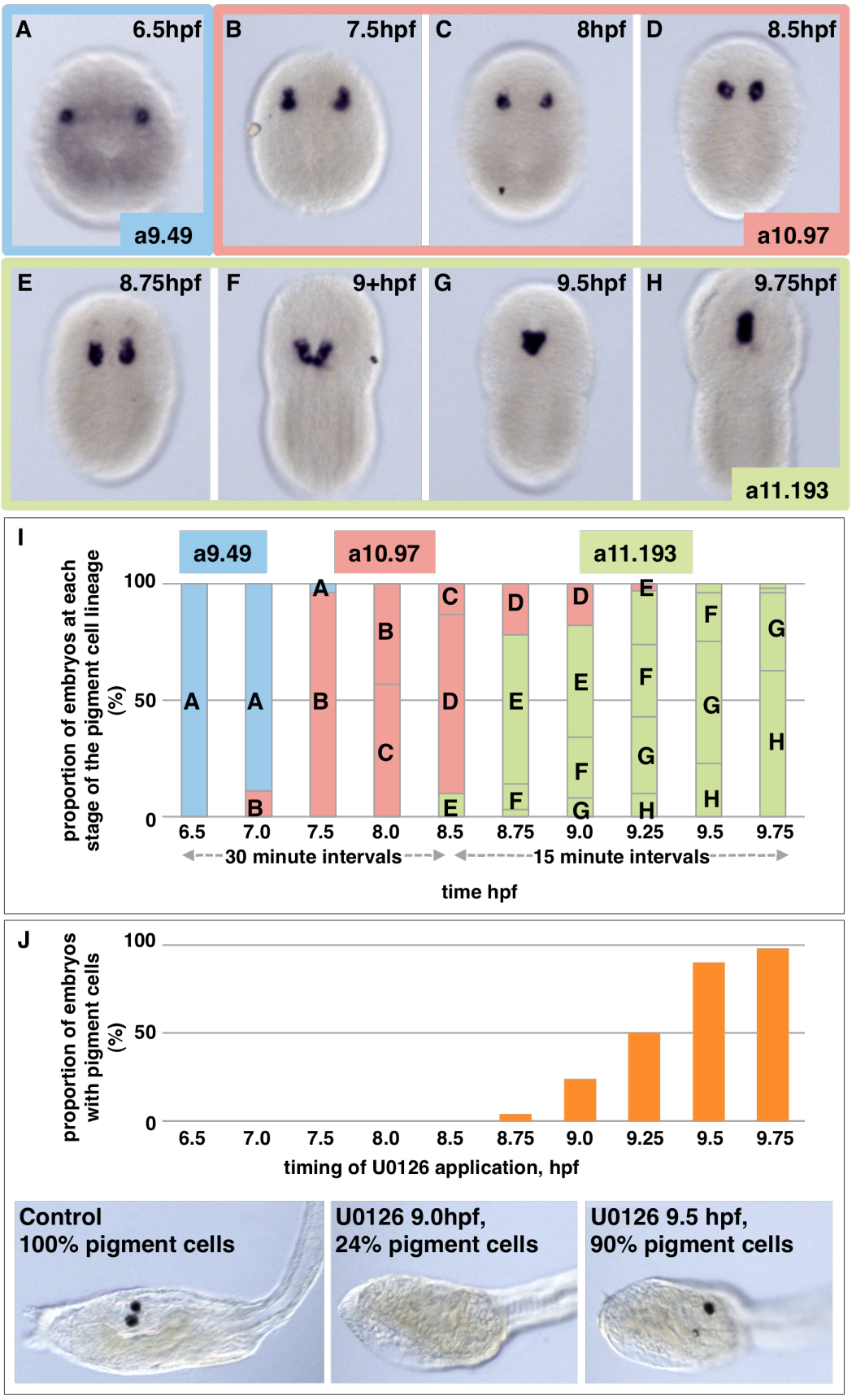
A 6.5hpf
B 7.5hpf
C 8hpf
D 8.5hpf
a9.49
a10.97
E 8.75hpf
F 9+hpf
G 9.5hpf
H 9.75hpf
a11.193
I
a9.49
a10.97
a11.193
proportion of embryos at each stage of the pigment cell lineage (%)
100
50
0
6.5
7.0
7.5
8.0
8.5
8.75
9.0
9.25
9.5
9.75
30 minute intervals
15 minute intervals
time hpf
J
proportion of embryos with pigment cells (%)
timing of U0126 application, hpf
Control
100% pigment cells
U0126 9.0hpf,
24% pigment cells
U0126 9.5 hpf,
90% pigment cells

Figure 5 | Pigment cell formation depends on MEK1/2 signals until early tailbud stage. a-h, Expression of *Trp* at different stages of the pigment cell lineage as indicated by the colored boxes. See text for details. Time points are hours post fertilization (hpf) at 18°C; the time indicated reflects the embryological stage seen for the majority of embryos at each time point (as shown in **i**). **i**,**j**, In these experiments, one half of the embryos were fixed for *Trp* in situ hybridization to determine the precise stage of U0126 treatment (n= 36-75), the other half were treated with U0126 until larval stages in order to monitor pigment cell formation (n=34-81). **i**, The color code of the graph represents the stage of the pigment cell lineage, defined as a9.49 (blue), a10.97 (red) and a11.193 (green). Bars are further broken down into the proportion of embryos representing the precise embryological stage, as represented in **a-h**. **j**, Bars represent the proportion of embryos with any pigmented cells at each time point. Representative resultant larvae after treatment with U0126 from the time points indicated are shown.

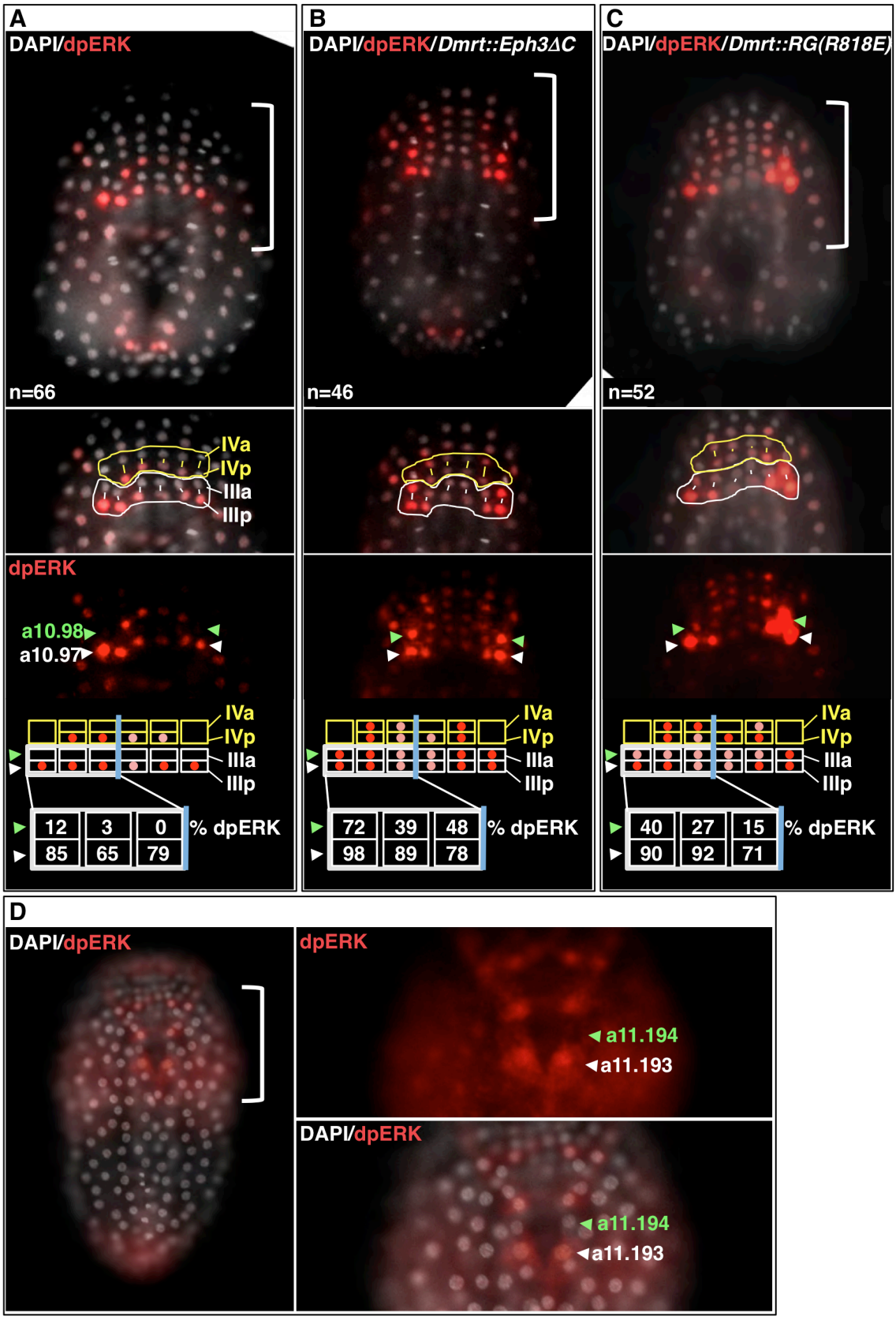
A
DAPI/dpERK
n=66
IVa
IVp
IIIa
IIIp
dpERK
a10.98
a10.97
IVa
IVp
IIIa
IIIp
12 3 0
85 65 79
% dpERK
B
DAPI/dpERK/Dmrt::Eph3ΔC
n=46
IVa
IVp
IIIa
IIIp
72 39 48
98 89 78
% dpERK
C
DAPI/dpERK/Dmrt::RG(R818E)
n=52
IVa
IVp
IIIa
IIIp
40 27 15
90 92 71
% dpERK
D
DAPI/dpERK
dpERK
a11.194
a11.193
DAPI/dpERK
a11.194
a11.193

Figure 6 | Eph/ephrin signals control the spatial extent of ERK1/2 activation at the 12-row neurula stage. a-c, Experimental conditions are indicated on the top panels. Embryos were stained for activated ERK1/2 (dpERK1/2) in red, with nuclei (DAPI) in white. For this analysis embryos were also co-electroporated with *Msx>LacZ* or *Dmrt>LacZ* followed by LacZ immunofluorescence to ensure our cell identification was correct (not shown). The top panel shows the entire embryo and the bracket indicates the annotated region in the lower panels. The divided rows III and IV are outlined in white and yellow respectively in the middle panel. At the stage of analysis, the lateral precursors of row IV have not yet divided. In the lower panel, only the dpERK immunofluorescence is shown for clarity. The interpretation of the dpERK immunofluorescence intensity is depicted by red and pink dots on the schematic of divided rows III and IV. The percentage of dpERK1/2 detection in each cell of row IIIa and IIIp is indicated on the lower schematic, representing independent scoring for each embryo half. **d**, Late neurula embryos stained for dpERK1/2 (red) and DAPI (white). Enlarged region is indicated by bracket on whole embryo panel.

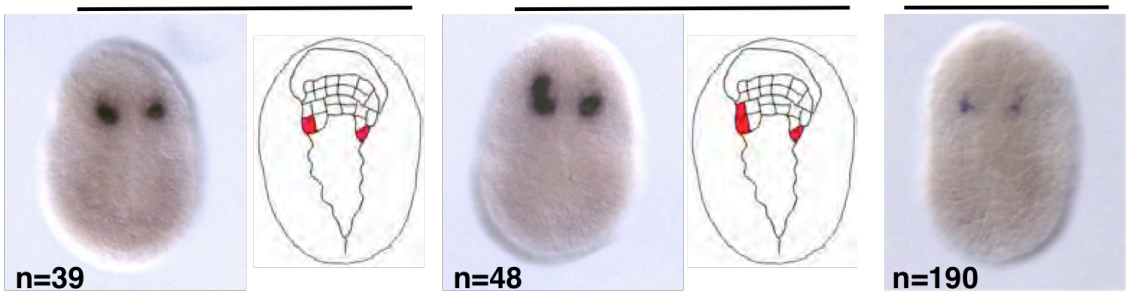
n=39
n=48
n=190

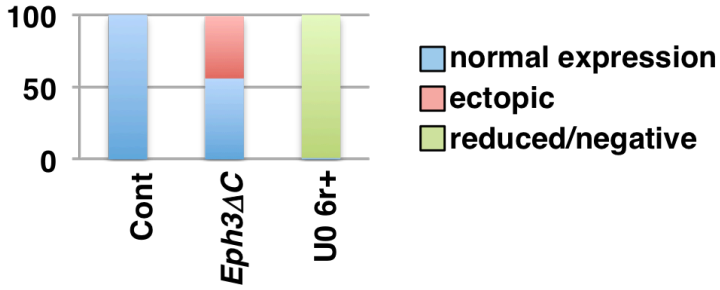
100
50
0
Cont
Eph3ΔC
U0 6r+
normal expression
ectopic
reduced/negative

Figure 7 | Ectopic *Trp* expression in a10.98 following inhibition of Eph/ephrin signals. Expression of *Trp* at 12-row neurula stage in control embryos, embryos electroporated with *Dmrt>Eph3ΔC.* or embryos treated with U0126 just after the 6-row stage (UO 6row+). In these experiments, U0126-treatment began once embryos started to leave the 6-row neural plate stage and the cells in row II begin to divide. Each embryo half was scored independently and the quantification is shown in the graph.

Chapter IV:

The pre-vertebrate origins of neurogenic placodes

Summary:

The sudden appearance of neural crest and neurogenic placodes in early branching vertebrates has puzzled biologists for over a century[79]. These embryonic tissues contribute to the development of the cranium and associated sensory organs, which were crucial for the evolution of the vertebrate "new head"[9,10]. A recent study suggests that rudimentary neural crest cells existed in ancestral chordates[42]. However, the evolutionary origins of neurogenic placodes has remained obscure due to a paucity of embryonic data from tunicates, the closest living relatives to the vertebrates[5]. Here we show that the tunicate *Ciona intestinalis* exhibits a proto-placodal ectoderm (PPE) that requires BMP inhibition and expresses the key regulatory determinant *Six1/2* and its co-factor *Eya,* a developmental process conserved across vertebrates. The *Ciona* PPE is shown to produce ciliated neurons that express gonadotropin-releasing hormone (*GnRH*), a G protein-coupled receptor for relaxin-3 (*RXFP3*), and a functional cyclic nucleotide-gated channel (*CNGA*), suggestive of dual chemosensory and neurosecretory activities. These observations provide the first evidence that *Ciona* has a neurogenic proto-placode, which forms neurons that appear to be related to those derived from the olfactory placode and hypothalamic neurons of vertebrates. We discuss the possibility that the PPE-derived GnRH neurons of *Ciona* resemble an ancestral cell type, a progenitor to the complex neuronal circuit that integrates sensory information and neuroendocrine functions in vertebrates.

Introduction:

Neurogenic placodes contribute to cranial sensory systems mediating hearing, smell and taste[10]. They are considered a vertebrate innovation[4], and the full repertoire, including olfactory, otic, epibranchial, and trigeminal placodes are already present in jawless hagfish and lampreys. It has been argued that the evolution of neurogenic placodes was a crucial event facilitating the transition from filter feeding invertebrate chordates to predatory vertebrates[9].

Comparative embryological studies have failed to identify any clear evolutionary precursors of neurogenic placodes in invertebrate chordates. It has been suggested that the pre-oral organ of amphioxus, Hatschek's pit, is related to the adenohypophyseal (anterior pituitary) placode of vertebrates, however the fate map of this tissue remains unresolved[80]. In addition, the atrial primordia of *Ciona* have been likened to the otic and lateral line placodes of fish, but they are

not specified until tailbud stages and do not derive from the anterior neural plate border (see below)[13]. Finally, previous studies provided evidence for a placodal-like tissue in *Ciona,* but it was homologized to the adenohypophyseal placode[13,14], which lacks neurogenic potential. We show that the latter tissue does in fact produce ciliated sensory neurons that express *GnRH* and *RXFP3*, signatures of neuroendocrine cell types found in vertebrates[9].

Results:

Neurogenic placodes develop from a specific domain anterior to the neural plate of vertebrate embryos[10]. All placode subtypes arise from this U-shaped domain, termed the preplacodal ectoderm[12]. This tissue expresses the transcription factor *Six1*, and mutations in *Six1* cause craniofacial defects in humans, including deafness[81]. We found that the *Ciona* homolog of *Six1, Six1/2*, as well as its co-factor *Eya*, are initially expressed in a row of eight cells located immediately anterior to the neural plate, as marked by *Zicl* (Fig. 1a, Appendix N). This pattern is recapitulated by a Six1/2 regulatory sequence driving expression of an mCherry reporter gene (Six1/2>mCherry; Fig. 1b, Supplementary Movie 4). At tailbud stages the Six1/2+ cells intercalate and become situated above the anterior brain (i.e., sensory vesicle), surrounding the future oral opening (Appendix O).

In vertebrates, the preplacodal ectoderm is specified by a two-step process whereby a gradient of BMP signalling establishes preplacodal competence in the non-neural ectoderm during the blastula/early gastrula stage, followed by subsequent inhibition of BMP signalling during gastrulation[12]. BMP signalling may not be required for establishing proto-placodal competence in *Ciona*, but inhibition of BMP signalling appears to be crucial for its specification. We observe conserved expression of *BMP2/4* and the *Chordin* antagonist in ventral and dorsal regions, respectively, at the time when the PPE is specified during gastrulation and neurulation (Appendix P).

Localized *Chordin* expression at the lateral edges of the *Ciona* PPE (Fig. 1b) suggests a role in antagonizing BMPs emanating from ventral regions, similar to the situation seen in vertebrates[82]. We therefore explored the possibility that inhibition of BMP signalling might be required for the activation or maintenance of *Six1/2* expression. We sought to overcome the presumed inhibitory effect of Chordin by the targeted misexpression of BMP ligands or constitutively active forms of BMP receptors. These experiments were achieved using a previously described *Dmrt* regulatory DNA (i.e., *Dmrt>GFP*)[52], which drives expression throughout the anterior neural plate and adjacent anterior ectoderm (Appendix N).

The co-electroporation of *Dmrt>BMP2/4*, *Dmrt>GFP*, and *Six1/2>mCherry* resulted in loss of *Six1/2* expression in the anterior neural plate border, consistent with similar experiments in vertebrates[83] (Fig. 1c). Conversely, misexpression of *BMP5/7* had no noticeable effect on expression of the *Six1/2*

reporter or embryo morphology (Fig. 1d). These observations suggest that Chordin may be specifically required to exclude BMP2/4 signals from the PPE.

Additional misexpression assays were performed with a constitutively active form of the BMP receptor (CA BMPR1), for cell-autonomous activation of BMP signalling. In these experiments, activation is restricted to *Dmrt*+ cells, which form the anterior neural plate and adjacent anterior ectoderm. Ectopic BMPR1 activity results in reduced expression of *Six1/2* (Fig. 1e), similar to the results obtained upon misexpression of the BMP2/4 ligand. However, the phenotype is less severe, with persistence of *Six1/2* expression in the medially derived regions of the PPE (compare Fig. 1d to Fig. 1e). Importantly, expression is lost in lateral regions, which are the source of the GnRH neurons (see below).

To demonstrate that the disruption of PPE formation is a specific result of ectopic BMP signalling, we misexpressed a constitutively active form of the TGF-β receptor throughout the anterior brain and adjacent ectoderm (*Dmrt>CA TGF-βR*). This had very little impact on the expression of *Six1/2*, despite severe defects in brain morphology (Fig. 1f). We therefore conclude that inhibition of BMP signalling is essential for the specification of the *Ciona* PPE, as observed in vertebrates[82,83]. However it is conceivable that this inhibition indirectly regulates *Six1/2* expression.

The olfactory placode is the anterior-most neurogenic placode in vertebrates and develops above the oral opening[80]. GnRH neurons arising from this placode migrate along the axonal tracts of olfactory neurons towards the hypothalamus[84,85]. They subsequently innervate the anterior pituitary and stimulate the release of gonadotropins, hormones vital for growth, sexual development and reproduction[86]. Previous studies have documented the expression of six different GnRH peptides encoded by two duplicated genes in *Ciona*[87]. *GnRH2* (hereafter referred to as *GnRH*) is expressed near the oral opening (Appendix Q) and we used the 5' regulatory sequences (*GnRH>GFP*) to label this lineage during development. During tailbud stages, the posterior-most *Six1/2+* cells acquire a distinctive cone-shaped morphology, permitting their direct visualization during morphogenesis (Fig. 2a, Appendix O). By larval stages, these cells have differentiated into neurons that co-express *GnRH>GFP* and *Six1/2>mCherry* (Fig. 2b, Supplementary Movie 5). The production of these neurons is strongly inhibited by BMP signalling (Appendix R).

Ciona PPE-derived GnRH neurons express two genes encoding G protein-coupled receptors (GPCRs) implicated in neurosecretion in vertebrates, a somatostatin, opioid, galanin/Chemokine-like receptor (*SOG/Chemokine-like*) and a relaxin-3 receptor (*RXFP3*) (Fig. 2c, d, Appendix Q, Supplementary Movie 5). The relationship of these *Ciona* GPCRs to human rhodopsin-class GPCRs is shown in a summary tree (Fig. 2e, Appendix S). In vertebrates, *RXFP3* is expressed in hypothalamic paraventricular nuclei that provide synaptic inputs for the secretion of GnRH within the hypothalamic-pituitary-gonadal (HPG) axis[88]. Interestingly, the PPE-derived *Ciona* GnRH neurons survive through metamorphosis despite extensive cell death and reorganization of most of the

larval nervous system (Fig. 2f). Moreover, injection of GnRH into mature *Ciona* causes the release of gametes and likely triggers spawning in wild populations.[89]

Since both GnRH1 and chemosensory neurons arise from the olfactory placode of vertebrates, we wondered if *Ciona* PPE-derived neurons might also possess chemosensory properties. Chemosensation by olfactory neurons occurs via odorant receptors in the tips of their cilia. Swimming larvae possess a group of neurons located behind the oral opening, previously described as the anterior apical trunk epidermal neurons (aATENs). These neurons possess cilia that are clearly visualized using an acetylated-α-tubulin antibody (Fig. 3a). Electroporation of *GnRH>mCherry* followed by acetylated-α-tubulin staining confirmed that the cilia project from the PPE-derived GnRH neurons (Fig. 3b). Moreover, comprehensive visualization of Six1/2+ cell morphogenesis reveals that the aATEN/GnRH neurons are derived from the a11.205 lineage (Appendix O). Ultrastructural analysis has shown that cilia of these neurons have a 9+2 microtubule arrangement[90], a shared characteristic attributed to non-motile cilia of vertebrate olfactory neurons[91].

Conventional odorant receptors have not been identified in the *Ciona* genome[80], but it is unlikely that a marine chordate would lack a means to detect odorants. Instead of examining divergent GPCRs, we focused on downstream effectors of chemosensory transduction. Cyclic nucleotide-gated cation channels (CNGs) are critical for mediating sensory perception in photoreceptors and olfactory neurons. The binding of odorants to receptors cause an intracellular increase in cyclic nucleotides that in turn results in an influx of calcium, which ultimately leads to the depolarization of sensory neurons[92]. In rats, *CNGA2* expression is detected in GnRH1 neurons but is not necessary for their activity. This expression might be due to prior activation in the shared progenitor of GnRH1 and olfactory neurons[93,94].

A homolog of vertebrate *CNGA1* is expressed in fully differentiated aATEN/GnRH neurons of *Ciona* (Fig. 3c). To determine whether *Ciona* CNGA forms a functional channel, we transfected a CNGA expression construct into Human Embryonic Kidney 293 cells incubated with the intracellular calcium indicator Fura-2 to test for a response to cyclic nucleotides. Indeed, application of either 8-Br-cGMP or 8-Br-cAMP elicited an increase in intracellular calcium concentration, with a higher sensitivity to cAMP than cGMP (Fig. 3d, Appendix T). The occurrence of a functional CNGA in PPE-derived neurons, in addition to the presence of a 9+2 cilium, suggests that they are likely to possess chemosensory activities. These observations provide the first evidence that putative sensory neurons arise from a placodal-like territory in a non-vertebrate.

Discussion:

Our data suggest that the aATEN/GnRH neurons have dual neurosecretory and chemosensory properties. In vertebrates, both neurosecretory and chemosensory cells arise from the olfactory placode and are

intimately linked. GnRH neuroblasts use the axon tracts of chemosensory neurons to guide them to their final destination in the hypothalamus. In adults, pheromones detected by chemosensory neurons cause a release of gonadotropins via hypothalamic GnRH neurons, a function vital for sexual reproduction. Furthermore, transneuronal tracing experiments have shown that olfactory and GnRH neurons form a coherent neuronal circuit[95,96], a connection that likely arose long ago.

It has been proposed that neuronal circuits evolve from the functional segregation of specialized cell types from multifunctional ancestral cells, akin to the well-known mechanism of gene duplication and subfunctionalization. It was predicted that a chemosensory-neurosecretory precursor likely existed in ancestral chordates prior to the diversification of the HPG axis seen in vertebrates[15,97]. We have presented evidence that the PPE-derived aATEN/GnRH neurons in *Ciona* provide a particularly vivid example of such an ancestral cell type. Over the course of evolution within the vertebrate lineage, the proposed chemosensory and neurosecretory functions of these neurons may have become segregated into dedicated cell types that work together within a coherent circuit (Fig. 3e). Such cellular subfunctionalization might be a generally important mechanism of neuronal circuit evolution in vertebrates.

Methods:

Embryo preparation and imaging

Ciona intestinalis adults were obtained, *in vitro* fertilized, and electroporated for transient transgenesis as described[52]. For each electroporation, typically 70 µg of DNA was resuspended in 100 µl buffer. Embryos were fixed at the appropriate developmental stage for 15 minutes in 4% formaldehyde. The tissue was then cleared in a series of washes of 0.01% Triton-X in PBS. Actin was stained overnight with Alexa-647-conjugated phalloidin (Fisher, A22287) at a dilution of 1:500.

For the acetylated-α-tubulin staining, larvae were fixed for 10 minutes in 2% paraformaldehyde, then washed three times in 0.01% Triton-X in PBS for 10 minutes, and blocked with 1% normal goat serum for 10 minutes. Afterwards samples were incubated with a monoclonal anti-acetylated tubulin antibody (Sigma-Aldrich, T6793) at a dilution of 1:1000 overnight at 4°C. Next the tissue was washed in 0.01% Triton-X in PBS, three times for 30 minutes each. Then the samples were incubated with an Alexa Fluor 488 donkey anti-mouse IgG (H+L) antibody (Fisher, A21202) at a dilution of 1:500 in 1% normal goat serum for 2 hours at room temperature, and finally washed in 0.01% Triton-X in PBS, three times for 30 minutes each.

Samples were mounted in 50% glycerol in PBS with 2% DABCO for microscopy. Confocal images were acquired on a Zeiss LSM 700 microscope using a plan-apochromat 20x, 40x, or 63x objective. Confocal stacks contained approximately 50 optical slices at a thickness of 1-2 µm each. Images were rendered using Volocity 6 with the 3D opacity, extended focus or XY plane visualization tools. Time-lapse images were taken on a Zeiss LSM 700 microscope at intervals of 3-4 minutes. Brightfield micrographs of larval *in situs* were acquired on a Zeiss Axio Imager microscope using an EC Plan-Neofluar 40x objective with a ProgRes C14 plus camera.

Experimental perturbations were performed in triplicate and two biological replicates were scored. The scored replicates were totaled and are indicated in the appropriate figure legends. Phenotypes were scored in animals exhibiting transgenesis (i.e., using a reporter unaffected by a given perturbation such as *Dmrt>GFP* in Fig. 1). Unfertilized animals or those that failed to gastrulate were excluded from the analysis. No randomization or blinding was performed on samples.

Molecular cloning

The University of California Santa Cruz Genome Browser Gateway facilitated the identification of conserved non-coding sequences between *Ciona intestinalis* and *Ciona savignyi*. Putative enhancer sequences were PCR amplified and cloned into a pCESA vector using *AscI*/*NotI* restriction sites for *Chordin* (KH.C6.145; 5'-CGGTTACGTTAAGTTCGTGCG-3' and 5'-CTTTGTTCCTGCTCGAAGTGAG-3'), *Six1/2* (KH.C3.553; 5'-GTGACAGGAAACGTCTAGG-3' and 5'-TGGCTCTGAGGCCGTGATTGTAG-3'), *GnRH* (KH.C9.484; 5'-GTGTACGATTGACAAGTTGG-and 5'-TGTTACGTTATCTCTCTAGAAG-3'), *SOG/Chemokine receptor-like* (ci0100133186; 5'-GGCAGATTTGACCTCAACTTG-3' and 5'-GGCGTTTCCGAAAAGCCCTTT-3'), *RXFP3* (KH.C6.184; 5'-CCGTGATTGTAATACGTATGAC-3' and 5'-GCACAGTATTGTGTTATATACC-3'), and *CNGA* (KH.C2.249; 5'-GTGGAGATGCCGATTTCAACC-3' and 5'-CACTTTGTTTGGCATTATTCC-3'). The *Dmrt* and *ZicL* enhancers have been previously described[52]. A similar cloning method was used to create misexpression vectors using *NotI*/*EcoRI* sites for the *BMP2/4* (KH.C4.125; 5'-ATGGTGGCGCTTACGGATTGGAC-3' and 5'-CTATCTACACCCACAAGCTTGC-3') and *BMP5/7* (KH.C2.336; 5'-ATGACTTGTCATCGCAATAAAG-3' and 5'-TCAGTTGCACCCGCATGACAC-3') plasmids. The *CA TGF-βR* construct was made by site directed mutagenesis to introduce a Q154D missense mutation in the regulatory GS domain of the wild type receptor. A similar strategy was used to create the previously described *CA BMPR1*[98]. The coding sequence of *SOG/Chemokine receptor-like* was amplified from cDNA (ci0100133186; 5'-ATGTTGCTCGGAATCATGAAATC-3' and 5'-

GTATAAATATTCATACTTGTTTCTG-3') and cloned into a pCESA vector using *NotI*/*EcoRI* restriction sites.

For the calcium imaging experiments, cDNA fragments containing the full-length coding region of *Ciona intestinalis CNGA*, *CNGB*, and *CNGC* (Ghost Gene IDs: KH.C2.249, KH.L42.6, and KH.C7.605, respectively) were amplified from a cDNA pool of mid tailbud embryos (*CNGA*) or larvae (*CNGB* and *CNGC*) by PCR using a thermostable DNA polymerase exhibiting proofreading activity (Takara LATaq; Takara Bio) with gene-specific primers (5'-AGCTAACACAGATTTTAGTGTAATG-3' and 5'-GTTGCGGGTAAATTACATGTC-3' for *CNGA*; 5'-ATGGCATTGCACATAAATGCAA-3' and 5'-AGCAAAGACTTTGGTAAACATCAG-3' for *CNGB*; 5'-TAAGGTTGATACAGGTTTCATTGG-3' and 5'-GACGTAATCATGACGAAACTGTG-3' for *CNGC*). The PCR products were subcloned into a pcDNA6 plasmid vectors and sequenced on both strands by the cycle sequencing method with an Applied Biosystems 3100 Genetic Analyzer (Applied Biosystems, Foster City, CA, USA).

In situ hybridization

The fluorescent *in situ* hybridizations were performed as described[52]. The colorimetric *in situ* hybridizations on hatched larvae were executed as previously detailed[99]. The *in situ* hybridizations for Appendix P were performed as specified[100]. mRNA probes were synthesized using linearized cDNA clones for *Six1/2* (ciad46p13), *Eya* (cilv29d14), *Chordin* (ciclo16e09), *BMP2/4* (cicl060n01), *GnRH2* (cilv25p08), and *RXFP3* (cinc033n18) from Nori Satoh's (OIST, Okinawa, Japan) cDNA gene collection. Probe templates for *CNGA* (5'-ATGGCATTGCACATAAATGCAA-3' and 5'-AGCAAAGACTTTGGTAAACATCAG-3') and *SOG/Chemokine receptor-like* (5'-ATGTTGCTCGGAATCATGAAATC-3' and 5'-GTATAAATATTCATACTTGTTTCTG-3') were amplified from a cDNA pool of mid tailbud embryos and subcloned into a pBSKM vector.

Phylogenetic analysis

For the initial survey tree BLASTP[101] was used to assign the two *Ciona* GPCR sequences of interest to the rhodopsin class. We used the MAFFT E-INS-i algorithm[102] to align their seven-transmembrane domains with those of the proteins constituting the Pfam seed alignment for rhodopsin GPCRs[103], as well as most *Ciona* rhodopsin receptor-like proteins identified previously[104]. After removing ambiguously aligned amino acids with Gblocks[105], the 118-sequence data set (including five outgroup sequences for *Ciona* Glutamate, Smoothened, Frizzled and cAMP receptor-like proteins) contained 373 positions (including gaps). For optimal tree searches and measurement of nodal support, Minimum

Evolution (ME), Maximum Likelihood (ML) and Bayesian Inference (BI) criteria were used[106].

To classify the two *Ciona* GPCRs of interest with greater accuracy and support, a second set of analyses was done using a more focused sequence sampling. Based on the initial survey tree and the identifications made by Kamesh et al.[104], we selected presumed members of: the specific clade containing the two *Ciona* GPCRs of interest, its large "Chemokine Cluster" sister clade, and its two closest rootward sister clades (i.e., members of the "SOG" rhodopsin subclass). For these selections, GPCRDB Tools[107] was used to build an alignment of human seven-transmembrane domain sequences from the Swiss-Prot database. Using Clustal Omega[108], seven relevant *Ciona* sequences from Kamesh et al.[104] were integrated into the GPCRDB Tools alignment. After hand-editing in Jalview[109], this 75-sequence data set contained 208 positions. As stated above, ME, ML and BI were used to analyze the final alignment.

Calcium imaging

Human embryonic kidney (HEK) 293 cells were grown under 5% CO_2 and 100% relative humidity in DMEM medium supplemented with 10% (v/v) fetal bovine serum and 0.1 mM non-essential amino acids. HEK 293 cells do not express endogenous CNG channels[110]. Each *Ciona CNG* construct was transfected into HEK 293 cells using Targefect F-1 reagent (Targeting Systems, Santee, CA, U.S.A.) according to the manufacturer's instructions, and the cells were incubated for 48 hours.

To quantitatively visualize cyclic nucleotide-induced intracellular calcium ion, transfected HEK 293 cells were incubated for 30 minutes in a solution containing 140 mM NaCl, 5.4 mM KCl, 5 mM CaCl2, 5.6 mM glucose, 10 mM HEPES (pH7.4), and 2 μM Fura 2 AM (Dojindo Laboratories, Kumamoto, Japan). After washing with PBS, cells were placed in a solution containing 140 mM NaCl, 5.4 mM KCl, 5 mM CaCl2, 5.6 mM glucose, and 10 mM HEPES (pH7.4). 8-Br-cAMP (Sigma B7880) or 8-Br-cGMP (Sigma B1381) at various concentrations was administrated to the cells in a perfusion system. Fluorescence signals were monitored using an Argus-50/CA system (Hamamatsu photonics, Shizuoka, Japan). Each experiment was performed in at least two biological replicates.

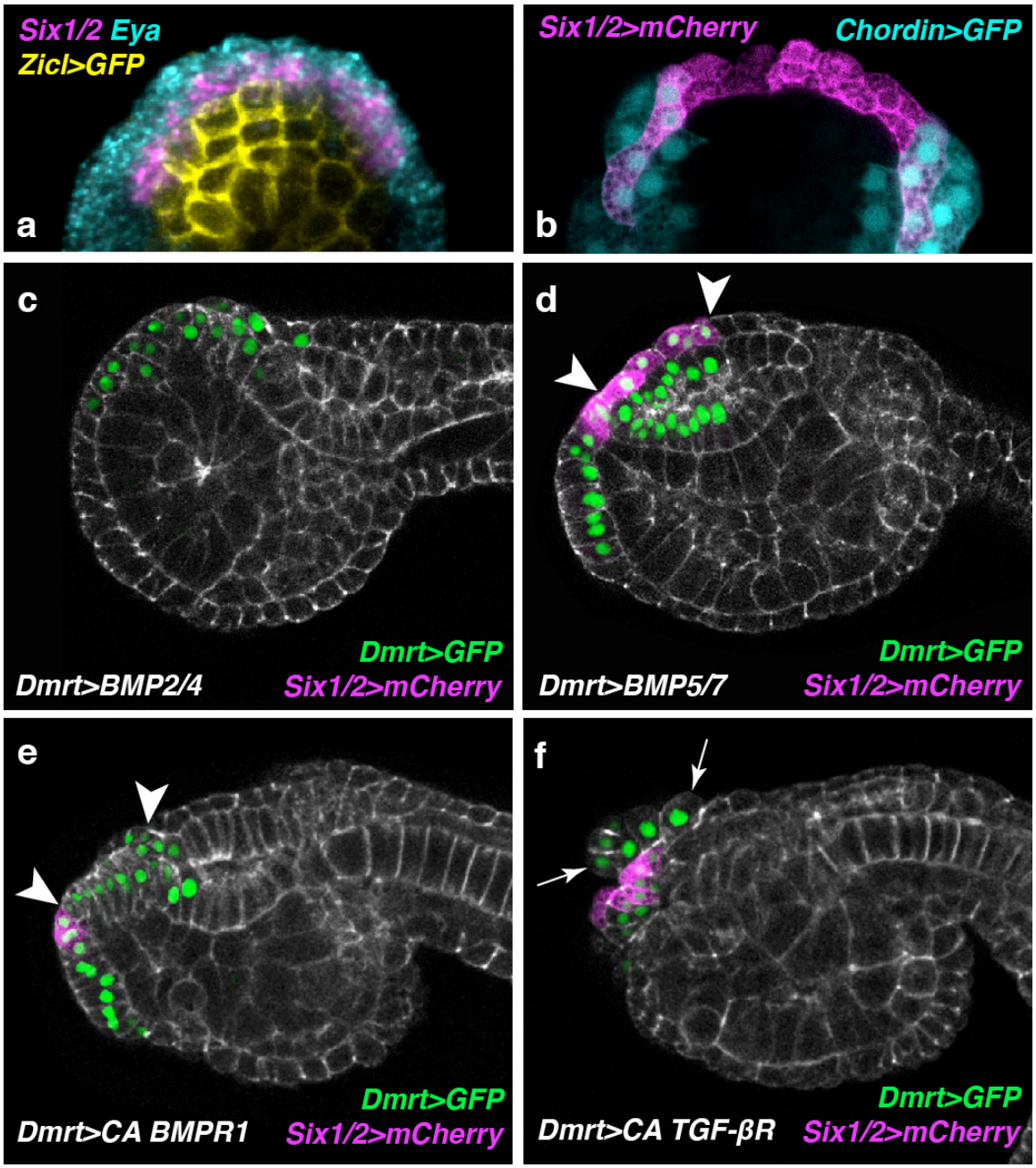
Six1/2 Eya
Zicl>GFP
a
Six1/2>mCherry
Chordin>GFP
b
c
Dmrt>BMP2/4
Dmrt>GFP
Six1/2>mCherry
d
Dmrt>BMP5/7
Dmrt>GFP
Six1/2>mCherry
e
Dmrt>CA BMPR1
Dmrt>GFP
Six1/2>mCherry
f
Dmrt>CA TGF-βR
Dmrt>GFP
Six1/2>mCherry

Figure 1 | *Six1/2* expression requires BMP attenuation. a, Dorsal view of an early neural stage embryo electroporated with *Zicl>GFP* and hybridized with *Six1/2* and *Eya* mRNA probes. **b**, Dorsal view of a mid-neural stage embryo co-electroporated with *Six1/2>mCherry* and *Chordin>GFP* after an additional division (16 *Six1/2+* cells total). **c-f**, Tailbud electroporated with *Six1/2>mCherry* and *Dmrt>GFP*, counterstained with phalloidin (grey). **c**, Co-electroporated with *Dmrt>BMP2/4* (131/135 had no *Six1/2>mCherry* expression). **d**, Co-electroporated with *Dmrt>BMP5/7* (120/135 displayed a full expression pattern for *Six1/2>mCherry*). **e**, Co-electroporated with *Dmrt>CA BMPR1* (95/135 had partial anterior *Six1/2>mCherry* expression). **f**, Co-electroporated with *Dmrt>CA TGF-βR* (93/135 displayed a full expression pattern for *Six1/2>mCherry* and anterior neural tube defects). Arrowheads in **d** and **e** flank the derivatives of the anterior ectoderm that normally co-express *Six1/2>mCherry* and *Chordin>GFP* in control embryos (see panel **b**). Arrows show extrusion of sensory vesicle cells in **f**.

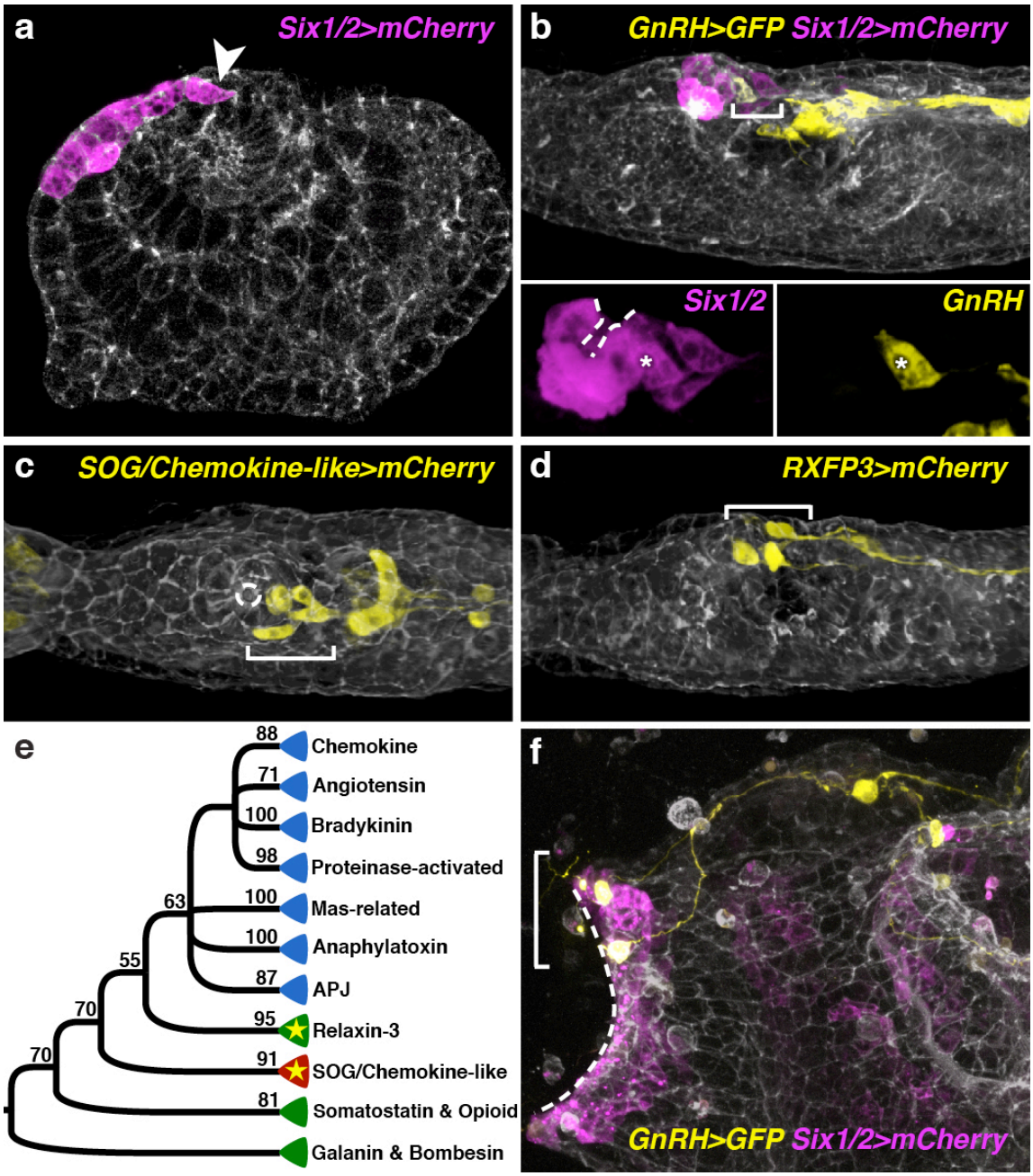
a
Six1/2>mCherry
b
GnRH>GFP Six1/2>mCherry
Six1/2
GnRH
c
SOG/Chemokine-like>mCherry
d
RXFP3>mCherry
e
88
Chemokine
71
Angiotensin
100
Bradykinin
98
Proteinase-activated
63
100
Mas-related
100
Anaphylatoxin
55
87
APJ
70
95
Relaxin-3
70
91
SOG/Chemokine-like
81
Somatostatin & Opioid
Galanin & Bombesin
f
GnRH>GFP Six1/2>mCherry

Figure 2 | PPE-derived GnRH neurons express *RXFP3*. a, Tailbud electroporated with *Six1/2>mCherry*. Arrowhead indicates the posterior most *Six1/2*+ cell that undergoes neurogenesis. **b**, Larva co-electroporated with *GnRH>GFP* and *Six1/2>mCherry*. Inset shows *Six1/2* expression surrounds the oral opening, dotted line in all panels. *GnRH+* neuron marked with asterisk. **c**, Dorsal view of larva electroporated with *SOG/Chemokine receptor-like>mCherry*. **d**, Larva electroporated with *RXFP3>mCherry*. **e**, Phylogenetic placement among human rhodopsin-class GPCRs of *Ciona RXFP3* and *SOG/Chemokine receptor-like*, indicated by the starred clades. Green clades comprise of *Ciona* and human orthologues, whereas no human orthologue was found for the red clade, and no known *Ciona* GPCR grouped within the blue clades. Support values are Bayesian posterior probability percentages. **f**, Juvenile co-electroporated with *GnRH>GFP* and *Six1/2>mCherry. Ciona* were counterstained with phalloidin (grey) in panels **a-d**, and **f**. Brackets indicate PPE-derived GnRH neurons. Panels **a**, **b**, **d**, and **f** are lateral anterior views.

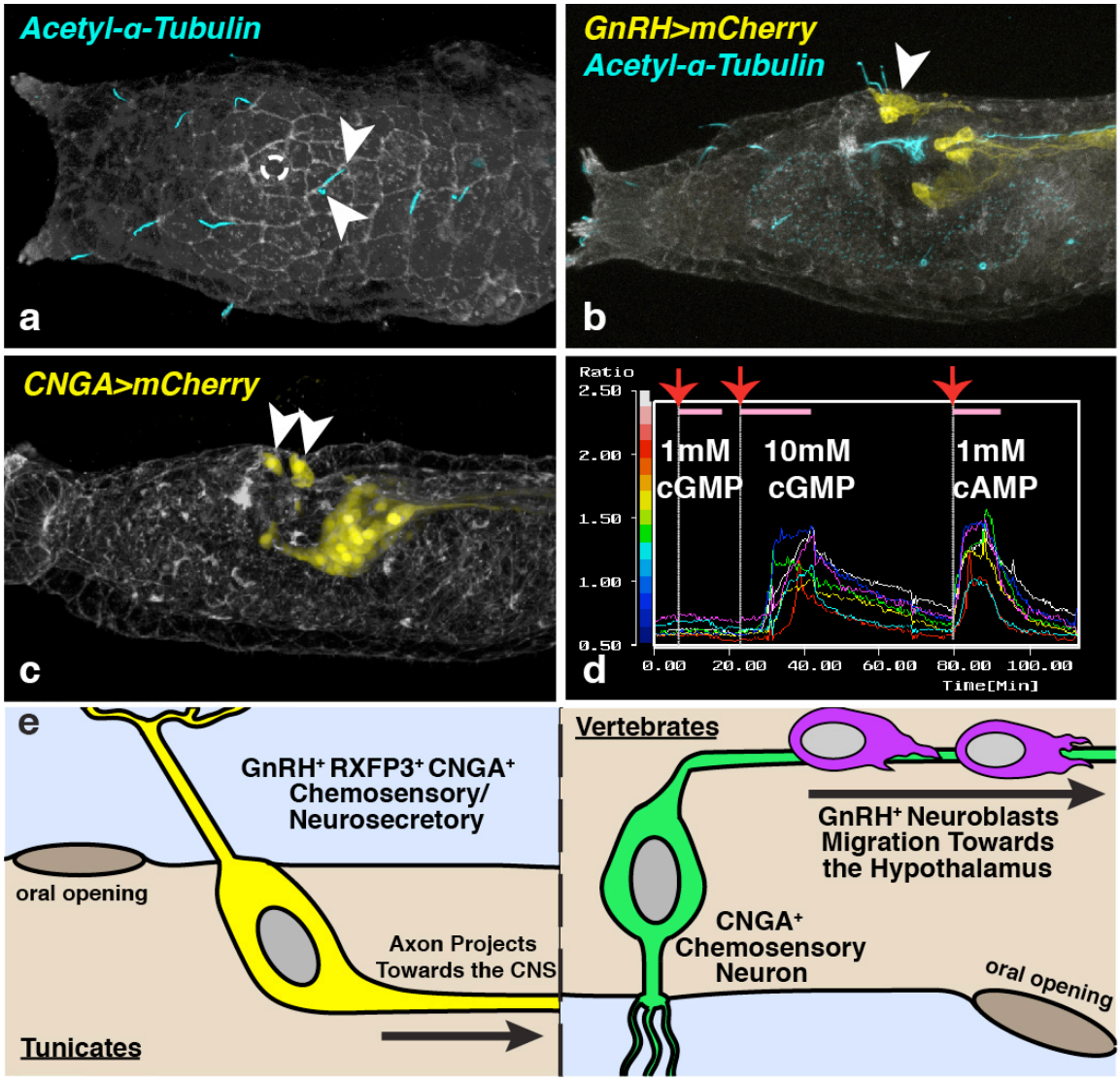
Acetyl-α-Tubulin
a
GnRH>mCherry
Acetyl-α-Tubulin
b
CNGA>mCherry
c
Ratio
2.50
2.00
1.50
1.00
0.50
1mM cGMP
10mM cGMP
1mM cAMP
0.00
20.00
40.00
60.00
80.00
100.00
Time[Min]
d
e
GnRH+ RXFP3+ CNGA+ Chemosensory/ Neurosecretory
oral opening
Axon Projects Towards the CNS
Tunicates
Vertebrates
GnRH+ Neuroblasts Migration Towards the Hypothalamus
CNGA+ Chemosensory Neuron
oral opening

Figure 3 l Ciliated GnRH neurons express functional *CNGA*. a-c, Larva stained with phalloidin (grey). **a**, Dorsal view of larva stained with an acetylated-α-tubulin antibody, dotted line indicates the oral opening. **b**, Lateral view of larva electroporated with *GnRH>mCherry* and stained with an acetylated-α-tubulin antibody. **c**, Lateral view of larva electroporated with *CNGA>mCherry*. Arrowheads indicate PPE-derived GnRH neurons in all panels. **d**, Ratiometric calcium imaging of HEK 293 cells transfected with *Ciona* CNGA assayed by the intracellular Ca^{2+} indicator Fura-2 AM. The graph shows the efficiency of response of CNGA to the cyclic nucleotide analogues 8-Br-cGMP and 8-Br-cAMP in seven individual cells (colored lines) over the 120-minute period. Indicated are the time points (red arrow) and durations (pink bar) of each analog perfusion. **e**, Schematic compares the PPE-derived GnRH neurons in *Ciona* and olfactory derived neurons in vertebrates.

Chapter V:

Conclusion

Vertebrate evolution is a perplexing topic, especially when many of the defining characteristics are considered innovations that lack homologs in invertebrate chordates. This narrow thinking however is not how evolution occurs. New features are built upon previous rudiments found in the last shared common ancestor. Neural crest and placodes are no exception as I have detailed in my dissertation.

The melanocyte lineage of *Ciona* may prove to be not the only neural crest homolog in tunicates. Several cells along the neural plate border in *Ciona*, such as the epidermal tail neurons, have neurogenic potential. The last common ancestor of tunicates and vertebrates might have had a neural plate border that produced peripheral neurons and even melanocytes along the entire length of the anterior-posterior axis. It is not beyond the realm of possibilities that the last shared ancestor had bona fide migratory neural crest cells that were lost in the tunicate lineage.

Using the current available knowledge of vertebrate neural crests we have identified the melanocyte lineage of *Ciona* as the best-known homolog. However, as new information becomes available a more complete picture of neural crest development will emerge. Previous inputs into the gene regulatory network may be modified and reworked. This may lead to new studies drawing comparison between neural crest and various invertebrate chordate cell types.

However, the acquisition of migratory capabilities and potential to give rise to ectomesenchyme may remain an attribute found only in vertebrate neural crest cells. How this rewiring event actually precipitated is an interesting topic of its own. Did a mesenchymal gene such as *Twist* come under control of new cis-regulatory sequences or was *Twist* activated at the neural plate via other means? In the future transcription profiling of individual cells and genome studies may uncover such evolutionary novelties.

Likewise, the concept of the ancestral cell is ripe for exploration in a simple organism such as *Ciona*. If the model holds true, then individual neurons in *Ciona* may prove to be evolutionarily linked to neuronal circuits found in vertebrates. This theory may provide evolutionary insights into how certain parts of the vertebrate nervous system formed. *Ciona* researchers are only beginning to uncover the function of various neurons and how they coordinate together to elicit behaviors in this system. This avenue of research will benefit tremendously from CRISPR-generated transgenic lines.

Moving forward the sea squirt will continue to impress both as a developmental biology model and as a tool for uncovering the mysteries of vertebrate evolution. As a principal investigator I plan on using both *Ciona* and Zebrafish for comparative evo-devo studies.

References

1 Wada, H. & Makabe, K. Genome duplications of early vertebrates as a possible chronicle of the evolutionary history of the neural crest. *Int. J. Biol. Sci.* **2**, 133-141 (2006).

2 Braasch, I., Volff, J. N. & Schartl, M. The Endothelin System: Evolution of Vertebrate-Specific Ligand-Receptor Interactions by Three Rounds of Genome Duplication. *Mol. Biol. Evol.* **26**, 783-799, (2009).

3 Yu J. K., Meulemans, D., McKeown, S. J. & Bronner-Fraser, M. Insights from the amphioxus genome on the origin of vertebrate neural crest. *Genome Res.* **18**, 1127-1132 (2008).

4 Shimeld, S. M., & Holland, P. W. H. Vertebrate innovations. *Proc. Natl. Acad. Sci. USA* **97**, 4449-4452 (2000).

5 Delsuc, F., Brinkmann, H., Chourrout, D. & Philippe, H. Tunicates and not cephalochordates are the closest living relatives of vertebrates. *Nature* **439**, 965-968 (2006).

6 Imai, K. S., Levine, M., Satoh, N. & Satou, Y. Regulatory blueprint for a chordate embryo. *Science* **312**, 1183-1187 (2006).

7 Stolfi, A. & Levine, M. Neuronal subtype specification in the spinal cord of a protovertebrate. *Development* **138**, 995-1004 (2011).

8 Le Douarin, N. M. *et al.* Neural crest cell plasticity and its limits. *Development* **131**, 4637-4650 (2004).

9 Gans, C. & Northcutt, R. G. Neural crest and the origin of vertebrates: a new head. *Science* **220**, 268-273 (1983).

10 Steventon, B., Mayor, R. & Streit, A. Neural crest and placode interaction during the development of the cranial sensory system. *Devl. Bio.* **389**, 28-38 (2014).

11 Meulemans, D. & Bronner-Fraser, M. Gene-regulatory interactions in neural crest evolution and development. *Dev. Cell* **7**, 291-299 (2004).

12 Kwon, H.J., Bhat, N., Sweet, E. M., Cornell, R. A. & Riley, B. B. Identification of early requirements for preplacodal ectoderm and sensory organ development. *PLoS Genet.* **6**, e1001133 (2010).

13 Mazet, F. *et al.* Molecular evidence from *Ciona intestinalis* for the evolutionary origin of vertebrate sensory placodes. *Devl. Bio.* **282**, 494-508 (2005).

14 Christiaen, L., Bourrat, F. & Joly, J. A modular cis-regulatory system controls isoform-specific pitx expression in ascidian stomodæum. *Devl. Bio.* **277**, 557-566 (2005).

15 Gorbman, A. Olfactory origins and evolution of the brain-pituitary endocrine system: facts and speculation. *Gen. Comp. Endocrinol.* **97**, 171-178 (1995).

16 Bronner, M. E. & Le Douarin, N. M. Evolution and development of the neural crest: An overview. *Dev. Biol.* **366**, 2-9 (2012).

17 Jeffery, W. R., Strickler, A. G. & Yamamoto, Y. Migratory neural crest-like cells form body pigmentation in a urochordate embryo. *Nature* **431**, 696-699 (2004).
18 Jeffery, W. R. Ascidian neural crest-like cells: phylogenetic distribution, relationship to larval complexity, and pigment cell fate. *J. Exp. Zool. B Mol. Dev. Evol.* **306**, 470-480 (2006).
19 Jeffery, W. R. *et al.* Trunk lateral cells are neural crest-like cells in the ascidian Ciona intestinalis: Insights into the ancestry and evolution of the neural crest. *Dev. Biol.* **324**, 152-160 (2008).
20 Tassy, O. *et al.* The ANISEED database: digital representation, formalization, and elucidation of a chordate developmental program. *Genome Res.* **20**, 1459-1468, (2010).
21 Russo, M. T. *et al.* Regulatory elements controlling Ci-msxb tissue-specific expression during Ciona intestinalis embryonic development. *Dev. Biol.* **267**, 517-528 (2004).
22 Squarzoni, P., Parveen, F., Zanetti, L., Ristoratore, F. & Spagnuolo, A. FGF/MAPK/Ets signaling renders pigment cell precursors competent to respond to Wnt signal by directly controlling Ci-Tcf transcription. *Development* **138**, 1421-1432 (2011).
23 Curran, K. *et al.* Interplay between Foxd3 and Mitf regulates cell fate plasticity in the zebrafish neural crest. *Dev. Biol.* **344**, 107-118, (2010).
24 Yajima, I. *et al.* Cloning and functional analysis of ascidian Mitf in vivo: insights into the origin of vertebrate pigment cells. *Mech. Dev.* **120**, 1489-1504 (2003).
25 Nishida, H. & Satoh, N. Determination and regulation in the pigment cell lineage of the ascidian embryo. *Dev. Biol.* **132**, 355-367 (1989).
26 Dorsky, R. I., Moon, R. T. & Raible, D. W. Control of neural crest cell fate by the Wnt signalling pathway. *Nature* **396**, 370-373 (1998).
27 Thomas, A. J., & Erickson, C. A. FOXD3 regulates the lineage switch between neural crest-derived glial cells and pigment cells by repressing MITF through a non-canonical mechanism. *Development* **136**, 1849-1858 (2009).
28 Imai, K. S., Satoh, N. & Satou, Y. An essential role of a FoxD gene in notochord induction in Ciona embryos. *Development* **129**, 3441-3453 (2002).
29 Yoshida, T., Vivatbutsiri, P., Morriss-Kay, G., Saga, Y. & Iseki, S. Cell lineage in mammalian craniofacial mesenchyme. *Mech. Dev.* **125**, 797-808 (2008).
30 Bildsoe, H. *et al.* Requirement for *Twist1* in frontonasal and skull vault development in the mouse embryo. *Dev. Biol.* **331**, 176-188 (2009).
31 Soo, K. *et al.* Twist function is required for the morphogenesis of the cephalic neural tube and the differentiation of the cranial neural crest cells in the mouse embryo. *Dev. Biol.* **247**, 251-270 (2002).

32 Hopwood, N. D., Pluck, A. & Gurdon, J. B. A Xenopus mRNA related to Drosophila twist is expressed in response to induction in the mesoderm and the neural crest. *Cell* **59**, 893-903 (1989).
33 Vincentz, J. W. *et al.* An absence of Twist1 results in aberrant cardiac neural crest morphogenesis. *Dev. Biol.* **320**, 131-139 (2008).
34 Tokuoka, M., Satoh, N. & Satou, Y. A bHLH transcription factor gene, Twist-like 1, is essential for the formation of mesodermal tissues of Ciona juveniles. *Dev. Biol.* **288**, 387-396 (2005).
35 Vlaeminck-Guillem, V. *et al.* The Ets family member Erg gene is expressed in mesodermal tissues and neural crests at fundamental steps during mouse embryogenesis. *Mech. Dev.* **91**, 331-335 (2000).
36 Hamada, M. *et al.* Expression of neuropeptide- and hormone-encoding genes in the *Ciona intestinalis* larval brain. *Dev. Biol.* **352**, 202-214, (2011).
37 Shi, W. & Levine, M. Ephrin signaling establishes asymmetric cell fates in an endomesoderm lineage of the Ciona embryo. *Development* **135**, 931-940 (2008).
38 Jiang, D., Tresser, J. W., Horie, T., Tsuda, M. & Smith, W. C. Pigmentation in the sensory organs of the ascidian larva is essential for normal behavior. *J. Exp. Biol.* **208**, 433-438, (2005).
39 Tsuda, M., Sakurai, D. & Goda, M. Direct evidence for the role of pigment cells in the brain of ascidian larvae by laser ablation. *J. Exp. Biol.* **206**, 1409-1417, (2003).
40 Lamb, T. D., Collin, S. P. & Pugh, E. N. Evolution of the vertebrate eye: opsins, photoreceptors, retina and eye cup. *Nat. Rev. Neurosci.* **8**, 960-976, (2007).
41 Sato, S. & Yamamoto, H. Development of pigment cells in the brain of ascidian tadpole larvae: Insights into the origins of vertebrate pigment cells. *Pigment Cell Res.* **14**, 428-436 (2001).
42 Abitua, P. B., Wagner, E., Navarrete, I. A. & Levine, M. Identification of a rudimentary neural crest in a non-vertebrate chordate. *Nature* **492**, 104-107, (2012).
43 Ivashkin, E. & Adameyko, I. Progenitors of the protochordate ocellus as an evolutionary origin of the neural crest. *Evodevo* **4**, (2013).
44 Nishida, H. Cell lineage analysis in ascidian embryos by intracellular injection of a tracer enzyme .III. Up to the tissue restricted stage. *Dev. Biol.* 121, 526-541 (1987).
45 Lemaire, P., Bertrand, V. & Hudson, C. Early steps in the formation of neural tissue in ascidian embryos. *Dev. Biol.* **252**, 151-169, (2002).
46 Nicol, D. & Meinertzhagen, I. A. Development of the central nervous-system of the larva of the ascidian, *Ciona Intestinalis* L .1. The early lineages of the neural plate. *Developmental Biology* **130**, 721-736, (1988).
47 Christiaen, L. *et al.* Evolutionary modification of mouth position in deuterostomes. *Semin. Cell Dev. Biol.* **18**, 502-511, (2007).

48 Cole, A. & Meinertzhagen, I. The central nervous system of the ascidian larva: mitotic history of cells forming the neural tube in late embryonic *Ciona intestinalis*. *Dev. Biol.* **271**, 239-262 (2004).
49 Taniguchi, K. & Nishida, H. Tracing cell fate in brain formation during embryogenesis of the ascidian *Halocynthia roretzi*. *Dev. Growth Differ.* **46**, 163-180 (2004).
50 Veeman, M. T., Newman-Smith, E., El-Nachef, D. & Smith, W. C. The ascidian mouth opening is derived from the anterior neuropore: Reassessing the mouth/neural tube relationship in chordate evolution. *Dev. Biol.* **344**, 138-149, (2010).
51 Mazet, F. The evolution of sensory placodes. *ScientificWorldJournal* **6**, 1841-1850, (2006).
52 Wagner, E. & Levine, M. FGF signaling establishes the anterior border of the Ciona neural tube. *Development* **139**, 2351-2359, (2012).
53 Guillemot, F. & Zimmer, C. From cradle to grave: The multiple roles of fibroblast growth factors in neural development. *Neuron* **71**, 574-588, (2011).
54 Hebert, J. M. FGFs: neurodevelopment's jack-of-all-trades - How do they do it? *Front. Neurosci.* **5**, 133, (2011).
55 Stuhlmiller, T. J. & Garcia-Castro, M. I. FGF/MAPK signaling is required in the gastrula epiblast for avian neural crest induction. *Development* **139**, 289-300, (2012).
56 Bertrand, V., Hudson, C., Caillol, D., Popovici, C. & Lemaire, P. Neural tissue in ascidian embryos is induced by FGF9/16/20, acting via a combination of maternal GATA and Ets transcription factors. *Cell* **115**, 615-627 (2003).
57 Hudson, C., Darras, S., Caillol, D., Yasuo, H. & Lemaire, P. A conserved role for the MEK signalling pathway in neural tissue specification and posteriorisation in the invertebrate chordate, the ascidian *Ciona intestinalis. Development* **130**, 147-159, (2003).
58 Hudson, C., Lotito, S. & Yasuo, H. Sequential and combinatorial inputs from Nodal, Delta2/Notch and FGF/MEK/ERK signalling pathways establish a grid-like organisation of distinct cell identities in the ascidian neural plate. *Development* **134**, 3527-3537, (2007).
59 Stolfi, A., Wagner, E., Taliaferro, J. M., Chou, S. & Levine, M. Neural tube patterning by Ephrin, FGF and Notch signaling relays. *Development* **140**, 481-481, (2012).
60 Ohta, N. & Satou, Y. Multiple signaling pathways coordinate to induce a threshold response in a chordate embryo. *PLoS Genet.* **9**, e1003818 (2013).
61 Picco, V., Hudson, C. & Yasuo, H. Ephrin-Eph signalling drives the asymmetric division of notochord/neural precursors in Ciona embryos. *Development* **134**, 1491-1497, (2007).

62 Haupaix, N. *et al.* p120RasGAP mediates ephrin/Eph-dependent attenuation of FGF/ERK signals during cell fate specification in ascidian embryos. *Development*, **140**, 4347-4352, (2013).
63 Irvine, S. Q., Cangiano, M. C., Millette, B. J. & Gutter, E. S. Non-overlapping expression patterns of the clusteredDll-A/B genes in the ascidian *Ciona Intestinalis*. *J. Exp. Zool. B: Mol. Dev. Evol.* **308**, 428-441, (2007).
64 Hotta, K. *et al.* A web-based interactive developmental table for the ascidian *Ciona intestinalis*, including 3D real-image embryo reconstructions: I. From fertilized egg to hatching larva. *Dev. Dyn.* **236**, 1790-1805 (2007).
65 Imai, K. S., Hino, K., Yagi, K., Satoh, N. & Satou, Y. Gene expression profiles of transcription factors and signaling molecules in the ascidian embryo: towards a comprehensive understanding of gene networks. *Development* **131**, 4047-4058, (2004).
66 Ikeda, T., Matsuoka, T. & Satou, Y. A time delay gene circuit is required for palp formation in the ascidian embryo. *Development* **140**, 4703-4708 (2013).
67 Whittaker, J. R. Quantitative control of end products in the melanocyte lineage of the ascidian embryo. *Dev. Biol.* **73**, 76-83, (1979).
68 Rothbacher, U., Bertrand, V., Lamy, C. & Lemaire, P. A combinatorial code of maternal GATA, Ets and β-TCF transcription factors specifies and patterns the early ascidian ectoderm. *Development* **134**, 4023-4032, (2007).
69 Davidson, B., Shi, W. Y., Beh, J., Christiaen, L. & Levine, M. FGF signaling delineates the cardiac progenitor field in the simple chordate, *Ciona intestinalis*. *Gene Dev.* **20**, 2728-2738, (2006).
70 Imai, K. S., Stolfi, A., Levine, M. & Satou, Y. Gene regulatory networks underlying the compartmentalization of the Ciona central nervous system. *Development* **136**, 285-293, (2009).
71 Kim, G. J. & Nishida, H. Role of the FGF and MEK signaling pathway in the ascidian embryo. *Dev. Growth Differ.* **43**, 521-533 (2001).
72 Shimauchi, Y., Murakami, S. D. & Satoh, N. FGF signals are involved in the differentiation of notochord cells and mesenchyme cells of the ascidian *Halocynthia roretzi*. *Development* **128**, 2711-2721 (2001).
73 Yasuo, H. & Hudson, C. FGF8/17/18 functions together with FGF9/16/20 during formation. of the notochord in Ciona embryos. *Dev. Biol.* **302**, 92-103, (2007).
74 Darras, S. & Nishida, H. The BMP/CHORDIN antagonism controls sensory pigment cell specification and differentiation in the ascidian embryo. *Dev. Biol.* **236**, 271-288 (2001).
75 Sardet, C. *et al.* Embryological methods in ascidians: The Villefranche-sur-Mer Protocols. *Methods Mol. Biol.* **770**, 365-400, (2011).

76 Hudson, C. & Yasuo, H. A signalling relay involving Nodal and Delta ligands acts during secondary notochord induction in Ciona embryos. *Development* **133**, 2855-2864, (2006).
77 Hudson, C., Kawai, N., Negishi, T. & Yasuo, H. β-Catenin-driven binary fate specification segregates germ layers in ascidian embryos. *Curr. biol.* **23**, 491-495, (2013).
78 Satou, Y. *et al.* A cDNA resource from the basal chordate *Ciona intestinalis. Genesis* **33**, 153-154, (2002).
79 Gaskell, W. H. *The origin of vertebrates*. (1908).
80 Patthey, C., Schlosser, G. & Shimeld, S. M. The evolutionary history of vertebrate cranial placodes - I: Cell type evolution. *Devl. Bio.* **389**, 82-97 (2014).
81 Ruf, R. G. *et al.* SIX1 mutations cause branchio-oto-renal syndrome by disruption of EYA1-SIX1-DNA complexes. *Proc. Natl. Acad. Sci. USA* **101**, 8090-8095 (2004).
82 Reichert, S., Randall, R. A. & Hill, C. S. A BMP regulatory network controls ectodermal cell fate decisions at the neural plate border. *Development* **140**, 4435-4444 (2013).
83 Ahrens, K. & Schlosser, G. Tissues and signals involved in the induction of placodal *Six1* expression in *Xenopus laevis*. *Devl. Bio.* **288**, 40-59 (2005).
84 Schwanzelfukuda, M. & Pfaff, D. W. Origin of luteinizing-hormone-releasing hormone neurons. *Nature* **338**, 161-164 (1989).
85 Wray, S., Grant, P. & Gainer, H. Evidence that cells expressing luteinizing hormone-releasing hormone mRNA in the mouse are derived from progenitor cells in the olfactory placode. *Proc. Natl. Acad. Sci. USA* **86**, 8132-8136 (1989).
86 Wray, S. From nose to brain: development of gonadotrophin-releasing hormone-1 neurones. *J. Neuroendocrinol.* **22**, 743-753 (2010).
87 Kusakabe, T. G. *et al.* A conserved non-reproductive GnRH system in chordates. *PloS one* **7**, e41955 (2012).
88 McGowan, B. M. *et al.* Relaxin-3 stimulates the hypothalamic-pituitary-gonadal axis. *Am. J. Physiol. Endocrinol. Metab.* **295**, E278-E286 (2008).
89 Terakado, K. Induction of gamete release by gonadotropin-releasing hormone in a protochordate, *Ciona intestinalis*. *Gen. Comp. Endocrinol.* **124**, 277-284 (2001).
90 Konno, A. *et al.* Distribution and structural diversity of cilia in tadpole larvae of the ascidian *Ciona intestinalis*. *Devl. Bio.* **337**, 42-62 (2010).
91 Reese, T. S. Olfactory cilia in the frog. *J. Cell Biol.* **25**, 209-230 (1965).
92 Kaupp, U. B. Olfactory signalling in vertebrates and insects: differences and commonalities. *Nat. Rev. Neurosci.* **11,** 1-13 (2010).
93 Constantin, S. & Wray, S. Gonadotropin-releasing hormone-1 neuronal activity is independent of cyclic nucleotide-gated channels. *Endocrinology* **149**, 279-290 (2008).

94 El Majdoubi, M. & Weiner, R. I. Localization of olfactory cyclic nucleotide-gated channels in rat gonadotropin-releasing hormone neurons. *Endocrinology* **143**, 2441-2444 (2002).
95 Boehm, U., Zou, Z. & Buck, L. B. Feedback loops link odor and pheromone signaling with reproduction. *Cell* **123**, 683-695 (2005).
96 Yoon, H., Enquist, L. W. & Dulac, C. Olfactory inputs to hypothalamic neurons controlling reproduction and fertility. *Cell* **123**, 669-682 (2005).
97 Arendt, D. The evolution of cell types in animals: emerging principles from molecular studies. *Nat. Rev. Genet.* **9**, 868-882 (2008).
98 Christiaen, L., Stolfi, A. & Levine, M. BMP signaling coordinates gene expression and cell migration during precardiac mesoderm development. *Devl. Bio.* **340**, 179-187 (2010).
99 Rehm, E. J., Hannibal, R. L., Chaw, R. C., Vargas-Vila, M. A. & Patel, N. H. Fixation and dissection of *Parhyale hawaiensis* embryos. *CSH Protocols* **2009** (2009).
100 Hudson, C. & Yasuo, H. Patterning across the ascidian neural plate by lateral Nodal signalling sources. *Development* **132**, 1199-1210 (2005).
101 Altschul, S. F. *et al.* Gapped BLAST and PSI-BLAST: a new generation of protein database search programs. *Nucleic Acids Res.* **25**, 3389-3402 (1997).
102 Katoh, K. & Standley, D. M. MAFFT multiple sequence alignment software version 7: Improvements in performance and usability. *Mol. Biol. Evol.* **30**, 772-780 (2013).
103 Finn, R. D. *et al.* Pfam: the protein families database. *Nucleic Acids Res.* **42**, D222-D230 (2014).
104 Kamesh, N., Aradhyam, G. K. & Manoj, N. The repertoire of G protein-coupled receptors in the sea squirt *Ciona intestinalis*. *BMC Evol. Biol.* **8**, 129 (2008).
105 Talavera, G. & Castresana, J. Improvement of phylogenies after removing divergent and ambiguously aligned blocks from protein sequence alignments. *Systematic Biol.* **56**, 564-577 (2007).
106 Winchell, C. J. & Jacobs, D. K. Expression of the Lhx genes *apterous* and *lim1* in an errant polychaete: implications for bilaterian appendage evolution, neural development, and muscle diversification. *Evodevo* **4** (2013).
107 Isberg, V. *et al.* GPCRDB: an information system for G protein-coupled receptors. *Nucleic Acids Res.* **42**, D422-425 (2014).
108 Sievers, F. *et al.* Fast, scalable generation of high-quality protein multiple sequence alignments using Clustal Omega. *Mol. Syst. Biol.* (2011).
109 Waterhouse, A. M., Procter, J. B., Martin, D. M., Clamp, M. & Barton, G. J. Jalview Version 2--a multiple sequence alignment editor and analysis workbench. *Bioinformatics* **25**, 1189-1191 (2009).

110 Dhallan, R. S., Yau, K. W., Schrader, K. A. & Reed, R. R. Primary structure and functional expression of a cyclic nucleotide-activated channel from olfactory neurons. *Nature* **347**, 184-187 (1990).

Appendix

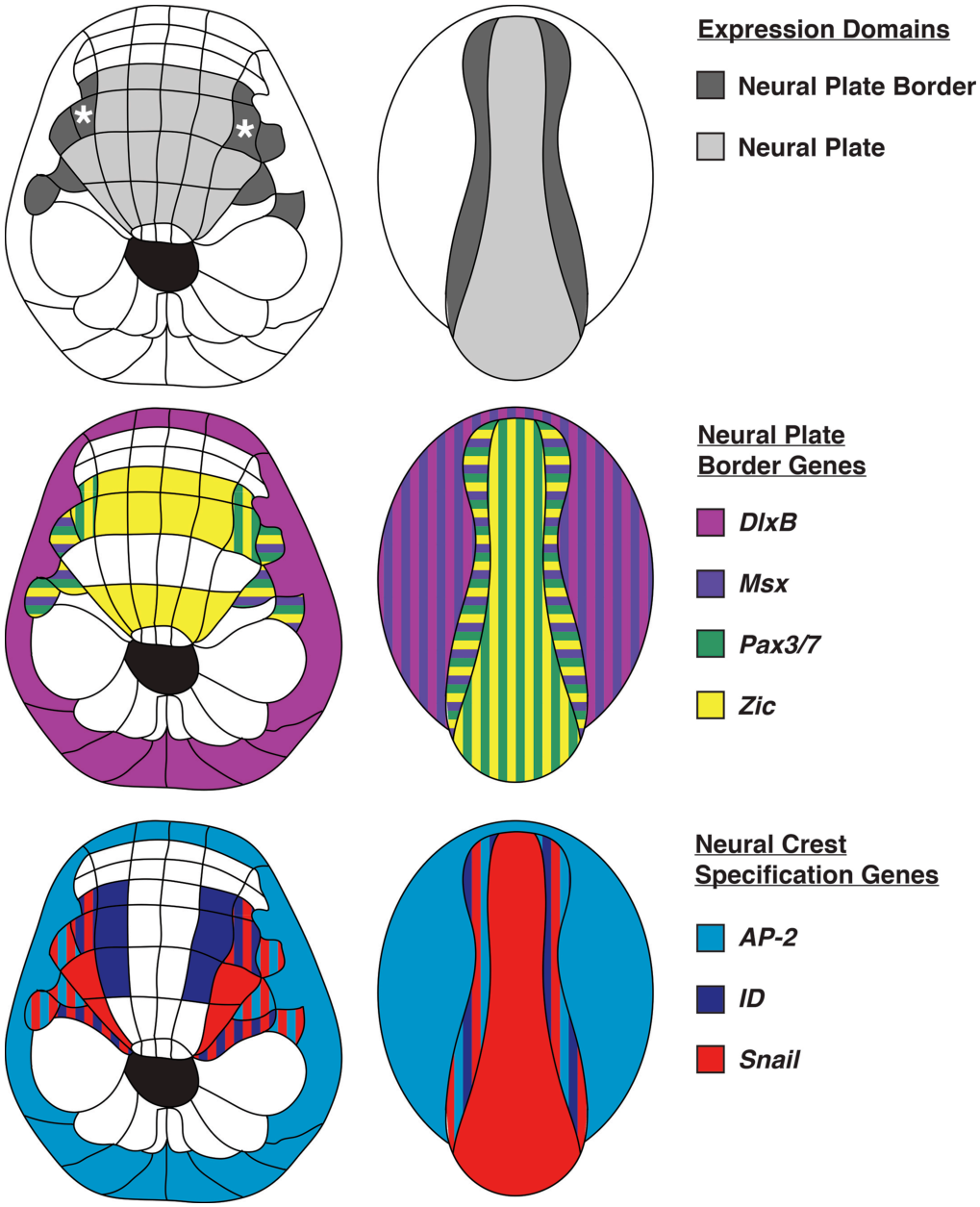
Expression Domains
Neural Plate Border
Neural Plate
Neural Plate Border Genes
DlxB
Msx
Pax3/7
Zic
Neural Crest Specification Genes
AP-2
ID
Snail

Appendix A | *Ciona intestinalis* and *Petromyzon marinus* neural crest expression domain comparison. Cartoon shows dorsal views of *Ciona* mid gastrula (left) and *Petromyzon* early neurula (right). The a9.49 lineage is marked by asterisks and in all images anterior is up. Initially in Ciona *DlxB* and *AP-2* are broadly expressed in the epidermis (including the mother of a9.49). Later *DlxB* is cleared from the neural ectoderm, whereas *AP-2* is maintained in the border as shown. During Ciona neurulation *Msx* expands medially into the a9.49 lineage and dorsal neural tube precursors. In both species *FoxD* is expressed only after neural tube formation is complete.

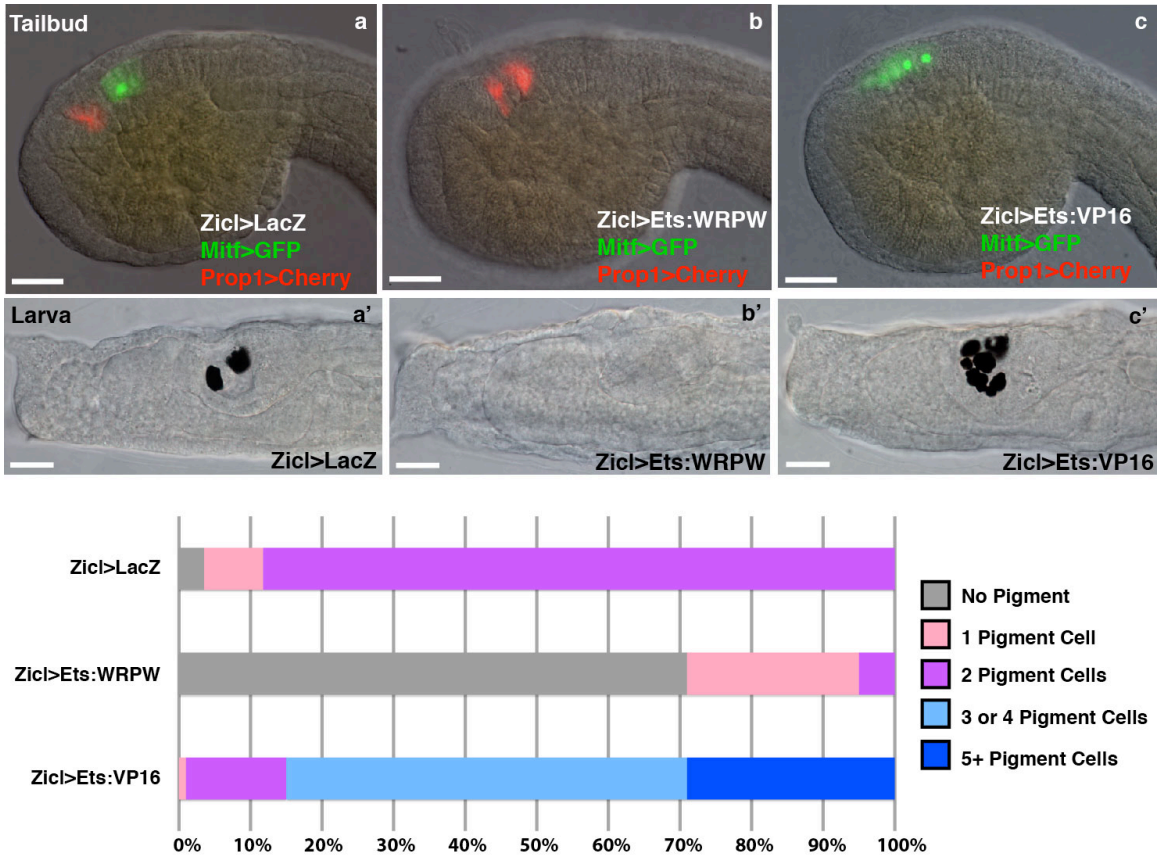
Tailbud
a
Zicl>LacZ
Mitf>GFP
Prop1>Cherry
b
Zicl>Ets:WRPW
Mitf>GFP
Prop1>Cherry
c
Zicl>Ets:VP16
Mitf>GFP
Prop1>Cherry
Larva
a'
Zicl>LacZ
b'
Zicl>Ets:WRPW
c'
Zicl>Ets:VP16
Zicl>LacZ
Zicl>Ets:WRPW
Zicl>Ets:VP16
0%
10%
20%
30%
40%
50%
60%
70%
80%
90%
100%
No Pigment
1 Pigment Cell
2 Pigment Cells
3 or 4 Pigment Cells
5+ Pigment Cells

Appendix B | Ets1/2 activity controls the number of pigmented cells. a,**a**' Tailbud embryo co-electroporated with *ZicL>LacZ*, *Prop1>mCherry*, *Mitf>GFP* (**a**) larva stage reveals two pigmented cells (**a'**) (n=85). **b**,**b**' Tailbud embryo co-electroporated with *ZicL>Ets:WRPW*, *Prop1>mCherry*, *Mitf>GFP* does not express *Mitf* reporter (**b**) resulting larva is not pigmented (**b'**) (n=100). **c**,**c**' Tailbud embryo co-electroporated with *ZicL>Ets:VP16*, *Prop1>mCherry*, *Mitf>GFP* shows expanded *Mitf* reporter at the expense of *Prop1* expression in the a10.99 lineage (**c**) resulting larva has supernumerary otoliths (**c'**) (n=100). In all images anterior is to the left and the scale bar represents 25 μm.

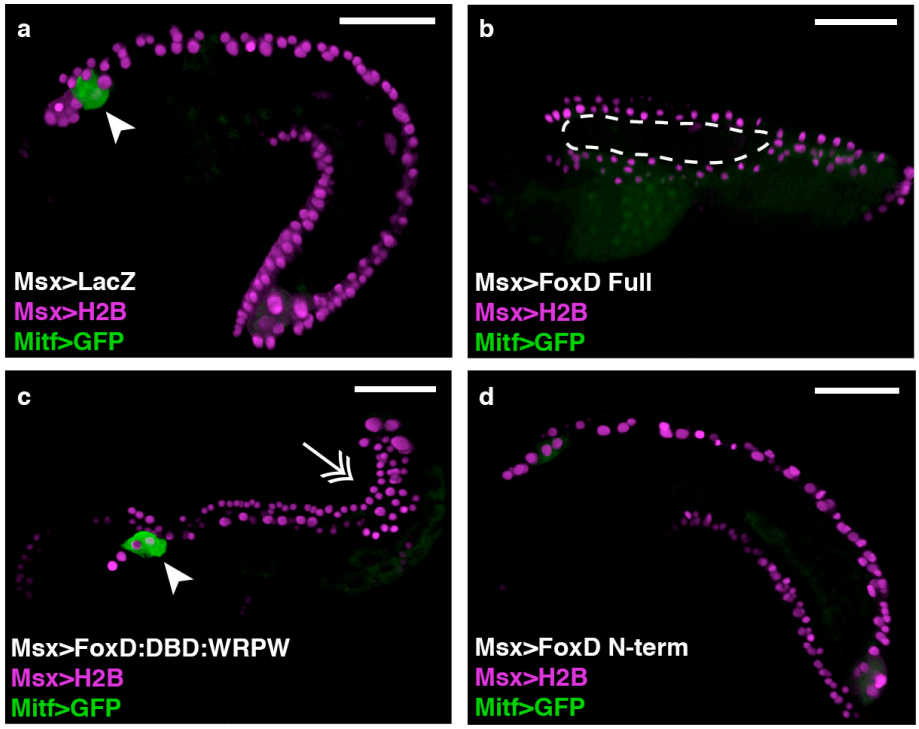
a
Msx>LacZ
Msx>H2B
Mitf>GFP
b
Msx>FoxD Full
Msx>H2B
Mitf>GFP
c
Msx>FoxD:DBD:WRPW
Msx>H2B
Mitf>GFP
d
Msx>FoxD N-term
Msx>H2B
Mitf>GFP

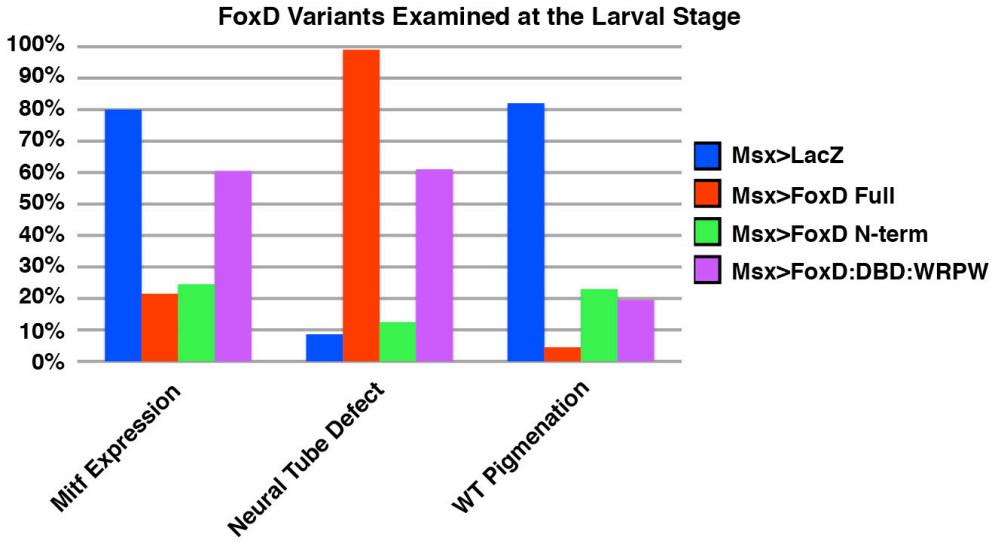
FoxD Variants Examined at the Larval Stage
100%
90%
80%
70%
60%
50%
40%
30%
20%
10%
0%
Mitf Expression
Neural Tube Defect
WT Pigmenation
Msx>LacZ
Msx>FoxD Full
Msx>FoxD N-term
Msx>FoxD:DBD:WRPW

Appendix C l Misexpression of FoxD constructs in the midline. a, Tailbud embryo co-electroporated with *Msx>LacZ*, *Msx>H2B mCherry*, and *Mitf>GFP*. Msx expression marks the midline and arrowheads show GFP expression in the a9.49 lineage in the series (n=176). **b**, Tailbud embryo co-electroporated with *Msx>FoxD* full length, *Msx>H2B mCherry*, and *Mitf>GFP*. Dotted line denotes the space between the neural folds that failed to intercalate (n=200). **c**, Tailbud embryo co-electroporated with *Msx>FoxD:DBD:WRPW*, *Msx>H2B mCherry*, and *Mitf>GFP*. Double arrow shows kinked tail resulting from a neural tube closure defect (n=200). **d**, Tailbud embryo co-electroporated with *Msx>FoxD* N-terminal, *Msx>H2B mCherry*, and *Mitf>GFP* (n=200). In all images anterior is to the left and the scale bar represents 50 μm. Graph indicates phenotypes observed at the larval stage.

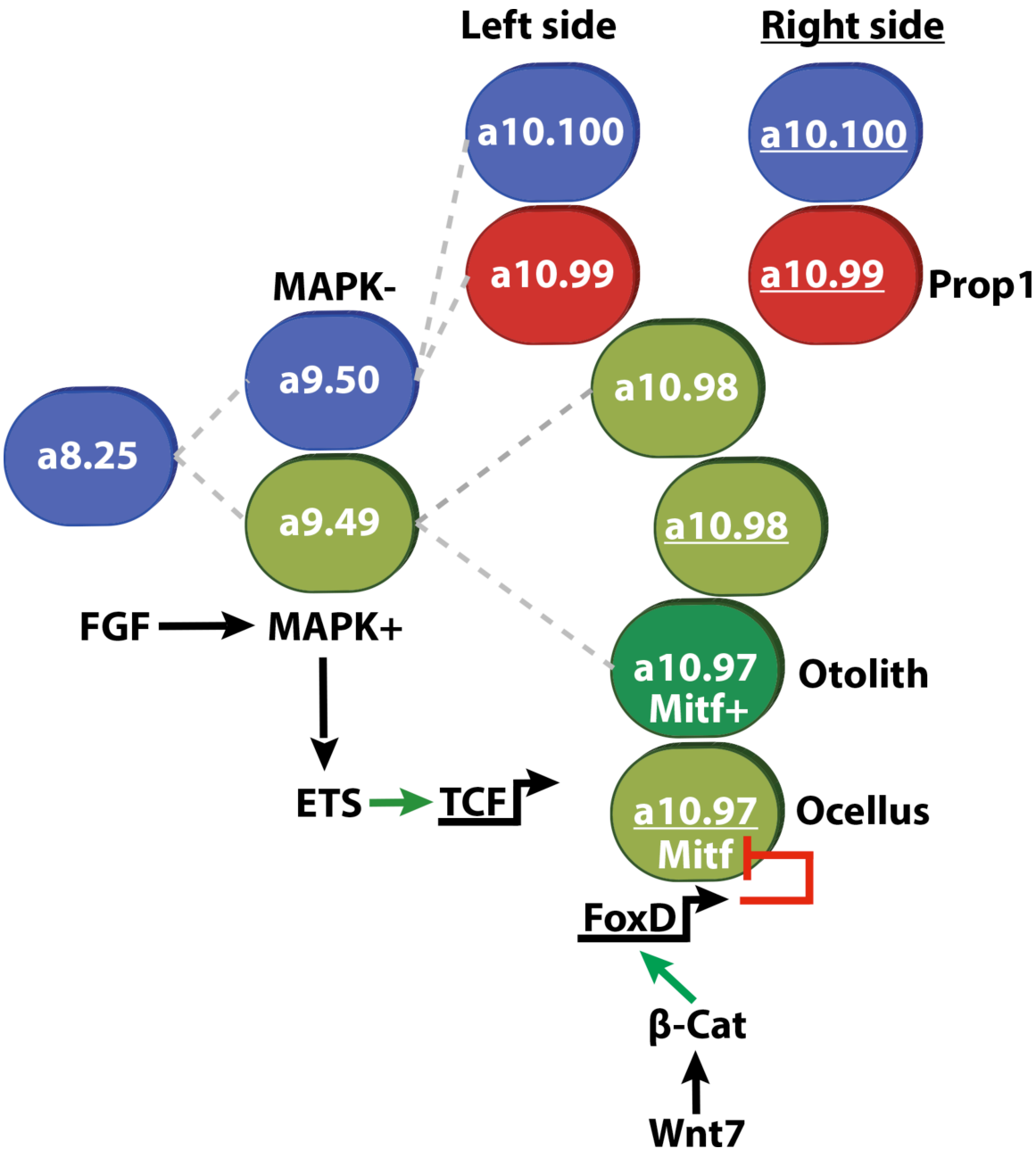
Left side
Right side
a10.100
a10.100
a10.99
a10.99
Prop1
MAPK-
a9.50
a10.98
a8.25
a9.49
a10.98
FGF
MAPK+
a10.97
Mitf+
Otolith
ETS
TCF
a10.97
Mitf
Ocellus
FoxD
β-Cat
Wnt7

Appendix D l Summary of the Mitf regulatory network. An FGF signal activates the MAPK pathway leading to the phosphorylation of Ets1/2 in a9.49 whose descendants are initially Mitf+ (green). The sister cell, a9.50, remains MAPK- and gives rise to the Prop1+ cell (red). Ets1/2 activation causes the transcription of *TCF* in the a10.97 pair allowing for Wnt competence. The left a10.97 and right a10.97 intercalate at the midline and the posterior cell receives the Wnt7 ligand leading to the expression of *FoxD* only in a10.97. FoxD represses *Mitf* in the presumptive ocellus while *Mitf* remains active in the otolith (dark green).

a

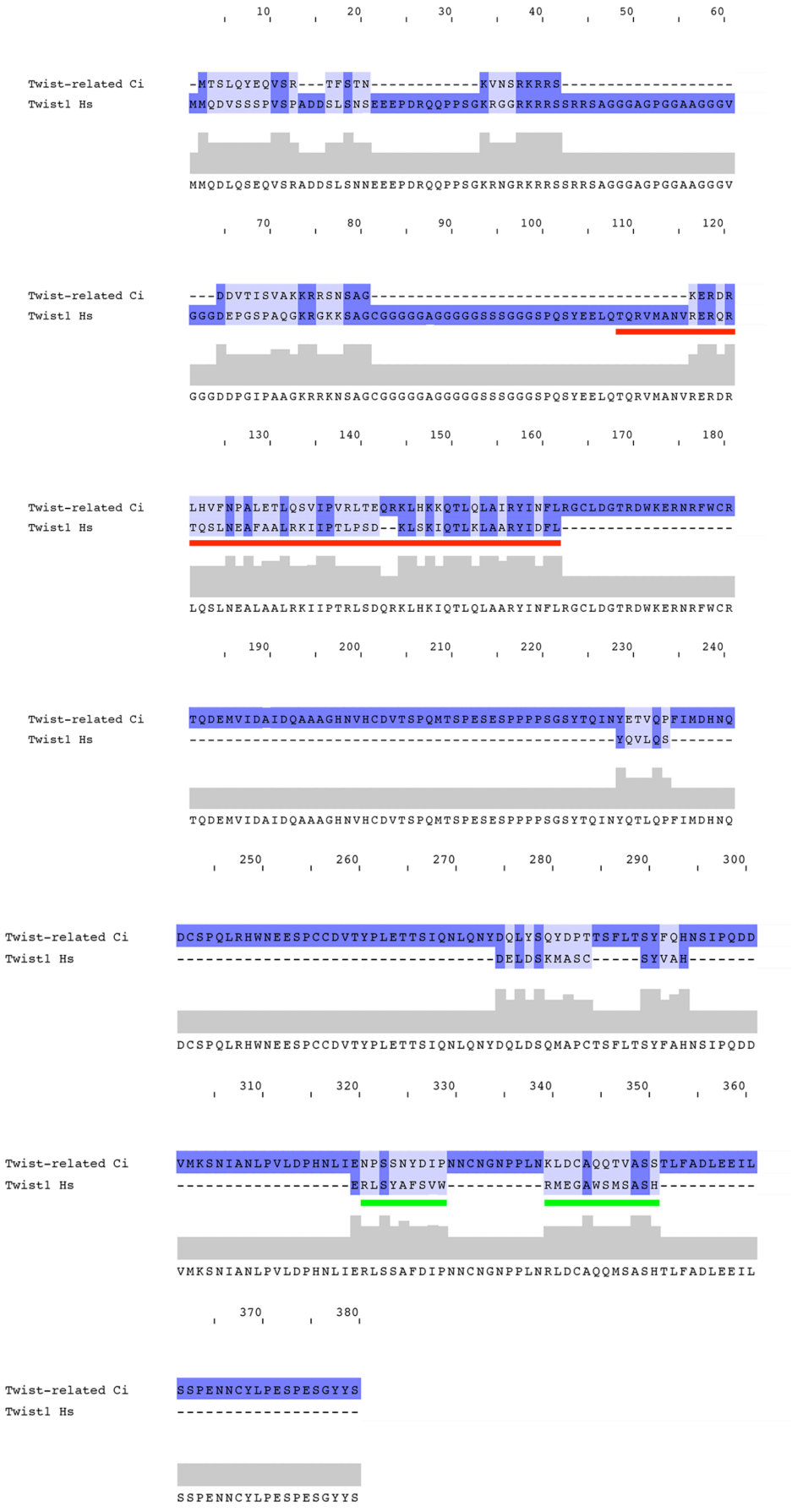
10 20 30 40 50 60
Twist-related Ci
Twist1 Hs
-MTSLQYEQVSR---TFSTN----------KVNSRKRRS----------
MMQDVSSSPVSPADDSLSNSEEEPDRQQPPSGKRGGRKRRSSRRSAGGGAGPGGAAGGGV
MMQDLQSEQVSRADDSLSNNEEEPDRQQPPSGKRNGRKRRSSRRSAGGGAGPGGAAGGGV
70 80 90 100 110 120
Twist-related Ci
Twist1 Hs
---DDVTISVAKKRRSNSAG----------KERDR
GGGDEPGSPAQGKRGKKSAGCGGGGGAGGGGGSSSGGGSPQSYEELQTQRVMANVRERQR
GGGDDPGIPAAGKRRKNSAGCGGGGGAGGGGGSSSGGGSPQSYEELQTQRVMANVRERDR
130 140 150 160 170 180
Twist-related Ci
Twist1 Hs
LHVFNPALETLQSVIPVRLTEQRKLHKKQTLQLAIRYINFLRGCLDGTRDWKERNRFWCR
TQSLNEAFAALRKIIPTLPSD--KLSKIQTLKLAARYIDFL----------
LQSLNEALAALRKIIPTRLSDQRKLHKIQTLQLAARYINFLRGCLDGTRDWKERNRFWCR
190 200 210 220 230 240
Twist-related Ci
Twist1 Hs
TQDEMVIDAIDQAAAGHNVHCDVTSPQMTSPESESPPPPSGSYTQINYETVQPFIMDHNQ
----------YQVLQS-------
TQDEMVIDAIDQAAAGHNVHCDVTSPQMTSPESESPPPPSGSYTQINYQTLQPFIMDHNQ
250 260 270 280 290 300
Twist-related Ci
Twist1 Hs
DCSPQLRHWNEESPCCDVTYPLETTSIQNLQNYDQLYSQYDPTTSFLTSYFQHNSIPQDD
----------DELDSKMASC-----SYVAH-------
DCSPQLRHWNEESPCCDVTYPLETTSIQNLQNYDQLDSQMAPCTSFLTSYFAHNSIPQDD
310 320 330 340 350 360
Twist-related Ci
Twist1 Hs
VMKSNIANLPVLDPHNLIENPSSNYDIPNNCNGNPPLNKLDCAQQTVASSTLFADLEEIL
----------ERLSYAFSVW----------RMEGAWSMSASH----------
VMKSNIANLPVLDPHNLIERLSSAFDIPNNCNGNPPLNRLDCAQQMSASHTLFADLEEIL
370 380
Twist-related Ci
Twist1 Hs
SSPENNCYLPESPESGYYS

SSPENNCYLPESPESGYYS

b

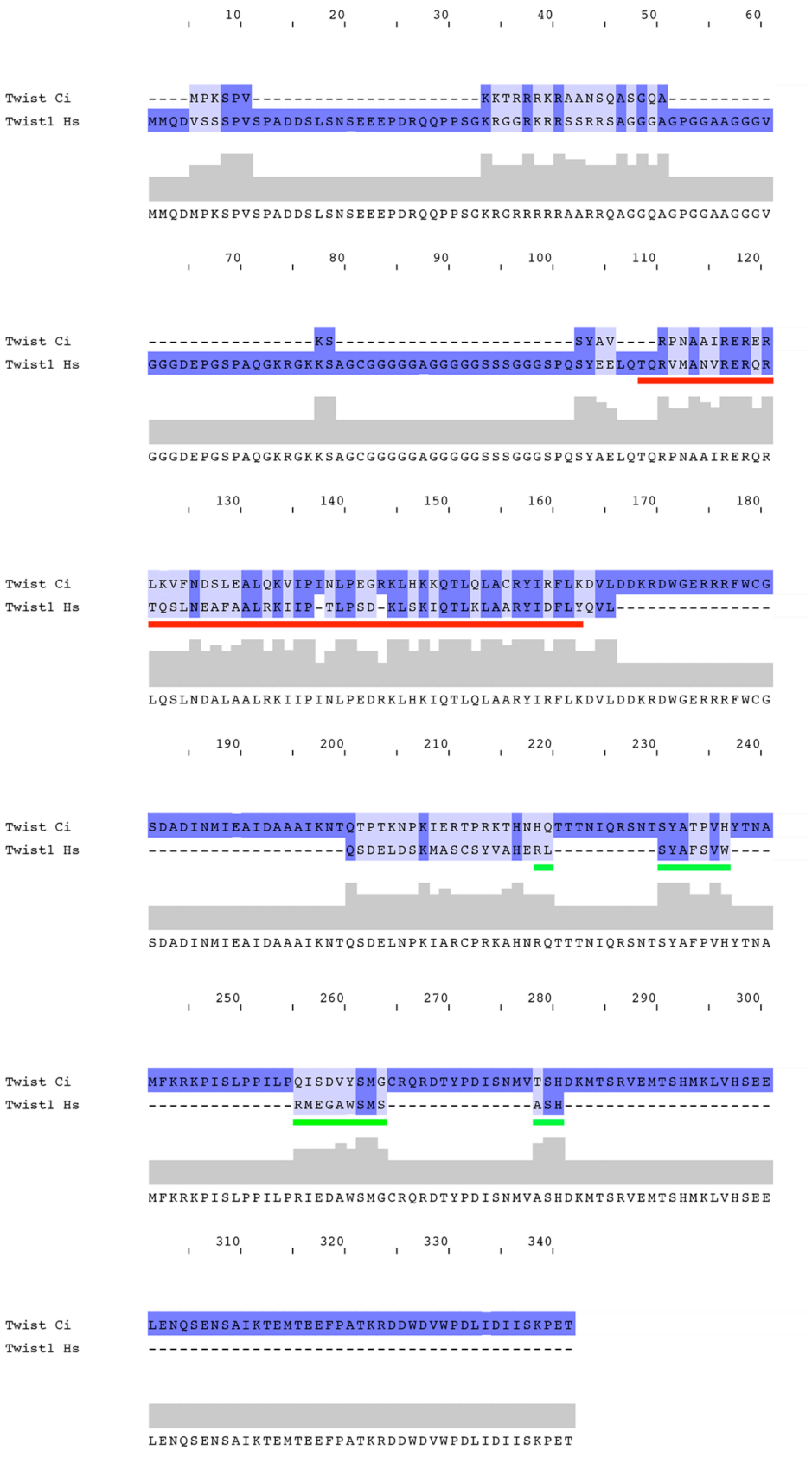
10 20 30 40 50 60
Twist Ci ----MPKSPV----------KKTRRRKRAANSQASGQA----------
Twist1 Hs MMQDVSSSPVSPADDSLSNSEEEPDRQQPPSGKRGGRKRRSSRRSAGGGAGPGGAAGGGV
MMQDMPKSPVSPADDSLSNSEEEPDRQQPPSGKRGRRRRRAARRQAGGQAGPGGAAGGGV
70 80 90 100 110 120
Twist Ci ----------KS----------SYAV----RPNAAIRERER
Twist1 Hs GGGDEPGSPAQGKRGKKSAGCGGGGGAGGGGGSSSGGGSPQSYEELQTQRVMANVRERQR
GGGDEPGSPAQGKRGKKSAGCGGGGGAGGGGGSSSGGGSPQSYAELQTQRPNAAIRERQR
130 140 150 160 170 180
Twist Ci LKVFNDSLEALQKVIPINLPEGRKLHKKQTLQLACRYIRFLKDVLDDKRDWGERRRFWCG
Twist1 Hs TQSLNEAFAALRKIIP-TLPSD-KLSKIQTLKLAARYIDFLYQVL----------
LQSLNDALAALRKIIPINLPEDRKLHKIQTLQLAARYIRFLKDVLDDKRDWGERRRFWCG
190 200 210 220 230 240
Twist Ci SDADINMIEAIDAAAIKNTQTPTKNPKIERTPRKTHNHQTTTNIQRSNTSYATPVHYTNA
Twist1 Hs ----------QSDELDSKMASCSYVAHERL----------SYAFSVW----
SDADINMIEAIDAAAIKNTQSDELNPKIARCPRKAHNRQTTTNIQRSNTSYAFPVHYTNA
250 260 270 280 290 300
Twist Ci MFKRKPISLPPILPQISDVYSMGCRQRDTYPDISNMVTSHDKMTSRVEMTSHMKLVHSEE
Twist1 Hs ----------RMEGAWSMS----------ASH----------
MFKRKPISLPPILPRIEDAWSMGCRQRDTYPDISNMVASHDKMTSRVEMTSHMKLVHSEE
310 320 330 340
Twist Ci LENQSENSAIKTEMTEEFPATKRDDWDVWPDLIDIISKPET
Twist1 Hs ----------
LENQSENSAIKTEMTEEFPATKRDDWDVWPDLIDIISKPET

Appendix E | *Ciona intestinalis* Twist is the closest homolog to human Twist1. a, *Ciona Twist*-related (model ID: KH.C5.554.v1.A.nonSL1-1) aligned to Human *Twist1*. The best blastp hit for *Twist*-related in the vertebrate database is atonal homolog 1a (*Danio rerio*). **b**, *Ciona Twist* (model ID: KH.C5.202.v1.A.ND1-1) aligned to Human *Twist1*. The best blastp hit for *Twist* in the vertebrate database is twist-related protein (*Xenopus laevis*), expressed in cranial neural crest. Alignment generated using webPRANK. The red underline indicates the annotated Human bHLH and the green underline shows the C-terminal Twist Box.

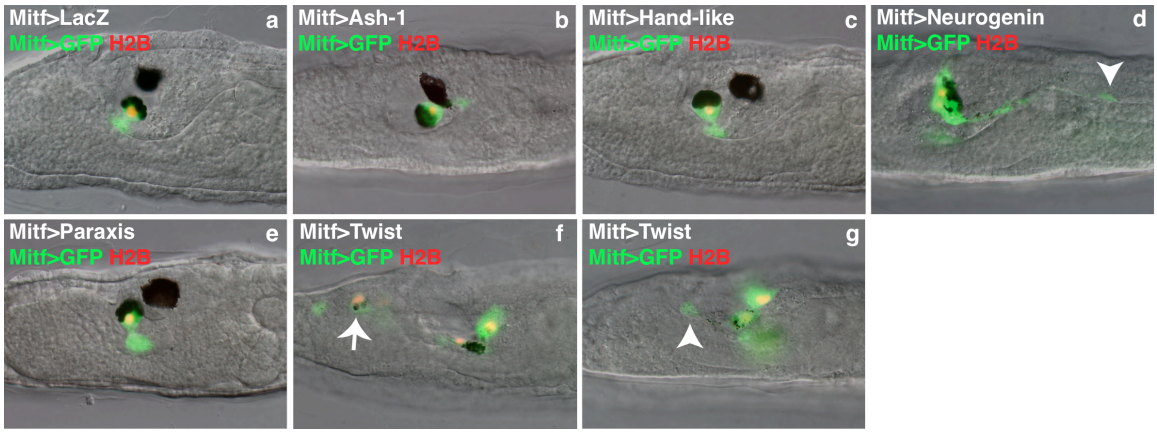
Mitf>LacZ
Mitf>GFP H2B
a
Mitf>Ash-1
Mitf>GFP H2B
b
Mitf>Hand-like
Mitf>GFP H2B
c
Mitf>Neurogenin
Mitf>GFP H2B
d
Mitf>Paraxis
Mitf>GFP H2B
e
Mitf>Twist
Mitf>GFP H2B
f
Mitf>Twist
Mitf>GFP H2B
g

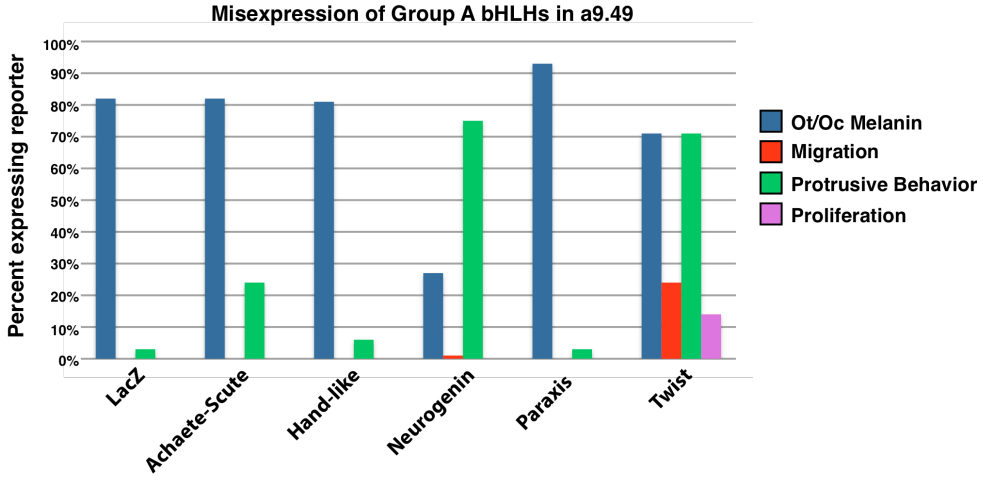
Misexpression of Group A bHLHs in a9.49
Percent expressing reporter
100%
90%
80%
70%
60%
50%
40%
30%
20%
10%
0%
LacZ
Achaete-Scute
Hand-like
Neurogenin
Paraxis
Twist
Ot/Oc Melanin
Migration
Protrusive Behavior
Proliferation

Appendix F | Related group A bHLH genes do not cause the same phenotype as Twist when misexpressed in a9.49. All larvae electroporated with *Mitf>GFP* and *Mitf>H2B mCherry* and 100 embryos were scored in each condition. **a**, Larva electroporated with *Mitf>LacZ*. **b**, Larva electroporated with *Mitf>Ash-1*. **c**, Larva electroporated with *Mitf>Hand-like*. **d**, Larva electroporated with *Mitf>Neurogenin*. **e**, Larva electroporated with *Mitf>Paraxis*. **f**,**g**, Larvae electroporated with *Mitf>Twist*. Graph summarizes the phenotypes for each condition. Larvae were scored positive for ot/oc melanin if both otolith and ocellus pigmentation were observed. H2B mCherry fluorescence found outside of the sensory vesicle was marked positive for migration (arrow). Larvae with irregular or elongated cell shapes were marked for protrusive behavior (arrowheads). Five or more Mitf+ cells seen in a larva was scored as positive for proliferation. In all images anterior is to the left.

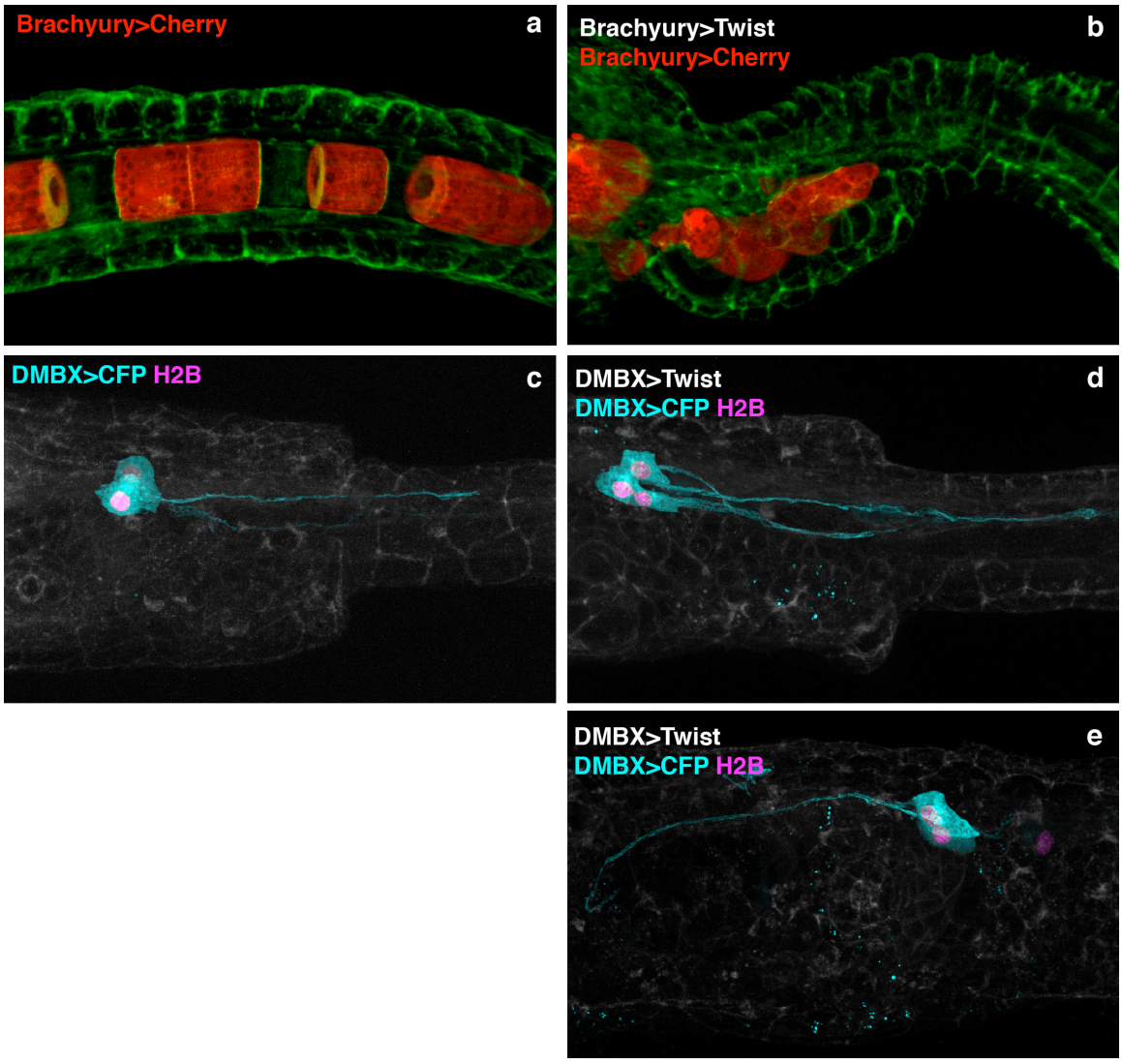
Brachyury>Cherry
a
Brachyury>Twist
Brachyury>Cherry
b
DMBX>CFP H2B
c
DMBX>Twist
DMBX>CFP H2B
d
DMBX>Twist
DMBX>CFP H2B
e

Appendix G | Misexpression of Twist in other lineages does not induce migratory cells. a, Tailbud embryo electroporated with *Brachyury>mCherry* labels the notochord. **b**, Tailbud embryo co-electroporated with *Brachyury>mCherry* and *Brachyury>Twist* displays a misshapen notochord causing a truncated tail. **c**, Larva electroporated with *DMBX>CFP* and *DMBX>H2B YFP* labels the A12.239 lineage within the motor ganglion. **d**, Larva co-electroporated with *DMBX>CFP, DMBX>H2B YFP, and DMBX>Twist.* An extra cell is seen but the lineage still projects axons posteriorly. **e**, Twist misexpression sometimes results in anteriorly projecting axons, but the cell morphology and position of cell body remain largely unaffected. In all images anterior is to the left.

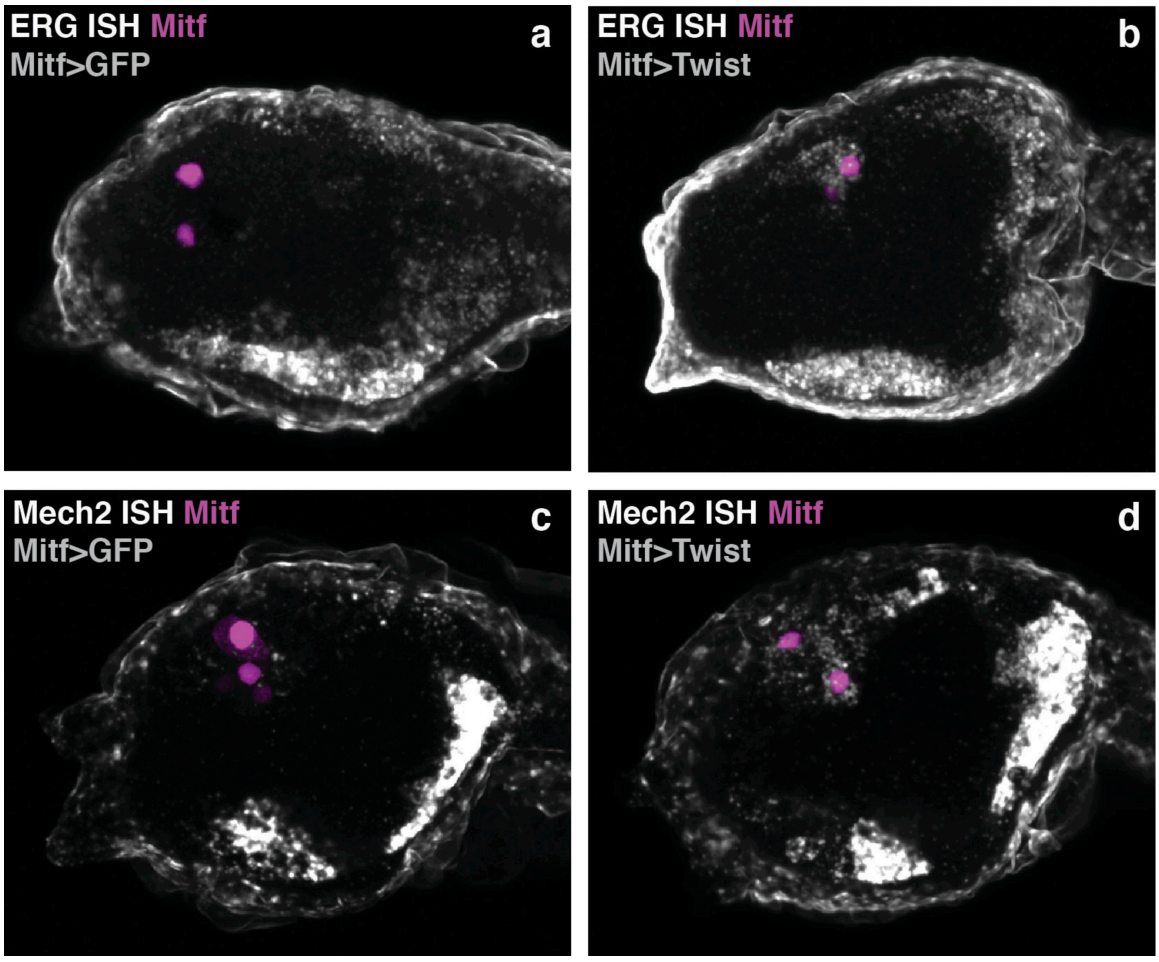
ERG ISH Mitf
Mitf>GFP
a
ERG ISH Mitf
Mitf>Twist
b
Mech2 ISH Mitf
Mitf>GFP
c
Mech2 ISH Mitf
Mitf>Twist
d

Appendix H | Misexpression of Twist in a9.49 causes the ectopic activation of mesenchyme genes. a, Late tailbud embryo hybridized with an *ERG* probe (white) and electroporated with *Mitf>GFP* (plasmid control) and *Mitf>LacZ*, which was detected with an antibody for β-gal (magenta). **b**, Late tailbud embryo hybridized with an *ERG* probe and electroporated with *Mitf>Twist* and *Mitf>LacZ*. Note the ectopic expression of ERG in a9.49. **c**, Late tailbud embryo hybridized with a *Mech2* probe and electroporated with *Mitf>GFP and Mitf>LacZ*. **d**, Late tailbud embryo hybridized with a *Mech2* probe and electroporated with *Mitf>Twist* and *Mitf>LacZ*. Note the ectopic expression of *Mech2* in a9.49.

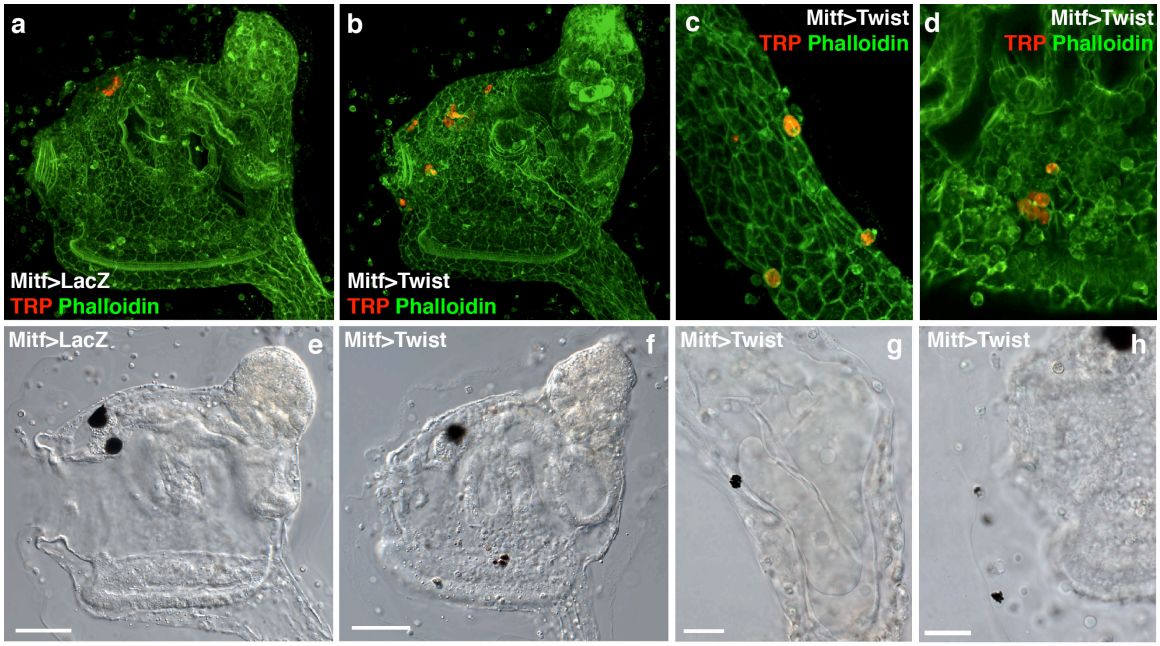
a
Mitf>LacZ
TRP Phalloidin
b
Mitf>Twist
TRP Phalloidin
c
Mitf>Twist
TRP Phalloidin
d
Mitf>Twist
TRP Phalloidin
Mitf>LacZ
e
Mitf>Twist
f
Mitf>Twist
g
Mitf>Twist
h

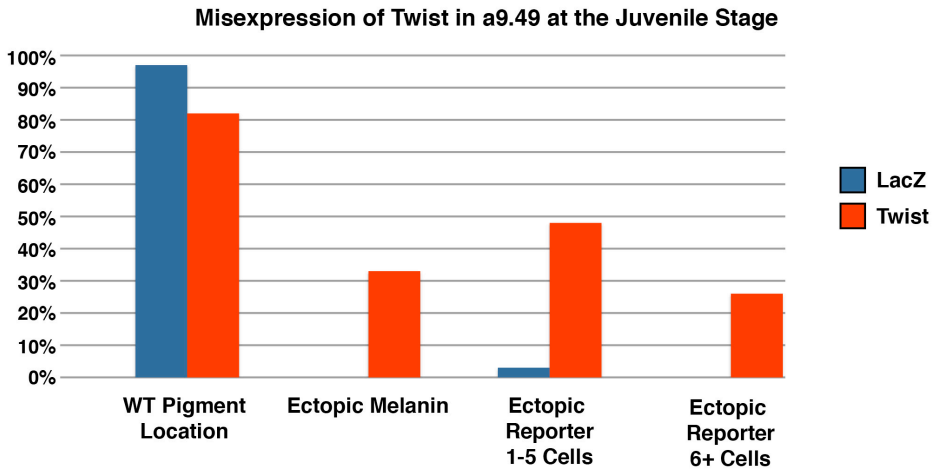
Misexpression of Twist in a9.49 at the Juvenile Stage
100%
90%
80%
70%
60%
50%
40%
30%
20%
10%
0%
WT Pigment Location
Ectopic Melanin
Ectopic Reporter 1-5 Cells
Ectopic Reporter 6+ Cells
LacZ
Twist

Appendix I | Twist misexpression causes ectopic a9.49 cells in juveniles. a, Juvenile electroporated with *Mitf>LacZ* and *TRP>mCherry* (n=100). **b**, Juvenile electroporated with *Mitf>Twist* and *TRP>mCherry* (n=100). **c**, Stalk of a juvenile electroporated with *Mitf>Twist* and *TRP>mCherry*. **d**, View of internal mesenchyme electroporated with *Mitf>Twist* and *TRP>mCherry*. **e**, DIC image of juvenile electroporated with *Mitf>LacZ* shows normal pigmentation. **f**, DIC image of juvenile electroporated with *Mitf>Twist* displays ventral ectopic pigment. **g**, DIC image of juvenile stalk electroporated with *Mitf>Twist* shows ectopic pigment. **h**, DIC image of juvenile tunic shows melanized tunic cells. In all images anterior is to the left. Scale bar represents 50 μm in e and f, and 25 μm in g and h.

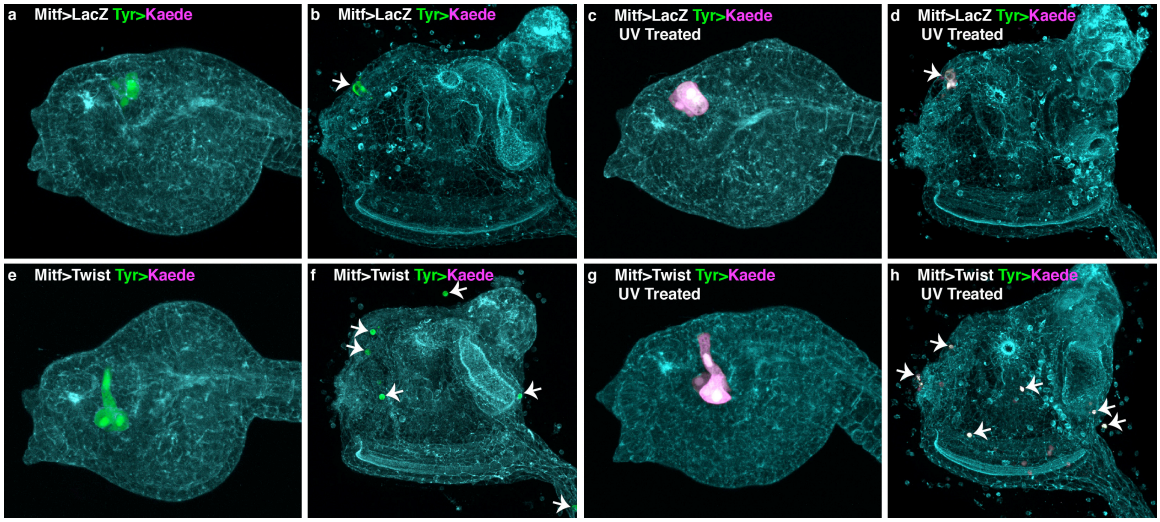
a Mitf>LacZ Tyr>Kaede
b Mitf>LacZ Tyr>Kaede
c Mitf>LacZ Tyr>Kaede
UV Treated
d Mitf>LacZ Tyr>Kaede
UV Treated
e Mitf>Twist Tyr>Kaede
f Mitf>Twist Tyr>Kaede
g Mitf>Twist Tyr>Kaede
UV Treated
h Mitf>Twist Tyr>Kaede
UV Treated

Appendix J | Lineage tracing of Mitf>Twist juveniles confirms ectopic cells arose from a9.49. a, Tailbud electroporated with *Mitf>LacZ* and *Tyr>Kaede* labeled the a9.49 lineage (green). **b**, Non-converted Kaede traced through the juvenile stage (arrow). **c**, Tailbud electroporated with *Mitf>LacZ* and *Tyr>Kaede* in which UV treatment converted the fluorescence (red). **d**, Photoconverted Kaede traced through the juvenile stage (arrow). **e**, Tailbud electroporated with *Mitf>Twist* and *Tyr>Kaede* labeled the a9.49 lineage (green). **f**, Non-converted Kaede traced through the juvenile stage (arrows). **g**, Tailbud electroporated with *Mitf>Twist* and *Tyr>Kaede* in which UV treatment converted the fluorescence (red). **h**, Photoconverted Kaede traced through the juvenile stage (arrows).

PCR Product Name	Forward Primer	Reverse Primer
Mitf 963 bp	ctgctaaaacaggctaacag	cgaatatctagtttacgagac
Prop1 1474 bp	tgttgctcatgctcgctgtc	aaaccaaacctaaacgcaaaggc
βγ-crystallin 1110 bp	gtccttacgtcataataaac	gccattgttccaccagcaac
Twist 1526 bp	accacagcttctattatatattaacctc	catcgtgtgttgattgatttgaaag
Ash-1 CDS	atggcgaccggaagtgacgaac	gtcacgtggtgatcagaaatg
Hand-like CDS	atgacaacagtagttatgcg	ttaataactttcgttgcgatg
Paraxis CDS	atgccagatcacgtggttcatacg	tcacaatcgaaccgtcgaagc
Neurogenin CDS	atgttggatttttcttcaaataagtcgg	ttatcggagtaaatgcatggagtag
Wnt7 CDS	atgtacaattggagcagctt	gcacttgtcagttgcaggta
Stabilized β-catenin CDS	acgatgggaacttccccgatac	ttagaggtcagtatcgagccatg
Twist CDS	atgccaaaatcaccagtcaag	ccacacattaagtttctggc
Foxd Full length CDS	atgatgacagtgcagtgttg	ttaagttctgccaaaacaaggcc
Foxd DBD CDS	cgaatcaaagaagaatgtaaaacctccg	ccggaacggatctctctg
Foxd N-term CDS	atgatgacagtgcagtgttg	cggtgatttcggcaaccag

Appendix K I Primer pairs used as described in the Methods of Chapter II.

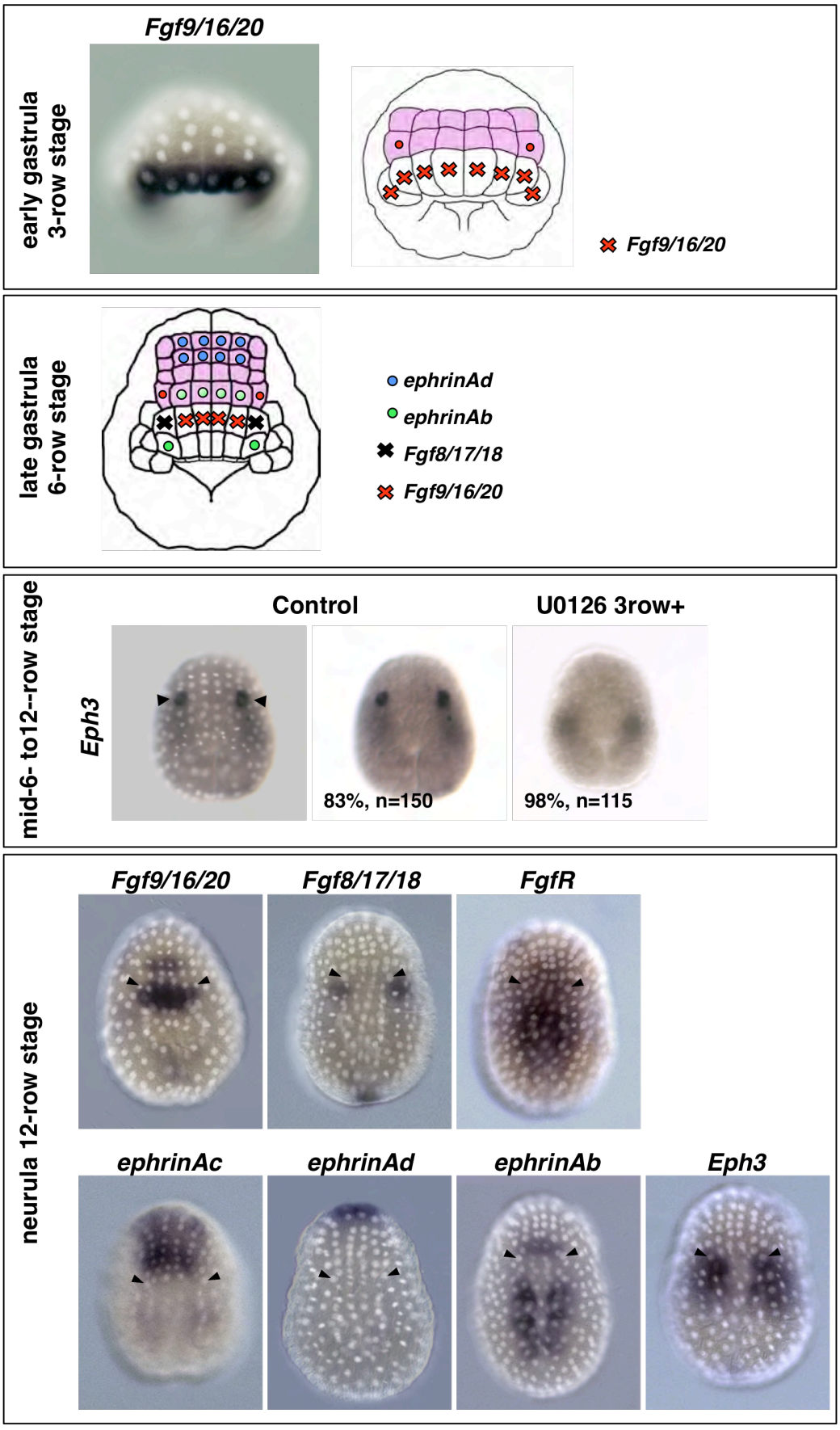
early gastrula
3-row stage
Fgf9/16/20
Fgf9/16/20
late gastrula
6-row stage
ephrinAd
ephrinAb
Fgf8/17/18
Fgf9/16/20
mid-6- to12--row stage
Eph3
Control
U0126 3row+
83%, n=150
98%, n=115
neurula 12-row stage
Fgf9/16/20
Fgf8/17/18
FgfR
ephrinAc
ephrinAd
ephrinAb
Eph3

Appendix L | Expression of *Fgf, ephrin FGFR* and *Eph3* at neural plate and neurula stages. A red dot indicates the pigment cell lineage on the schematics and a-line neural plate cells are colored in pink. *ephrinAc* is not expressed at the 6-row neural plate stage, but is expressed in all animal cells at the early gastrula stage. FGFRc and Eph3 are ubiquitous during early gastrula and neural plate stages. Broad low levels of expression are also detected at the 12-row neural plate stage, with specific domains of stronger expression also detected. Strong *Eph3* expression starts to be detected in the pigment cell lineage between the 6- and 12-row neural plate stage. This expression was dependent upon MEK activity; embryos were treated with U0126 from the 3-row neural plate stage. Arrowheads point to the nucleus of a9.49 in the middle panel and a10.97 in the lower panels.

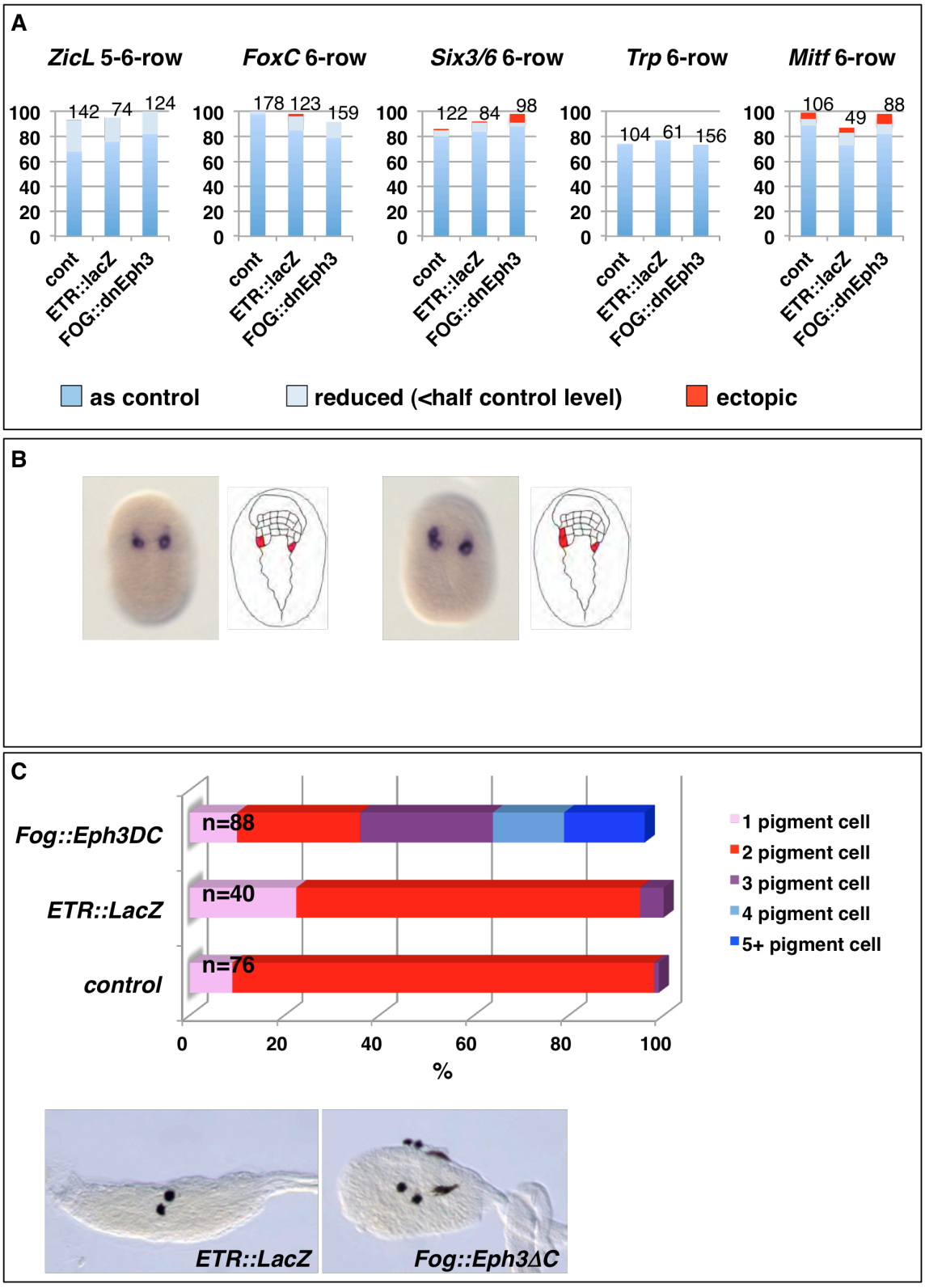
A
ZicL 5-6-row
FoxC 6-row
Six3/6 6-row
Trp 6-row
Mitf 6-row
100
80
60
40
20
0
142 74 124
178 123 159
122 84 98
104 61 156
106 49 88
cont
ETR::lacZ
FOG::dnEph3
as control
reduced (<half control level)
ectopic
B
C
Fog::Eph3DC
ETR::LacZ
control
n=88
n=40
n=76
0
20
40
60
80
100
%
1 pigment cell
2 pigment cell
3 pigment cell
4 pigment cell
5+ pigment cell
ETR::LacZ
Fog::Eph3ΔC

Appendix M | Gene expression and pigment cell formation in embryos electroporated with *Fog>Eph3ΔC*. **a**, Graphs show the expression of the genes indicated (above) in control and electroporated embryos. Embryos were scored following the key (below). **b**, *Trp* expression at 12-row neurula stage. Each embryo half was scored independently. Data is presented as percentage of embryos with stronger expression in a10.97 compared to a10.98 (a10.97>a10.98), equal expression between a10.97 and a10.98 (a10.97=a10.98) and expression in row IV cells, which was always in the lateral column. **c**, The number of pigment cells counted in electroporated embryos.

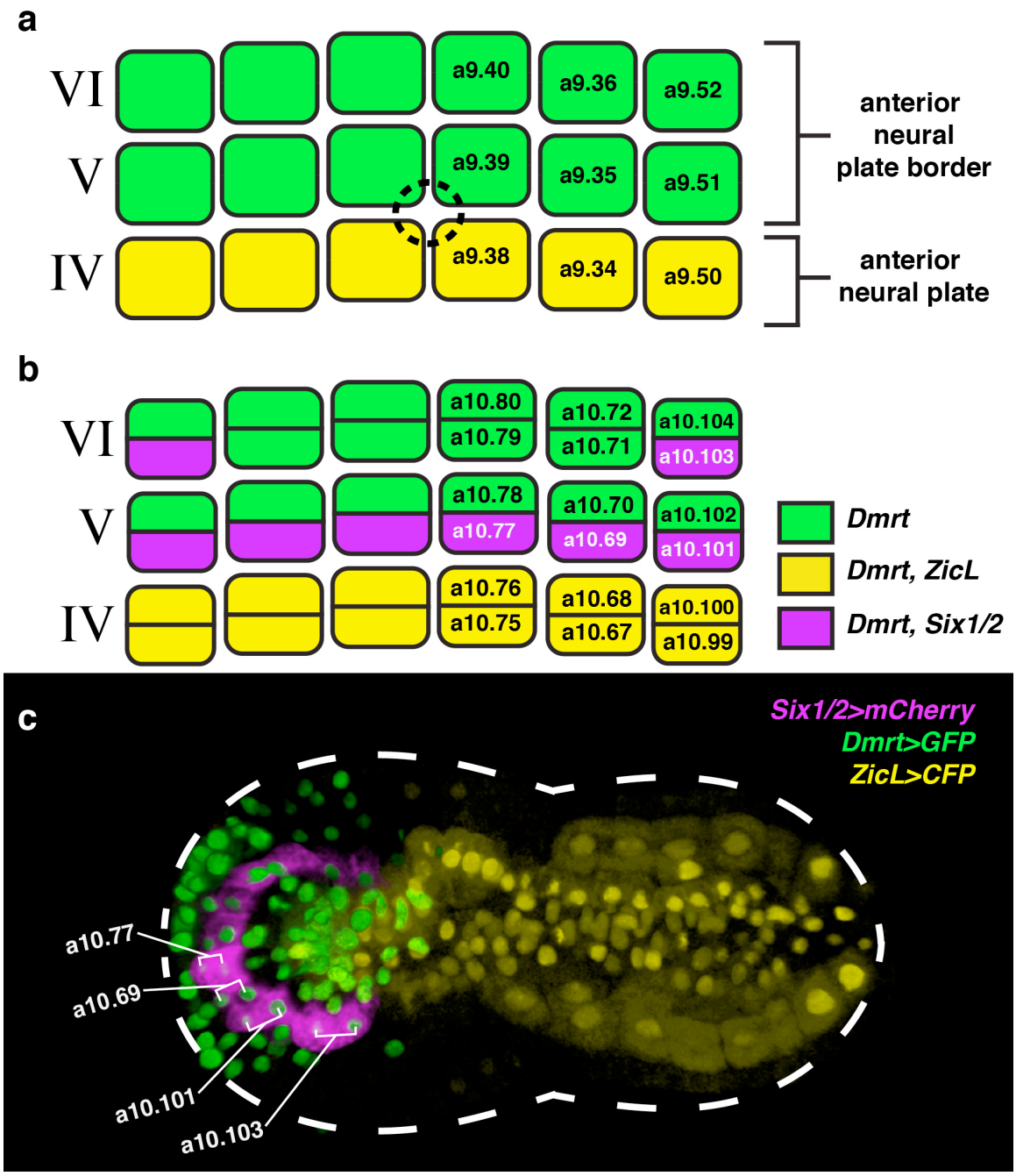
a
VI
V
IV
a9.40
a9.36
a9.52
a9.39
a9.35
a9.51
a9.38
a9.34
a9.50
anterior neural plate border
anterior neural plate
b
VI
V
IV
a10.80
a10.79
a10.72
a10.71
a10.104
a10.103
a10.78
a10.77
a10.70
a10.69
a10.102
a10.101
a10.76
a10.75
a10.68
a10.67
a10.100
a10.99
Dmrt
Dmrt, ZicL
Dmrt, Six1/2
c
Six1/2>mCherry
Dmrt>GFP
ZicL>CFP
a10.77
a10.69
a10.101
a10.103

Appendix N | Lineage information for *Six1/2* expression in *Ciona intestinalis* from the gastrula to initial tailbud stage. a, Schematic of the anterior neural plate border at the mid gastrula stage, including cell lineage nomenclature. *Dmrt* is initially activated in six blastomeres of 64-cell embryos (a7.9, a7.10 and a7.13). This lineage produces only the anterior neural plate, and adjacent anterior neural plate border, which forms the PPE. The anterior most *ZicL+* cells of row IV (yellow) mark the boundary of the neural plate, which gives rise to the anterior sensory vesicle in tailbud embryos. **b**, Schematic of the anterior neural plate border during the gastrula-neurula transition, indicating the lineage-specific expression of *Six1/2* in magenta. *Six1/2* is initially expressed in eight cells comprising the posterior row V cells and the posterior lateral cells of row VI. **c**, Dorsal view of initial tailbud embryo co-electroporated with *Six1/2>mCherry*, *Dmrt>GFP*, and *ZicL>CFP*. At this stage the cells initially expressing *Six1/2* have divided once, giving rise to 16 cells total. Brackets indicate the derivatives of the annotated lineages shown in **b**. Anterior is to the left.

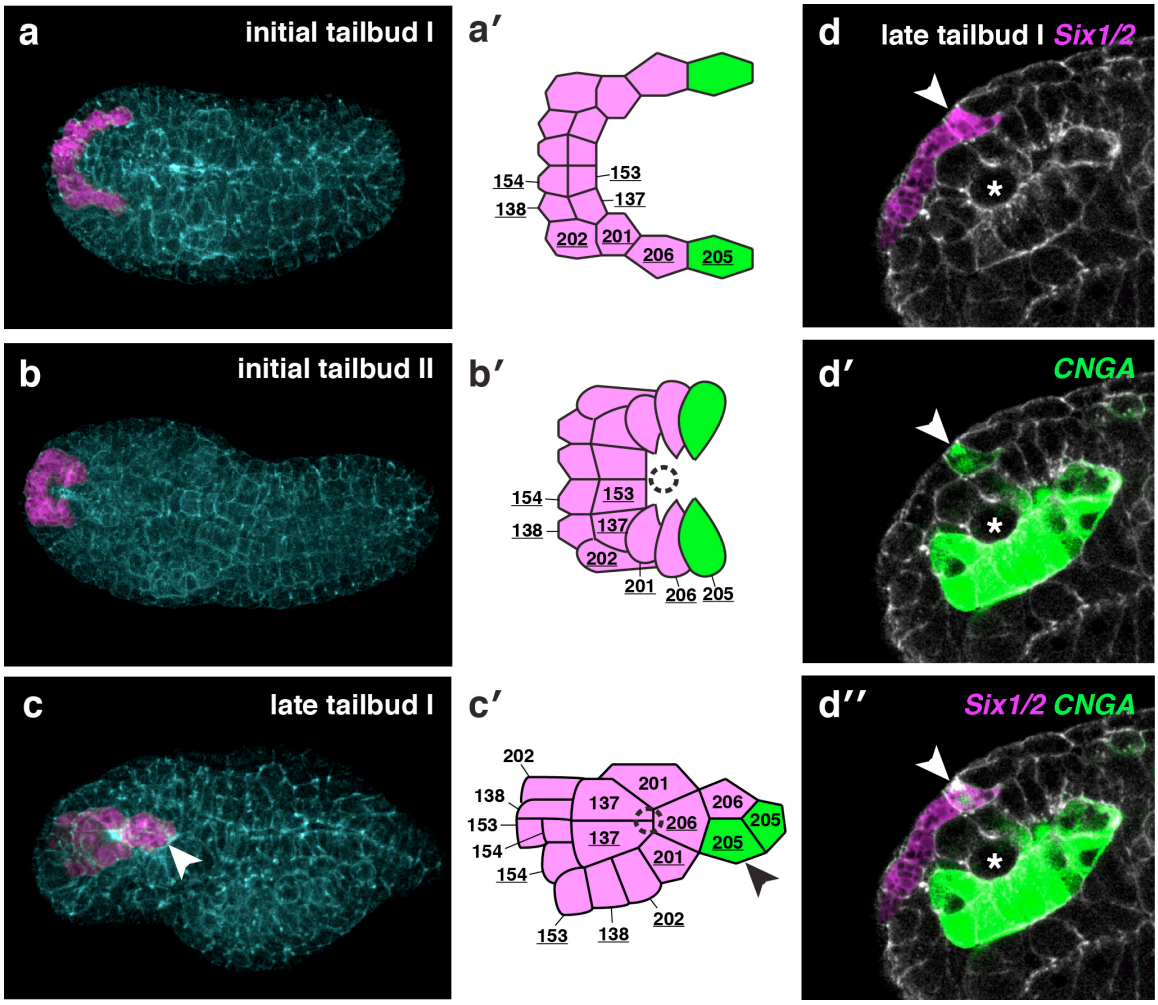
a
initial tailbud I
a′
154
153
138
137
202
201
206
205
d
late tailbud I Six1/2
b
initial tailbud II
b′
154
153
138
137
202
201
206
205
d′
CNGA
c
late tailbud I
c′
202
201
138
137
206
153
205
154
137
201
154
202
153
138
d″
Six1/2 CNGA

Appendix O I *Six1/2+* cell morphogenesis in *Ciona intestinalis* from the initial tailbud stage to late tailbud I. a-c, Dorsal views of tailbud embryos electroporated with *Six1/2>mCherry* (magenta) and counterstained with phalloidin (blue). Arrowheads identify PPE-derived cells fated to become GnRH neurons. **a**, At the initial tailbud stage I the *Six1/2+* cells are arranged in a U-shape, anterior to the neural plate. **a′**, Schematic indicates that the U-shape is composed of 16 cells total at the 11th generation (i.e., a11.154, a11.138, etc.). There are no further divisions of these cells until after the late tailbud I stage. The green colored cells indicate a11.205, which are fated to become PPE-derived GnRH neurons. **b**, At the initial tailbud stage II the lateral edges of the *Six1/2+* cells begin to intercalate towards the midline. **b′**, Schematic shows a dotted circle where the future opening of the oral siphon forms. **c**, At the late tailbud I stage the *Six1/2+* cells have completed intercalation. The bright phalloidin signal in the center of the pattern marks the apically localized actin of cells constricted towards the oral opening. At this stage the *Six1/2+* cells are positioned on top of the anterior sensory vesicle over the ocellus. **c′** Schematic shows a dotted circle where the oral opening forms. More anterior cells have undergone local cellular rearrangements. Underlined cell lineages are derived from the left side of the embryo (i.e., a11.154). **d-d′′**, Anterior lateral view of late tailbud I stage embryo electroporated with *Six1/2>GFP* and *CNGA>mCherry.* Asterisks indicate the ocellus. **d,** Shows the *Six1/2>GFP* channel. **d′,** Shows the *CNGA>mCherry* channel (see Fig. 3c for larval expression). **d′′**, Shows the merge of *Six1/2>GFP* and *CNGA>mCherry*.

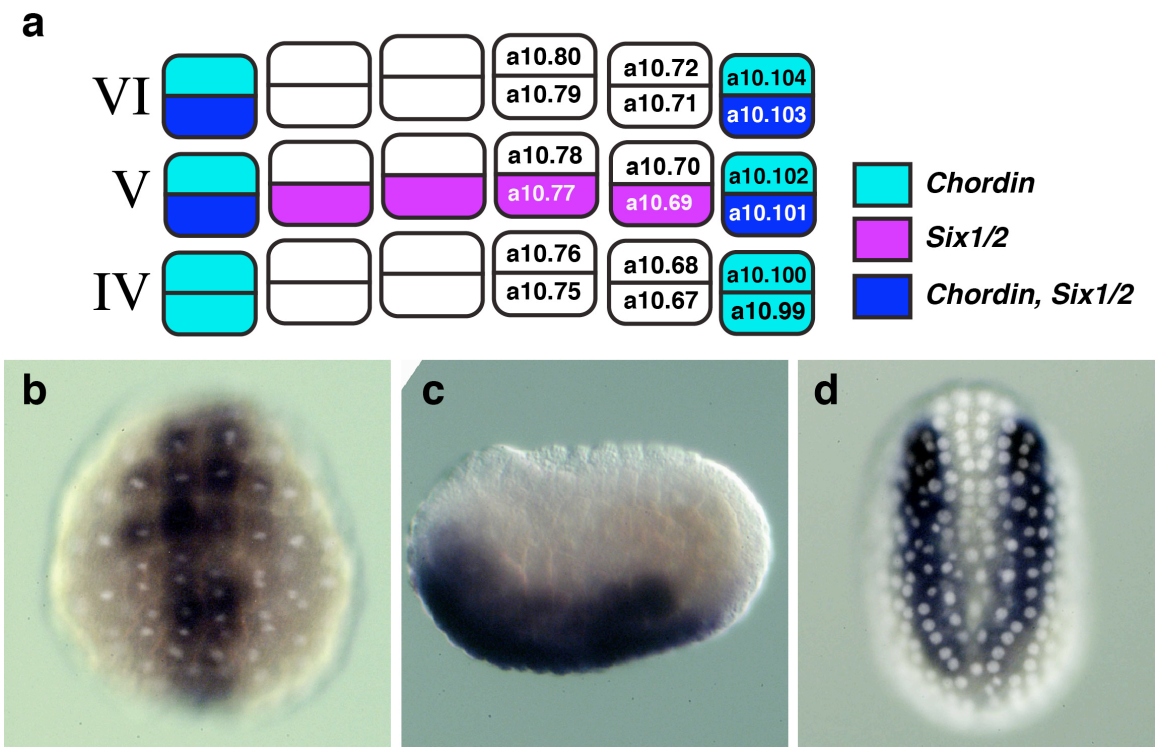
a
VI
V
IV
a10.80
a10.79
a10.78
a10.77
a10.76
a10.75
a10.72
a10.71
a10.70
a10.69
a10.68
a10.67
a10.104
a10.103
a10.102
a10.101
a10.100
a10.99
Chordin
Six1/2
Chordin, Six1/2
b
c
d

Appendix P | Dorsal-ventral BMP patterning during PPE specification in *Ciona intestinalis*. a, Schematic of the anterior neural plate border during the gastrula-neurula transition, includes cell lineage nomenclature. *Chordin* and *Six1/2* are co-expressed in the lateral posterior derivatives of row V and VI (dark blue, Fig. 1b). **b**, Ventral view of mid gastrula stage embryo hybridized with a *BMP2/4* mRNA probe and merged with a DAPI nuclear counterstain. **c**, Lateral view of an embryo during the gastrula-neurula transition hybridized with a *BMP2/4* mRNA probe. Anterior is to the left. **d**, Dorsal view of an embryo during the gastrula-neurula transition hybridized with a *Chordin* mRNA probe and merged with a DAPI nuclear counterstain.

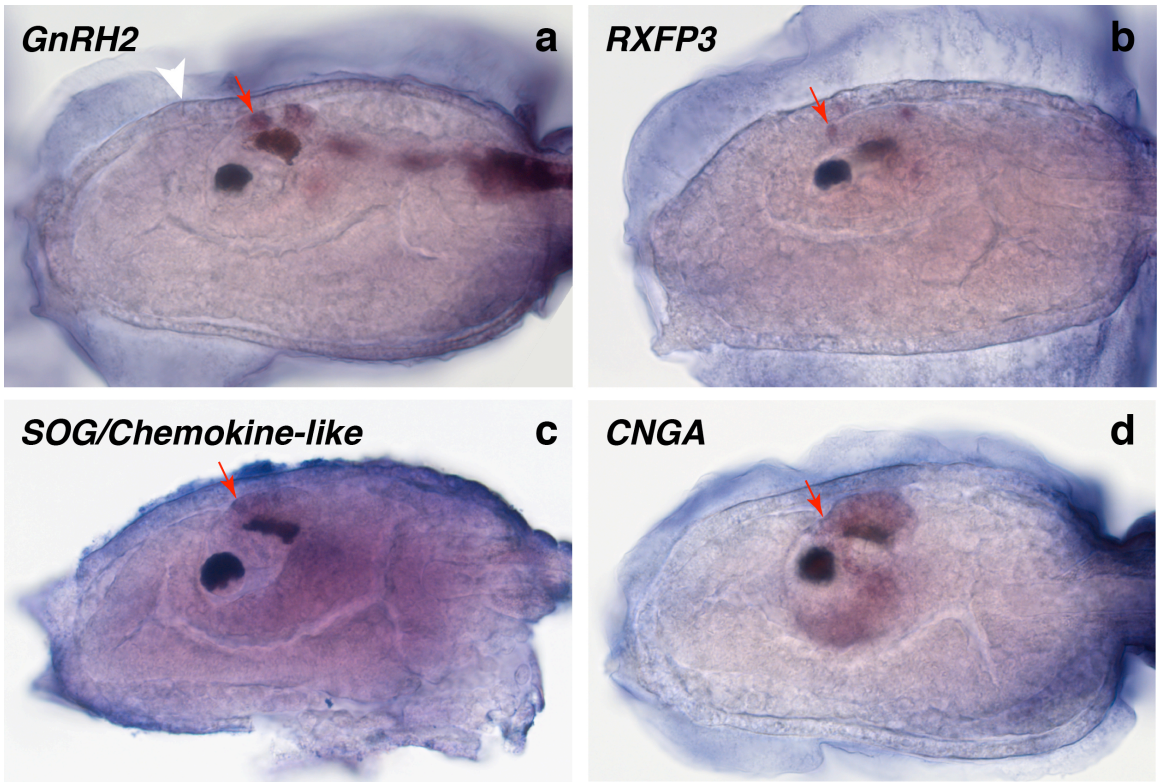
GnRH2
a
RXFP3
b
SOG/Chemokine-like
c
CNGA
d

Appendix Q | Endogenous expression of newly described reporter genes in *Ciona* hatched larvae. a-d, Brightfield anterior lateral views. **a**, Animal hybridized with a *GnRH2* mRNA probe. White arrowhead indicates the position of the oral opening. **b**, Animal hybridized with an *RXFP3* mRNA probe. **c**, Animal hybridized with a *SOG/Chemokine-like* mRNA probe. The heavily stained tunic was manually removed to reveal expression signal. **d**, Animal hybridized with a *CNGA* mRNA probe. Red arrows mark areas of comparable expression throughout the panels in presumed PPE-derived neurons. Adjacent signal in the ocellus associated photoreceptors makes it difficult to discriminate expression in PPE-derived neurons in panel **d**.

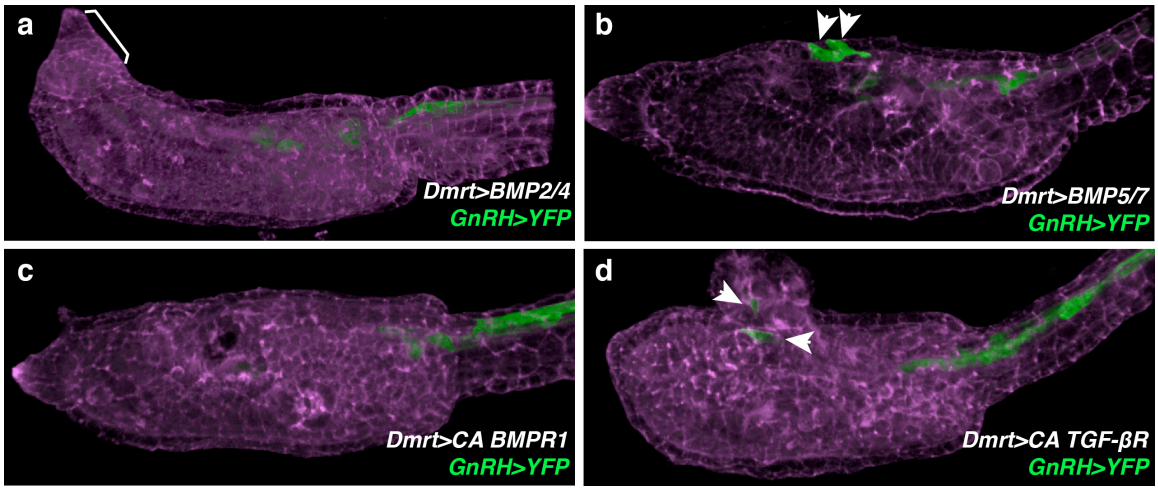
a
Dmrt>BMP2/4
GnRH>YFP
b
Dmrt>BMP5/7
GnRH>YFP
c
Dmrt>CA BMPR1
GnRH>YFP
d
Dmrt>CA TGF-βR
GnRH>YFP

Appendix R | *GnRH* expression requires BMP attenuation. a-d, Lateral view of larva electroporated with *GnRH>YFP* and counterstained with phalloidin (violet). **a**, Co-electroporated with *Dmrt>BMP2/4*. 196/200 larvae had no GnRH>YFP expression in anterior apical trunk epidermal neurons (aATENs) and displayed mild to severe morphogenetic defects. Bracket shows mild anterior morphological defect. **b**, Co-electroporated with *Dmrt>BMP5/7.* 124/200 larvae had *GnRH>YFP* expression in aATENs. **c**, Co-electroporated *Dmrt>CA BMPR1*. 197/200 larvae had no *GnRH>YFP* expression in aATENs. **d**, Co-electroporated with *Dmrt>CA TGF-βR*. 130/200 larvae had *GnRH>YFP* expression in aATENs and most displayed severe anterior neural tube defects. Arrowheads indicate the position of *GnRH* expression in aATENs. Anterior is to the left in all images.

a

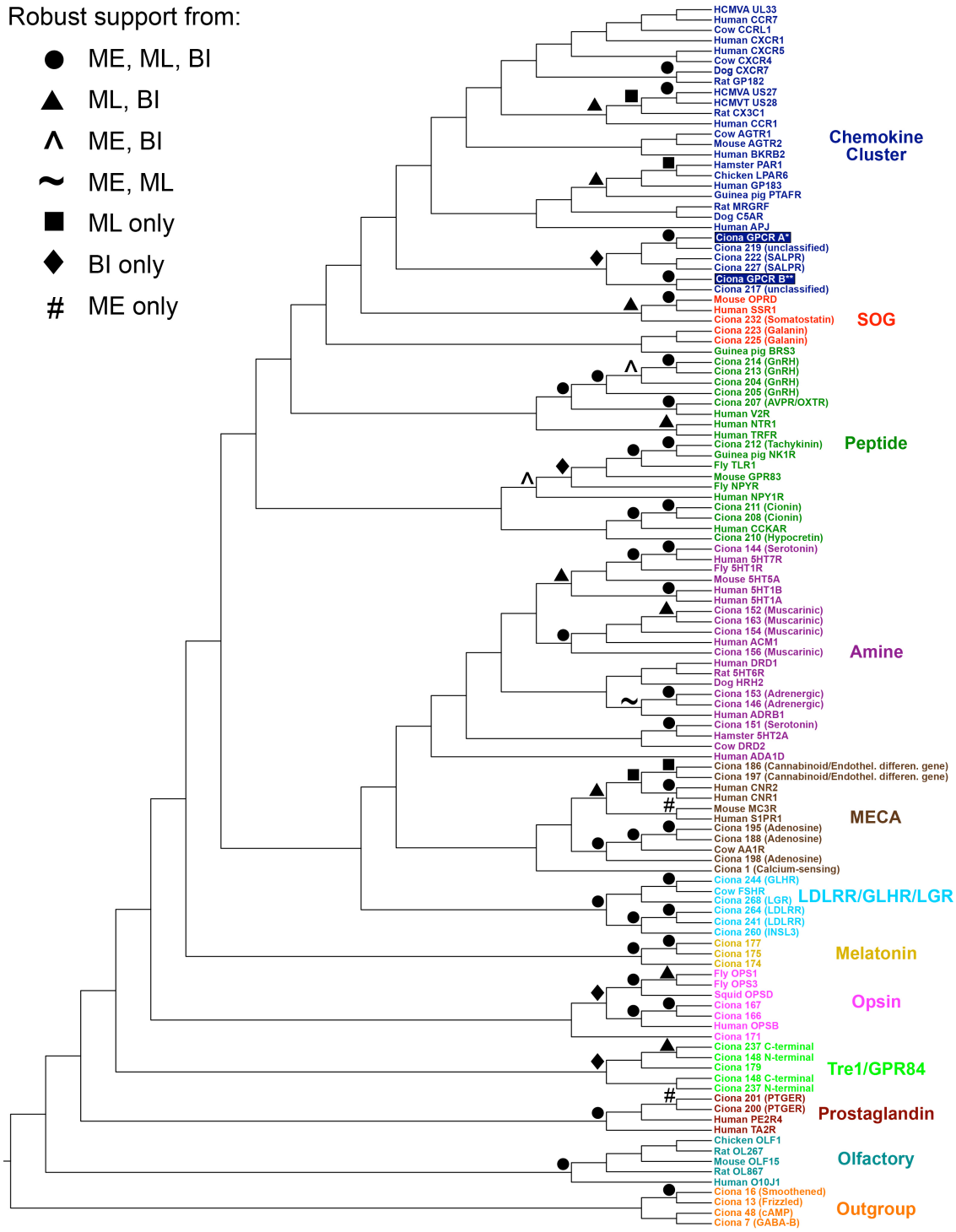
Robust support from:
ME, ML, BI
ML, BI
ME, BI
ME, ML
ML only
BI only
ME only
HCMVA UL33
Human CCR7
Cow CCRL1
Human CXCR1
Human CXCR5
Cow CXCR4
Dog CXCR7
Rat GP182
HCMVA US27
HCMVT US28
Rat CX3C1
Human CCR1
Cow AGTR1
Mouse AGTR2
Human BKRB2
Hamster PAR1
Chicken LPAR6
Human GP183
Guinea pig PTAFR
Rat MRGRF
Dog C5AR
Human APJ
Ciona GPCR A*
Ciona 219 (unclassified)
Ciona 222 (SALPR)
Ciona 227 (SALPR)
Ciona GPCR B**
Ciona 217 (unclassified)
Mouse OPRD
Human SSR1
Ciona 232 (Somatostatin)
Ciona 223 (Galanin)
Ciona 225 (Galanin)
Guinea pig BRS3
Ciona 214 (GnRH)
Ciona 213 (GnRH)
Ciona 204 (GnRH)
Ciona 205 (GnRH)
Ciona 207 (AVPR/OXTR)
Human V2R
Human NTR1
Human TRFR
Ciona 212 (Tachykinin)
Guinea pig NK1R
Fly TLR1
Mouse GPR83
Fly NPYR
Human NPY1R
Ciona 211 (Cionin)
Ciona 208 (Cionin)
Human CCKAR
Ciona 210 (Hypocretin)
Ciona 144 (Serotonin)
Human 5HT7R
Fly 5HT1R
Mouse 5HT5A
Human 5HT1B
Human 5HT1A
Ciona 152 (Muscarinic)
Ciona 163 (Muscarinic)
Ciona 154 (Muscarinic)
Human ACM1
Ciona 156 (Muscarinic)
Human DRD1
Rat 5HT6R
Dog HRH2
Ciona 153 (Adrenergic)
Ciona 146 (Adrenergic)
Human ADRB1
Ciona 151 (Serotonin)
Hamster 5HT2A
Cow DRD2
Human ADA1D
Ciona 186 (Cannabinoid/Endothel. differen. gene)
Ciona 197 (Cannabinoid/Endothel. differen. gene)
Human CNR2
Human CNR1
Mouse MC3R
Human S1PR1
Ciona 195 (Adenosine)
Ciona 188 (Adenosine)
Cow AA1R
Ciona 198 (Adenosine)
Ciona 1 (Calcium-sensing)
Ciona 244 (GLHR)
Cow FSHR
Ciona 268 (LGR)
Ciona 264 (LDLRR)
Ciona 241 (LDLRR)
Ciona 260 (INSL3)
Ciona 177
Ciona 175
Ciona 174
Fly OPS1
Fly OPS3
Squid OPSD
Ciona 167
Ciona 166
Human OPSB
Ciona 171
Ciona 237 C-terminal
Ciona 148 N-terminal
Ciona 179
Ciona 148 C-terminal
Ciona 237 N-terminal
Ciona 201 (PTGER)
Ciona 200 (PTGER)
Human PE2R4
Human TA2R
Chicken OLF1
Rat OL267
Mouse OLF15
Rat OL867
Human O10J1
Ciona 16 (Smoothened)
Ciona 13 (Frizzled)
Ciona 48 (cAMP)
Ciona 7 (GABA-B)
Chemokine Cluster
SOG
Peptide
Amine
MECA
LDLRR/GLHR/LGR
Melatonin
Opsin
Tre1/GPR84
Prostaglandin
Olfactory
Outgroup

b

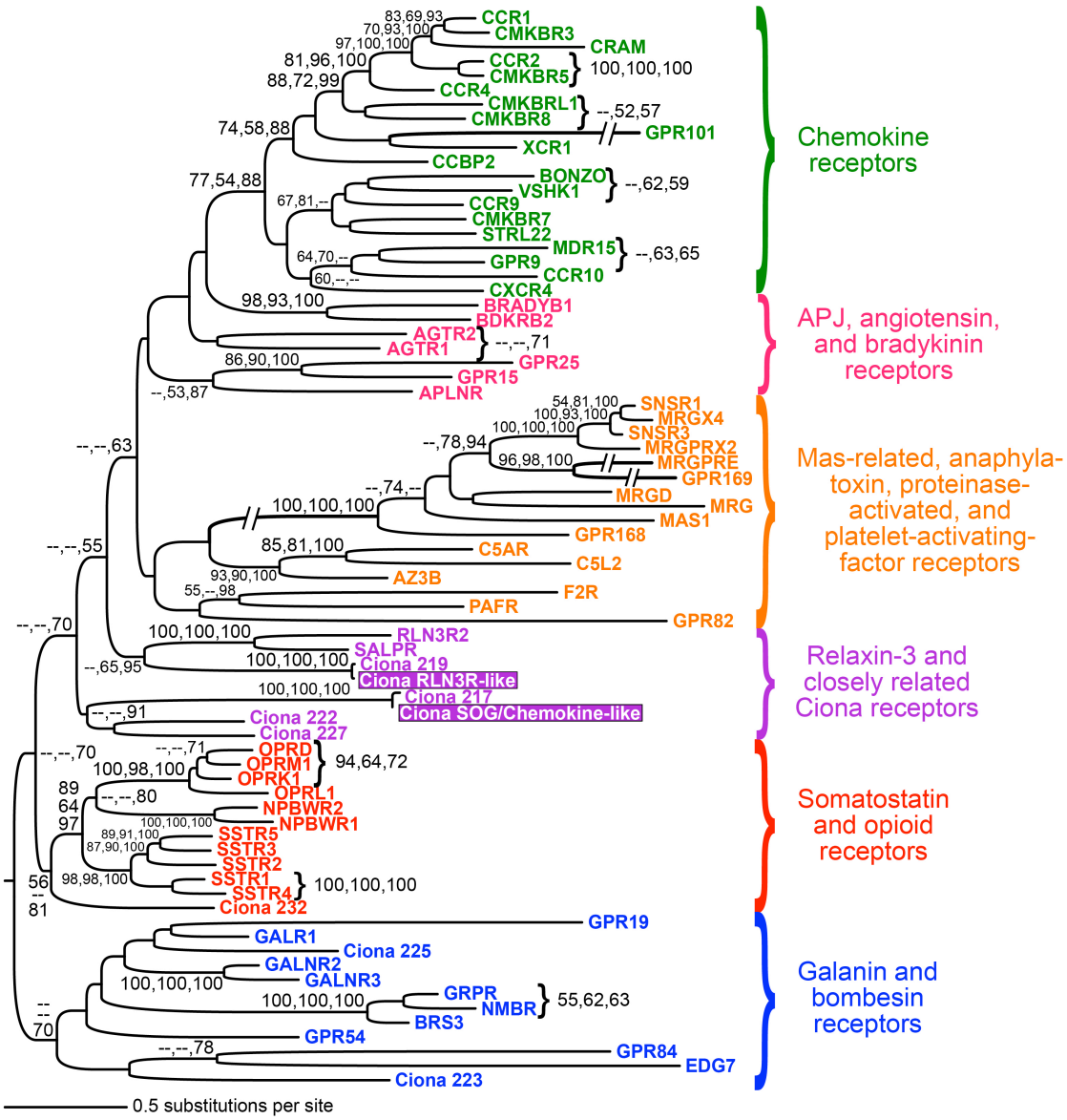
CCR1
CMKBR3
CRAM
CCR2
CMKBR5
CCR4
CMKBRL1
CMKBR8
GPR101
XCR1
CCBP2
BONZO
VSHK1
CCR9
CMKBR7
STRL22
MDR15
GPR9
CCR10
CXCR4
BRADYB1
BDKRB2
AGTR2
AGTR1
GPR25
GPR15
APLNR
SNSR1
MRGX4
SNSR3
MRGPRX2
MRGPRE
GPR169
MRGD
MRG
MAS1
GPR168
C5AR
C5L2
AZ3B
F2R
PAFR
GPR82
RLN3R2
SALPR
Ciona 219
Ciona RLN3R-like
Ciona 217
Ciona SOG/Chemokine-like
Ciona 222
Ciona 227
OPRD
OPRM1
OPRK1
OPRL1
NPBWR2
NPBWR1
SSTR5
SSTR3
SSTR2
SSTR1
SSTR4
Ciona 232
GPR19
GALR1
Ciona 225
GALNR2
GALNR3
GRPR
NMBR
BRS3
GPR54
GPR84
EDG7
Ciona 223
0.5 substitutions per site
Chemokine receptors
APJ, angiotensin, and bradykinin receptors
Mas-related, anaphylatoxin, proteinase-activated, and platelet-activating-factor receptors
Relaxin-3 and closely related Ciona receptors
Somatostatin and opioid receptors
Galanin and bombesin receptors

Appendix S I Phylogenetic analysis of two GPCRs expressed in the PPE-derived neurons of *Ciona intestinalis*. a, Maximum Likelihood phylogeny of Rhodopsin-class G protein-coupled receptors. This initial survey aimed to find the approximate placement of the two GPCRs of interest (boxed in blue). All non-*Ciona* sequences were downloaded in bulk from pfam.xfam.org; they comprise the Pfam "seed" alignment of seven-transmembrane receptors for the GPCRs. The rhodopsin subclass names are given to the right of each colored group. The asterisk and double-asterisk indicate, respectively, the genes labeled "RXFP3" and "SOG/Chemokine-like" in Fig. 2e. We judge robust nodal support as: bootstrap percentages > 70 for Minimum Evolution (ME) and Maximum Likelihood (ML) and posterior probability percentages > 95 for Bayesian Inference (BI). **b**, Maximum Likelihood phylogeny of a refined set of human and *Ciona* rhodopsin-class GPCRs. The *Ciona* GPCRs expressed in the aATENs/GnRH neurons are highlighted with violet boxes. The three nodal support values are, in order: ME bootstrap percentage, ML bootstrap percentage and BI posterior probability (only values > 50 are shown). Branch lengths are proportional to molecular change (amino acid substitutions/site) between nodes; see scale bar for measurement.

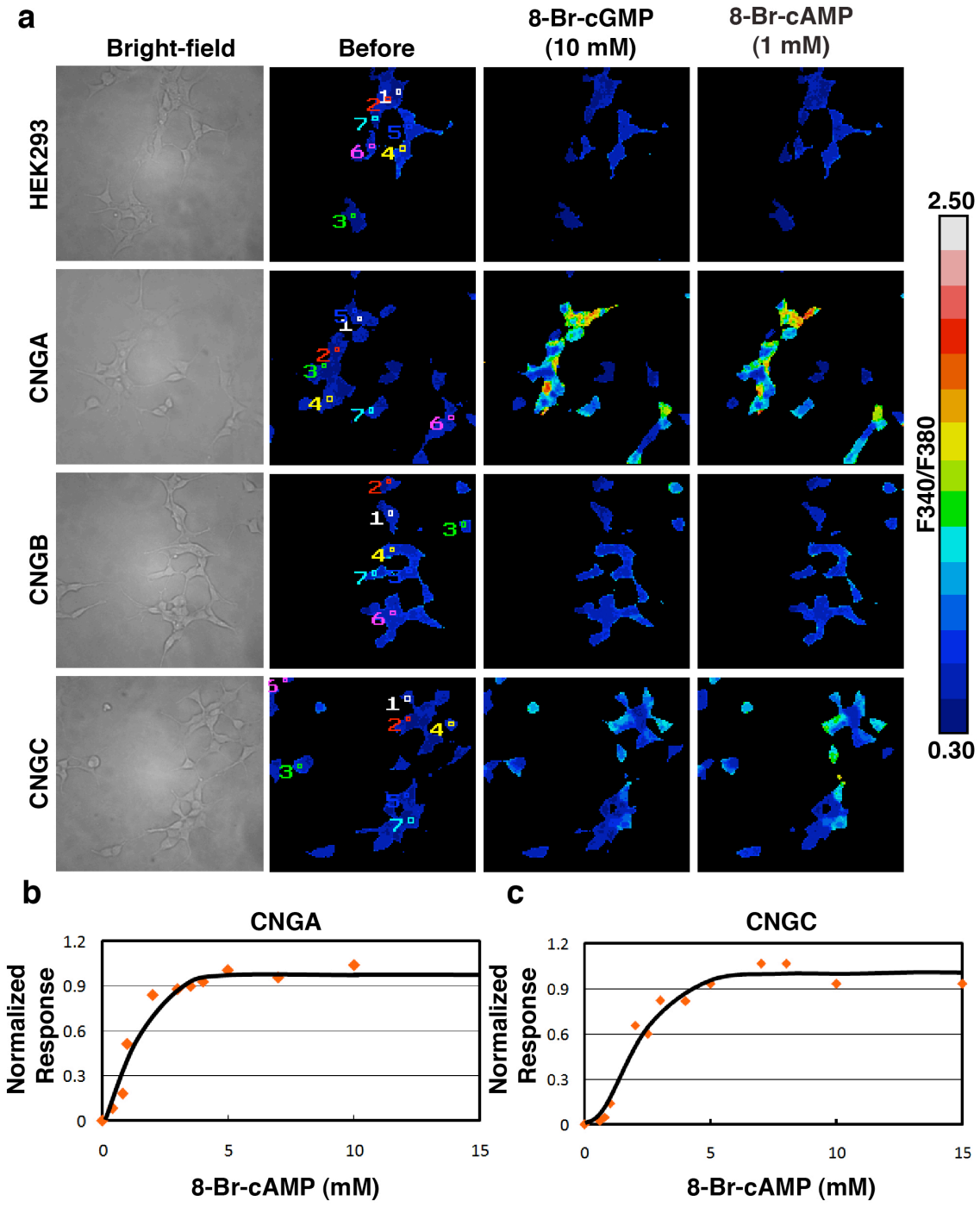
a
Bright-field
Before
8-Br-cGMP (10 mM)
8-Br-cAMP (1 mM)
HEK293
CNGA
CNGB
CNGC
2.50
F340/F380
0.30
b
CNGA
Normalized Response
8-Br-cAMP (mM)
c
CNGC
Normalized Response
8-Br-cAMP (mM)

Appendix T I Elevation of intracellular Ca^{2+} concentration in cells expressing *Ciona* CNG channels in response to cyclic nucleotides. **a**, Intracellular Ca^{2+} was visualized by Fura-2 AM ratiometric calcium imaging. Ca^{2+} influx into HEK 293 cells transfected with CNGA and CNGC was induced by 10 mM 8-Br-cGMP and 1 mM 8-Br-cAMP. In contrast, no Ca^{2+} influx was observed when HEK 293 cells transfected with CNGB were treated with either 10 mM 8-Br-cGMP or 1 mM 8-Br-cAMP. Colored numbers in the "before" panels indicate cells that were subjected to a quantitative measurement of fluorescence. **b**, Dose dependent response of HEK 293 cells transfected with CNGA to 8-Br-cAMP. Data were obtained from at least seven different cells in each of 16 different transfections. **c**, Dose dependent response of HEK 293 cells transfected with CNGC to 8-Br-cAMP. Data were obtained from at least seven different cells in each of seven different transfections.

Supplementary Movie Information

Supplementary Movie 1
This movie shows the lateral view of a *Mitf>Twist* expressing larva labeled with *Tyr>mCherry.* The time-lapse covers a period of about 168 minutes, during which time the protrusive behavior of the a9.49 lineage is seen. The a9.49 lineage misexpressing *Twist* commonly forms filopodia, which is indicative of cellular reprogramming to mesenchymal fate (QuickTime; 2.4 MB).

Supplementary Movie 2
Lateral view of a *Mitf>Twist* expressing early juvenile labeled with *Tyr>mCherry* (grey is UV autofluorescence). The time-lapse covers about 6 hours of development, during which time the ectopic a9.49 lineage can be seen migrating around the periphery like the endogenous migrating tunic cells. The movie loops twice and during the second time the migrating descendants of a9.49 are labeled with asterisks. Other *Tyr>mCherry* that have been incorporated into the mesenchyme remain stationary (QuickTime; 20.3 MB).

Supplementary Movie 3
Time-lapse movie of an embryo electroporated with *Dmrt>H2BYFP* to label rows III-VI and *ZicL>H2BCFP* to label rows I-IV. The movie begins just after the cells in row III have divided and runs until the pigment cell precursors intercalate at the midline. Image stacks were taken every 3 min for 2 hours at 21°C. Annotations refer to the cell lineage nomenclature at the tenth generation except for the final division of the pigment cells. The final division of a10.97 (labeled "97") gives rise to a11.193 (labeled "193") and a11.194 (labeled "194"). Similarly, cells a10.68 and a10.67 of row IV can also be seen dividing (QuickTime; 69.1 MB).

Supplementary Movie 4
This movie shows the neurulation of an embryo co-electroporated with *Dmrt>H2B:YFP* and *Six1/2>mCherry* from a dorsal view. The time-lapse covers a period of about 120 minutes, during which time *Six1/2>mCherry* becomes expressed in posterior row V cells. The movie pauses to show the derivatives of row III-IV (orange) and row V-VI (white) at the 10^{th} generation (i.e., a10.97, a10.98, etc.). *Six1/2>mCherry* is initially expressed in the derivatives of a10.77, a10.69, a10.101, and a10.103 (QuickTime; 31 MB).

Supplementary Movie 5
This movie shows lateral views of the co-localization of *SOG/Chemokine receptor-like>mCherry*, *RXFP3>mCherry*, and *CNGA>mCherry* with *GnRH>GFP* in three larval stage embryos respectively. In each larva the *mCherry* reporter is shown first, as the plane of the Z-section pans through the left and right side of the animal. Then the *GnRH>GFP* signal is gradually faded in to show co-localization in the PPE-derived neurons. These neurons are located behind the oral opening and are the only site of co-expression (QuickTime; 32 MB).